Electron correlation and screening in model nanostructures

Jack Wetherell

Doctor of Philosophy

University of York
Physics

November 2018

Abstract

Accurate models of electron correlation are key to understanding and predicting important physical characteristics that underpin the development of many modern quantum technologies. One of the most widely used approaches to modeling correlation is the *GW* approximation within many-body perturbation theory (MBPT). There are a large number of 'flavors' of the *GW* approximation, with varying levels of computational cost and accuracy. Our aim is to elucidate the various deficiencies and develop novel corrections in order to ameliorate such failings.

In this thesis we study simple model systems, whose properties can be determined exactly by numerical solution of the Schrödinger equation, that exhibit the key physical properties present in real quantum systems such as atoms and molecules. We then are able to compare the exact results to that of existing methods to identify the fundamental source of shortcomings, using this insight to develop new approximations. We find that a common systematic error across all flavors of the *GW* approximation is the 'self-screening' error. We develop a conceptually and computationally simple correction that removes the unwanted effect of this error on the charge density and ionization potential.

We demonstrate that MBPT methods exhibit Kohn's concept of advantageous 'nearsightedness', unlike the computationally cheaper Kohn-Sham density functional theory (KS-DFT). We attribute this to the non-locality of the potentials used in MBPT. We highlight that this allows approximations to more easily encapsulate advanced aspects of exchange and correlation to be made within MBPT. Hybrid functionals contain these non-local potentials and so benefit from this nearsightedness, and when enforced to obey physically justified constraints, yield extremely accurate densities and ionization potentials.

We also extend our investigation to the time-dependent properties of correlated systems. A form of time-dependent many-body perturbation theory, that brings together the simplicity of time-dependent DFT (TDDFT) and sophisticated correlation effects of MBPT is investigated. We show that this approach significantly outperforms common approximations to TDDFT without requiring the more onerous computational cost of non-equilibrium Green's function methods.

I would like to dedicate this thesis to Mike Wetherell.

Contents

List of Figures

List of Tables

Acknowledgements

First and foremost I would like to thank my supervisor Rex Godby and collaborator Matt Hodgson for their invaluable advice, insight and guidance throughout.

I would also like to thank Leopold Talirz, for his crucial improvements to the iDEA code and for leading the development of the public release. In addition thanks to the many people also involved in the continued development of the iDEA code; Matt Hodgson, Razak Elmaslmane, Mike Entwistle, Ewan Richardson and Ryan Cocking. Special thanks to Razak Elmaslmane and Keith McKenna for our immensely enjoyable collaborative project presented in Chapter 7 of this thesis.

For helpful discussions which have had a great impact on this work I thank Matt Hodgson, Leopold Talirz, Lucia Reining, Krister Karlsson, Peter Elliot, Hardy Gross, Razak Elmaslmane, Mark van Schilfgaarde, Phil Hasnip, Ewan Richardson and Mike Entwistle.

I am also thankful of the unwavering support of my family and Sian Bissell O'Sullivan. Finally, I acknowledge funding from the York Centre for Quantum Technologies (YCQT).

Declarations

I declare that the work presented in this thesis, except where otherwise stated, is based on my own research and has not been submitted previously for a degree in this or any other university. Parts of the work reported in this thesis have been published in: Physical Review B, Physical Review B Rapid Communications and Physical Review Materials Rapid Communications.

Chapter 4 describes collaborative work that is currently in preparation to be submitted for publication: J. Wetherell, L. Talirz, M. J. P. Hodgson, and R. W. Godby, 'Electron densities and Kohn-Sham potentials from many-body perturbation theory', *In Preparation*. I participated fully in the development of the code and the formulation and analysis of the research and executed all calculations shown in the paper, and prepared the first draft of the paper.

Chapter 5 describes collaborative work that has been published: J. Wetherell, M. J. P. Hodgson, and R. W. Godby, '*GW* self-screening error and its correction using a local density functional', *Physical Review B (Rapid Communications)* **97**, 121102(R) (2018). I participated fully in the development of the code and the formulation and analysis of the research and executed all calculations shown in the paper, and prepared the first draft of the paper.

Chapter 6 describes collaborative work that has been published J. Wetherell, M. J. P. Hodgson, L. Talirz, and R. W. Godby, 'Advantageous nearsightedness of many-body perturbation theory contrasted with Kohn-Sham density functional theory', *Physical Review B* **99**, 045129 (2019). I participated fully in the development of the code and the formulation and analysis of the research and executed all calculations shown in the paper, and prepared the first draft of the paper.

Chapter 7 describes collaborative work that has been published: A. R. Elmaslmane*, J. Wetherell*, M. J. P. Hodgson, K. P. McKenna, and R. W. Godby, 'Accuracy of electron densities obtained via Koopmans-compliant hybrid functionals', *Physical Review Materials (Rapid Communications)* **2**, 040801(R) (2018) (* authors contributed equally). A. R. Elmaslmane and I participated equally in the development of the code and the formulation and analysis of the research and execution of calculations shown in the paper. A. R. Elmaslmane prepared the first draft of the paper.

Chapter 8 describes collaborative work that is currently in preparation to be submitted for publication: J. Wetherell, M. J. P. Hodgson, and R. W. Godby, 'Time-dependent electron densities from many-body perturbation theory', *In Preparation*. I participated fully in the development of the code and the formulation and analysis of the research and executed all calculations shown in the paper, and prepared the first draft of the paper.

During the course of this project I also contributed to the collaborative work that has been published: M. T. Entwistle, M. J. P. Hodgson, J. Wetherell, B. Longstaff, J. D. Ramsden and R. W. Godby, Local density approximations from finite systems, *Physical Review B* **94** 205134 (2016). I participated in the computational development of the iDEA code for these calculations and in the collaborative writing of the paper. M. T. Entwistle executed the calculations shown in the paper, and prepared the first draft of the paper. This is not included explicitly in a chapter of this thesis as it does not directly contribute to the main messages; references are made to this work where appropriate.

Chapter 1

Introduction

One of the principal contributors to the rapid advancement of modern technology is the successful quantum mechanical simulation of matter. One of the most challenging quantum phenomena to accurately and efficiently model is electron correlation. Correlation is the part of the interaction between electrons that causes the motion of one to effect the motion of all others, as they tend to exclude each other from their surrounding vicinity due to their Coulomb repulsion. This effect gives rise to the screening of the Coulomb interaction due to the response of mobile electrons. While correlation contributes only a small amount to the total description of the interaction of electrons, it is absolutely essential to describe many fundamental properties of matter, such as the accurate prediction of the bonding of atoms to form molecules [1, 2], the energies to break such bonds [3] and the London dispersion forces between molecules [4].

Due to the extremely rapid miniaturization of semiconductor electronics, silicon based integrated circuits are reaching the limit of Moores' law [5], as the size of individual components are becoming of the order of the length scale of tens of atoms [6]. Attempts overcome this limitation has lead to a drive in development of an alternative type of electronics that takes a bottom-up approach, constructing components out of individual atoms and molecules rather than etching components into bulk semiconductors. One such approach is molecular junctions, that consist of a single molecule connected between two conducing leads [7, 8, 9]. However, it still remains a challenge to accurately model the flow of electronic currents through these small structures in the presence of a strong, quickly switching, electric field [10, 11, 12]. Such models require an accurate and computationally tractable description of correlation.

The approach we take in this thesis is to study simple model systems, whose properties are designed to capture the physical features present in molecules, for which the many-electron Schrödinger equation can be solved exactly. We then implement existing approaches and compare to the exact results. This simplicity allows us to delve into the fundamental quantities in order to gain a solid understanding of what is the root cause of the known shortcomings of existing methods. This allows us to develop new and improved methods that aim to overcome such deficiencies. We then test these novel approaches for our set of challenging model systems to quantify the improvements made and to what extent further advancement is needed.

There are several methods used to model the properties of molecules at equilibrium, one of the most widely used is many-body perturbation theory (MBPT) [13, 14, 15].

This theory describes how a system responds to the addition and removal of electrons; an in-depth account of MBPT is presented in chapter 2. The simplest and most practical approximation within MBPT is the Hartree-Fock method [16, 17, 18]. Despite its success at predicting molecular bond-lengths [12], the bond energy and dissociation limit, molecular gaps and inter-molecular forces are wholly incorrect [12]. This is due to the approximation totally neglecting electron correlation.

A usual approach to incorporating electron correlation into this picture is the *GW* approximation [19]. While this does in some cases improve upon HF for the addition and removal energies of molecular systems [20], it is highly dependent on which of the many 'flavors' of *GW* is used [20, 21]. The most sophisticated fully-self consistent flavor is known to perform very poorly, due to the lack of 'vertex terms' [22, 23, 24]. Also, little is known about the performance of *GW* for the charge density, which is crucially important to modeling the time-dependent evolution of the density and current density, as it is used as the starting point of such propagations.

In chapter 4 we investigate this problem in detail by comparing a wide range of existing and novel flavors of the *GW* approximation to the exact when applied to our set of characteristic model systems, in particular focusing on the quality of the charge density. We show that the accuracy of the densities and ionization potentials predicted vary considerably with the flavor used. We find an emerging systematic error is prevalent across all flavors, especially in the fully-self consistent case. We identity this as the self-screening error, a part of the self-interaction error present in *GW* calculations that causes each electron to screen its own removal [22]. This arises due to the neglect of vertex terms in the *GW* approximation to the self-energy [25]. Explicit vertex corrections are tremendously expensive, and usually do not significantly improve the performance of the calculations [23, 26, 27]. In chapter 5 we investigate this error in more detail to ascertain the root cause in the simplest possible case, and proceed to develop a simple, computationally inexpensive vertex correction [28]. In tests, this removes the self-screening errors in the density and ionization potential. We outline what further improvements are needed beyond our vertex correction.

In chapter 6 we illustrate that, unlike Kohn-Sham density functional theory [29, 30, 31], many-body perturbation theory methods such as Hartree-Fock and the GW approximation exhibit Kohn's concept of nearsightedness [32]. This means that the potential describing one subsystem needs not contain any additional features due to the presence of surrounding subsystems. This is of particular importance when modeling molecules [33]. We find that this is due to the spatial non-locality of the MBPT potentials. We illustrate, using a simple model system, that pathological features needed in exact Kohn-Sham theory are not required in the potentials of MBPT. We suggest that this allows for more advanced approximations to exchange and correlation to be formulated within MBPT. Hybrid functionals build upon the non-local exact exchange potential of Hartree-Fock, and hence also benefit from this nearsightedness. In chapter 7 we demonstrate that hybrid functionals that are designed to obey physically justified constraints yield extremely accurate densities [34].

A key theory when modeling the currents that form when systems are driven out of equilibrium by electric fields is time-dependent density functional theory (TDDFT) [35]. While in principle exact, this theory is requires approximation, most commonly by the adiabatic local density approximation (LDA). When used to predict the conductance properties of molecular junctions the adiabatic LDA is totally inadequate [12], this is due in part to the neglect of the memory effects required by exact

TDDFT. A usual alternative to TDDFT is the non-equilibrium Green's function approach via the propagation of the two-point Kadanoff-Baym equations [36, 37, 38]. This approach, while much more accurate than TDDFT, is limited due to the onerous computational cost; in particular the requirement to store the two-point Green's function, which requires several terra-bytes for even small molecular systems of simulation times of the order of ten femto-seconds [39], although optimizations are being developed [39].

In chapter 8 we apply our approach to the development of methods to compute time-dependent densities for a range of model systems driven out of equilibrium with an external perturbing field. We propose methods that exploit the simplicity and computational ease of propagating single-particle orbitals through time, as in the TDDFT case, but with potentials inspired from MBPT methods. In tests we find these methods yield much more accurate densities than the adiabatic LDA, without the demanding computational cost of propagating the non-equilibrium Green's functions.

Chapter 2

Theory of interacting electrons

2.1 Single-particle quantum mechanics

2.1.1 The wavefunction

The wavefunction of a single electron system fully describes the state of a system and is denoted

$$\psi(x), \tag{2.1}$$

where $\psi(x)$ must be a smooth, continuous, complex valued function[1]. The state of the system evolves with time and is represented by the time-dependence of the wavefunction

$$\psi(x,t). \tag{2.2}$$

The physical interpretation of the wavefunction is through the probability density $\rho(x)$. For a system in state $\psi(x)$ this is given by

$$\rho(x) = |\psi(x)|^2. \tag{2.3}$$

The integral of this quantity tells us the probability of finding the electron between points $x = A$ and $x = B$ in our system

$$P(A,B) = \int_A^B \rho(x)\,dx. \tag{2.4}$$

2.1.2 Observables and operators

We will now illustrate how to determine physical properties of a system that is in a state $\psi(x)$.

Every observable A has a corresponding Hermitian operator $\hat{A}$. As $\hat{A}$ is Hermitian it has an associated set of orthonormal eigenfunctions $\{\phi_i\}$ and set of real eigenvalues $\{a_i\}$, these sets are solutions to the operator's eigenequation

$$\hat{A}\phi_i = a_i\phi_i. \tag{2.5}$$

[1]This is written in one dimension (and will remain in one dimension throughout this section for simplicity of notation), but in general the wavefunction is a function of all the generalized coordinates of the system (e.g. $\psi(r,\theta,\phi)$).

As $\{\phi_i\}$ are orthonormal

$$\int_{\forall} \phi_i^* \phi_j dx = \delta_{ij}.^2 \tag{2.6}$$

If the state of the system is $\psi(x)$, we can determine the probability of observing the value of A to be a_i. As $\{\phi_i\}$ form a complete set, the wavefunction can be written in terms of the set of eigenfunctions of $\hat{A}$ as a basis:

$$\psi = \sum_i c_i \phi_i. \tag{2.7}$$

The system is now defined by a set of probability amplitudes $\{c_i\}$ in the basis of $\hat{A}$, these are determined by

$$c_i = \int_{\forall} \phi_i^*(x) \psi(x) dx. \tag{2.8}$$

The probability of the value of A being observed to be a_i is

$$P(a_i) = |c_i|^2. \tag{2.9}$$

The probability of observing all other non-eigenvalues is zero, therefore the value of A is quantised rather then continuous. The expectation value of the observable A is then

$$\langle A \rangle = \int_{\forall} \psi^*(x) \hat{A} \psi(x) dx \tag{2.10}$$

$$= \sum_i |c_i|^2 a_i. \tag{2.11}$$

If the system is in an eigenstate j of $\hat{A}$ then the expectation value is then simply a_j. The process of determining properties of an observable A of a system in a state ψ is summarized in the following process diagram:

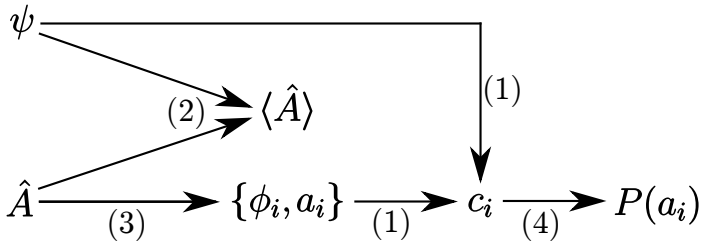

Figure 2.1: Process diagram describing how to determine values of an observable A of a system in a state ψ where step (1) is given by equation 2.8, step (2) by 2.10, step (3) by 2.5 and step (4) by 2.9.

2.1.3 Time-evolution of the wavefunction

We have shown how to calculate the physical properties of a system in a state ψ. To determine how these properties evolve with time the wavefunction is evolved in time to give $\psi(x,t)$ and then the process outlined in figure 2.1 can be applied at given time.

The single-particle Hamiltonian is defined as

$$\hat{H}_s = \hat{K}_s + \hat{V} = -\frac{\hbar^2}{2m}\frac{\partial^2}{\partial x^2} + V_{\text{external}}(x). \tag{2.12}$$

[2]Where $\forall$ denotes the integral over all space.

Where the system is defined by the external potential energy $V_{\text{external}}(x)$. We can determine the eigenfunctions and eigenvalues of this operator by solving its corresponding eigenequation

$$\hat{H}_s\phi_i = E_i\phi_i. \tag{2.13}$$

This special case of equation 2.5 is called the Time-Independent Schrödinger Equation (TISE). If this system is in the lowest energy eigenfunction of this Hamiltonian, we say that it is in the ground-state. The state of a system can then be written in the basis of $\hat{H}_s$:

$$\psi = \sum_n c_n\phi_n \tag{2.14}$$

As the state of the system evolves with time the probability amplitudes vary with time

$$\psi(x,t) = \sum_n c_n(t)\,\phi_n(x), \tag{2.15}$$

where the state that the system was initially prepared in $\psi(x,0)$ determines the initial values of the probability amplitudes

$$c_n(0) = \int_\forall \phi_n^*(x)\,\psi(x,0)\,dx. \tag{2.16}$$

The system evolves in time according to the Time-Dependent Schrödinger Equation (TDSE):

$$i\hbar\frac{\partial\psi}{\partial t} = \hat{H}_s\psi \tag{2.17}$$

Lets us consider an electron in one of the eigenstates $\psi(x,0) = \phi_s(x)$ where ϕ_s is one of the eigenfunctions of the Hamiltonian $\hat{H}_s$. This means that the particle is resting in the energy state of energy E_s as shown the figure below.

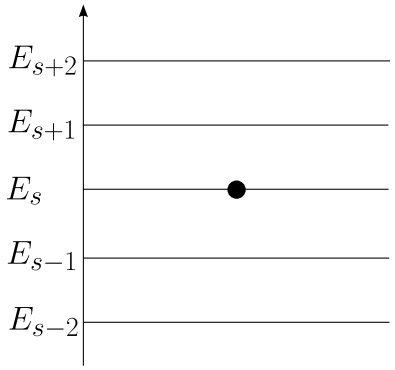

Figure 2.2: Energy diagram of an electron occupying energy state E_s

We now ask what happens if we perturb the system by turning on a driving potential at $t = 0$. What is the probability of the electron being excited to another energy state E_k after a time t due to this perturbation?

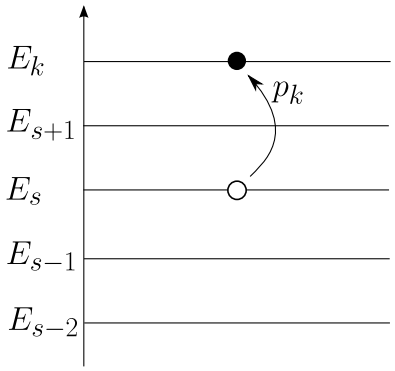

Figure 2.3: Probability of an electron being excited to state E_k from E_s

As the excitation only happens when the wavefunction collapses to the excited state, before the collapse the electron is being excited to all states simultaneously, we say the system is exploring excited states. The perturbation can be considered a perturbation to the system's Hamiltonian

$$\hat{H}' = \hat{H}_s + \Delta\hat{H}. \tag{2.18}$$

Written out fully this becomes

$$\hat{H}' = -\frac{\hbar^2}{2m}\frac{\partial^2}{\partial x^2} + V_{\text{external}}(x) + \Delta V(x,t). \tag{2.19}$$

The system will evolve according to the TDSE. This causes the probability amplitudes of each of the eigenstates of our system to evolve with more that just a phase factor. This represents the system exploring excited states

$$\psi(x,t) = \sum_n c_n(t)\, e^{-\frac{i}{\hbar}E_n t}\phi_n(x). \tag{2.20}$$

We can now solve the TDSE to determine this trajectory of the probability amplitudes $c_n(t)$.[3]

[3]We now have the phase factor taken out of the function $c_n(t)$ for convenience. Also note that the eigenstates ϕ_n are still the eigenstates of the unperturbed system.

2.2 Many-particle quantum mechanics

2.2.1 Non-interacting particles

So far we have discussed extracting the ground-state and time-dependent properties of a system that contains only one electron. Now we will investigate systems of several electrons. Initially we will consider the Coulomb force between the electrons to be zero as some new quantum mechanical effects occur even for non-interaction particles, and so for simplicity we will study these separately. The wavefunction of our N particle system is written as [4]

$$\Psi(x_1, x_2, \ldots, x_N) \tag{2.21}$$

And from this we can determine the probability density of finding a single electron:

$$\rho(x) = \int_{\forall} \cdots \int_{\forall} |\Psi(x, x_2, \ldots, x_N)|^2 dx_2 \ldots dx_n \tag{2.22}$$

and from this we can determine the charge density $n(x)$:[5]

$$n(x) = Ne\rho(x) \tag{2.23}$$

who's integral is the total charge between points A and B in system

$$Q\left(A, B\right) = \int_A^B n\left(x\right) dx. \tag{2.24}$$

It is important that when evaluating the probability density using equation 2.22 that it does not matter which x_i is replaced with x and is not integrated over (we picked x_1 in this case). This is because electrons are indistinguishable particles and when we observe an electron in a given region of our system, we cannot determine which electron we observed[6]. As our electrons are not interacting we are able to assemble the wavefunction from the single electron states $\{\phi_i\}$ (here called single-particle orbitals), but there are a few ways we can choose to do this and it is important that we choose the way that keeps our electrons indistinguishable. We will show that the only way to do this is to build the wavefunction in such a way that obeys the Pauli exclusion principle.

2.2.2 The Pauli exclusion principle

Pauli's exclusion principle states that no two identical fermions can occupy the same quantum state. In a two electron system this can be written in the position basis as

$$\Psi(x, x) = 0, \tag{2.25}$$

and more generally

$$\Psi(x_1, x_2) = -\Psi(x_2, x_1). \tag{2.26}$$

[4]The way we determine the physical properties of this state for an observable A is the same as in Figure 2.1.

[5]Where here e is the charge of the electron.

[6]Of course this only applies to electron with like-spin. Opposite spin electrons are 'distinguishable' fermions.

Therefore the many-body wavefunction must be antisymmetric upon exchange of particles. We will show that obeying this principle enforces indistinguishably of our electrons. Let's choose a way of constructing the wavefunction from the set of single-particle orbitals that does not obey this principle; a product state

$$\Psi_{\mathrm{PS}}(x_1, x_2) = \phi_1(x_1)\phi_2(x_2). \tag{2.27}$$

If we then calculate the charge density using equations 2.22 and 2.23 it depends on which value of x we choose to integrate over

$$n(x_1) = 2e|\phi_1(x_1)|^2 \tag{2.28}$$
$$n(x_2) = 2e|\phi_2(x_2)|^2. \tag{2.29}$$

Therefore the electrons are not indistinguishable, as by experimentally measuring the charge density we can determine which electron we are observing. Now let us instead choose a way to construct the wavefunction that obeys the Pauli exclusion principle, the Slater determinant (SD)

$$\Psi_{\mathrm{SD}}(x_1, x_2) = \frac{1}{\sqrt{2}} \begin{vmatrix} \phi_1(x_1) & \phi_2(x_1) \\ \phi_1(x_2) & \phi_2(x_2) \end{vmatrix}. \tag{2.30}$$

Now when we evaluate the charge density we yield

$$n(x_1) = |\phi_1(x_1)|^2 + |\phi_2(x_1)|^2 \tag{2.31}$$
$$n(x_2) = |\phi_1(x_2)|^2 + |\phi_2(x_2)|^2. \tag{2.32}$$

So obeying the Pauli exclusion principle ensures the electrons remain indistinguishable, this means that two indistinguishable electrons cannot occupy the same orbital, as the SD of such a case would yield a zero wavefunction. This effect, of multiple electrons (of the same spin) being forbidden to be in the same state is sometimes referred to as Pauli *repulsion*, and is purely a quantum effect between identical fermions (even when there is no Coulomb force present). This effect is called a repulsion due to the effect it has on the ground-state density of the system, as shown in figure 2.4.

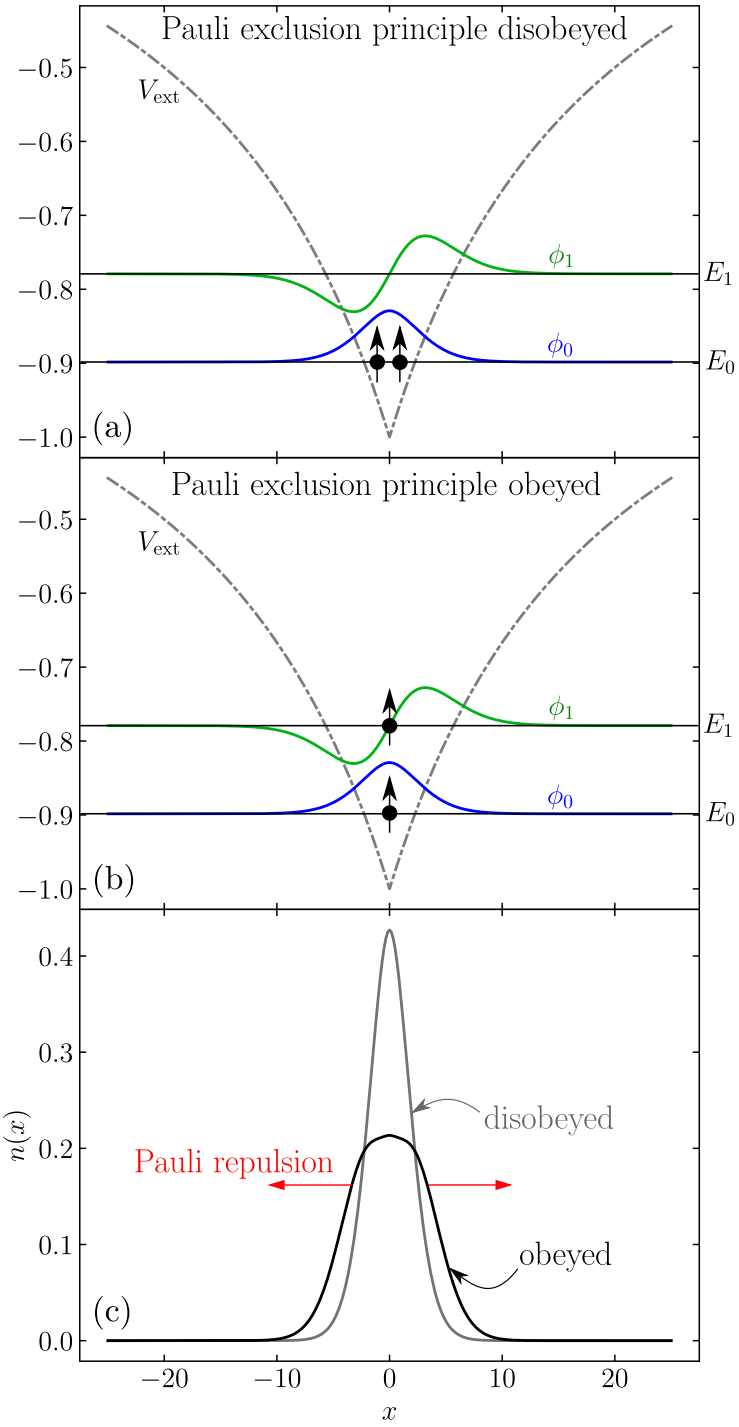

Figure 2.4: Demonstration of the Pauli repulsion for a model 1-dimensional non-interacting two-electron atom, where the electrons are treated as having the same spin (like-spin). Panel (a) shows the external potential of the model atom, the lowest two non-interacting orbitals ϕ_0 and ϕ_1 and the corresponding eigen-energies E_0 and E_1. In this case the Pauli exclusion principle is disobeyed and both electrons occupy state 0. Panel (b) shows the same as (a) but with the Pauli exclusion principle being obeyed, with each electron occupying its own orbital. Panel (c) compares the density of both cases. Switching from the principle being disobeyed to obeyed causes the electrons to appear to repel, as the density spreads out from the center of the well. This is why the effect is called the Pauli *repulsion*. It is worth noting that this effect is occurring despite the complete lack of Coulomb repulsion.

Therefore identical electrons (of like-spin) cannot occupy the same orbital and experience a Pauli repulsion. However, electrons of opposite-spin are not indistinguishable and therefore can occupy the same orbital and do not feel such a repulsion. So when filling non-interacting states with electrons, there can be one spin-up and one spin-down in each orbital.

2.2.3 The Coulomb interaction

We have shown that the many-body wavefunction of a non-interacting system of like-spin electrons can be constructed using a Slater determinant of single-particle orbitals, for example the general two electron case is given by

$$\Phi^{\mathrm{SD}}_{nm}(x_1, x_2) = \frac{1}{\sqrt{2}} \begin{vmatrix} \phi_n(x_1) & \phi_m(x_1) \\ \phi_n(x_2) & \phi_m(x_2) \end{vmatrix}. \tag{2.33}$$

An alternative way this wavefunction can be computed is by finding the eigenfunctions of the many-body non-interacting Hamiltonian

$$\hat{H} = \hat{K} + \hat{V} = -\frac{\hbar^2}{2m} \sum_n \frac{\partial^2}{\partial x_n^2} + \sum_n V_{\mathrm{ext}}(x_n), \tag{2.34}$$

$$\hat{H}\Phi_{nm} = E_{nm}\Phi_{nm}. \tag{2.35}$$

We now add in the Coulomb interaction into the Hamiltonian, by considering the interaction between all pairs of electrons[7]

$$\hat{H} = \hat{K} + \hat{V} + \hat{U} = -\frac{\hbar^2}{2m} \sum_n \frac{\partial^2}{\partial x_n^2} + \sum_n V_{\mathrm{ext}}(x_n) + \sum_{(n,m),n\neq m} \frac{e^2}{4\pi\varepsilon_0(|x_n - x_m| + 1)} \tag{2.36}$$

$$\hat{H}\Psi_i = E_i\Psi_i \tag{2.37}$$

Note that unlike the non-interacting case the interacting wavefunction is in most cases not able to be written as a single Slater Determinant of single-particle orbitals, due to the fact that each electron repels all other electrons and thus effects their energetics, and so the electrons cannot be treated as independent particles.

2.2.4 The Born-Oppenheimer approximation

In order to model a real, large-scale quantum system such as a molecule, we invoke the Born-Oppenheimer approximation (BOA). This states that the motion of the nuclei is negligible when compared to the motion of the electrons due to the much larger mass. Therefore the nuclei are simply included in the system's external potential V_{ext}. In order to find the ground state of a system we first guess the location of all the nuclei in the system, and solve the many-body Schrödinger equation to obtain the ground-state electron energy and charge density. We then minimize the

[7] The Coulomb term includes $+1$ in the denominator, as we are discussing the problem in 1D, and thus must use the 'softened' Coulomb interaction, which simulates the interaction of electrons in a nano-wire. In the 3D case the term would be the usual $\hat{U} = e^2/4\pi\varepsilon_0|\mathbf{r}|^2$.

ground-state energy with respect to the nuclei positions using the process of structure optimization via gradient decent. This then gives us the most energetically favorable configuration of nuclei. The ground-state energy and electron density can then be calculated using

$$\hat{H}\Psi_0 = E_0\Psi_0, \tag{2.38}$$

and from this the electronic structure of the system can be obtained. If we want to compute the time-dependent properties of this system in response to a given perturbation ΔV we begin with the system in the ground-state, and then evolve with time using the time-dependent many-body Shrödinger equation

$$i\hbar\frac{\partial\Psi}{\partial t} = \hat{H}'\Psi, \tag{2.39}$$

where $\hat{H}' = H + \Delta V$. So if we can solve the time-independent and time-dependent Schrödinger equation for a given system we can determine all of its physical properties. For example the total energy of the system, how it responds to an electric field or when illuminated with light, or the energy required to add and remove electron etc.

The problem is that in practice, these equations become intractably difficult to solve for systems of more than a few electrons, due to the unfavorable computational scaling. In order overcome this issue there are methods that allow us to approximately determine the physical properties of systems, without having to solve the many-body Shrödinger equation directly. Two such methods are many-body perturbation theory (MBPT), which considers how a system responds to the addition and removal of electrons, and Kohn-Sham density-functional theory (KS-DFT), which considers modeling a fictitious system of non-interacting electrons, that has the same ground-state charge density as the real interacting system.

2.3 The variational principle

In order to begin approximating the solution to the many-body time-independent Schödinger equation (MB-TISE) to obtain the ground-state wavefunction of a system of interacting electrons we make use of the variational principle. Let us calculate the expectation value of the total energy of our system in the state Ψ,[8]

$$\langle E \rangle = \langle \Psi | \hat{H} | \Psi \rangle. \tag{2.40}$$

If this system is in the ground-state Ψ_0 this gives us the ground-state energy of the system,

$$E_0 = \langle \Psi_0 | \hat{H} | \Psi_0 \rangle, \tag{2.41}$$

where E_0 is the lowest possible eigenstate of $\hat{H}$. We can then define the following functional of the many-body wavefunction:

$$E[\Psi] = \langle \Psi | \hat{H} | \Psi \rangle. \tag{2.42}$$

The variation principle therefore states that the minimum of this functional with respect to the wavefunction gives us the ground-state energy of our system,

$$E_0 = \min_{\Psi} \left\{ \langle \Psi | \hat{H} | \Psi \rangle \right\}. \tag{2.43}$$

Therefore, if we search over all possible wavefunctions, we will eventually arrive at the global minimum of $E[\Psi]$, which is the ground-state many-body wavefunction and from this all ground-state properties of the system can be computed.

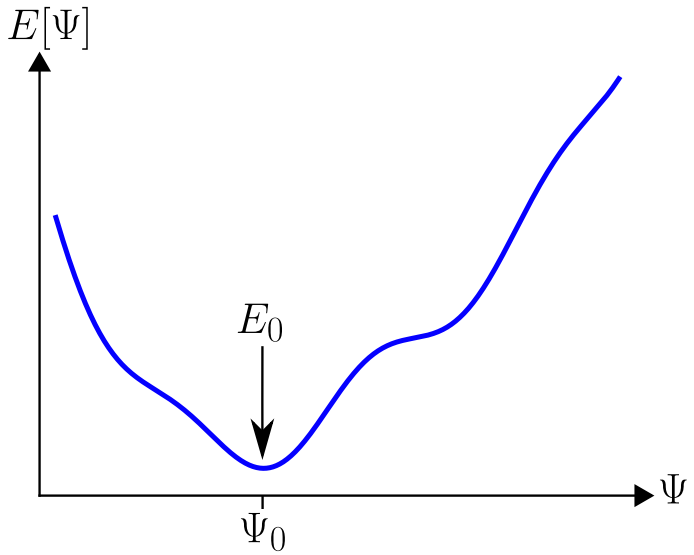

Figure 2.5: Illustration of the functional $E[\Psi]$ along with the ground-state energy E_0 shown as the minimum of this functional, along with the ground-state wavefunction Ψ_0.

[8] This is the form of equation 2.10 with Dirac notation

2.3.1 The Hartree approximation

As a first attempt we will limit the wavefunction to taking the form of a product state of single-particle orbitals,

$$\Psi_{\mathrm{PS}}(x_1, x_2, \ldots, x_N) = \phi_1(x_1)\phi_2(x_2)\ldots\phi_N(x_N). \tag{2.44}$$

This greatly reduces the amount of wavefunction space we need to look through when performing the minimisation as shown in equation 2.43. Performing this minimization gives us the single-particle Hamiltonian (termed the 'Hartree' Hamiltonian $\hat{H}_{\mathrm{s}}^{H}$) whose eigenfunctions are the $\{\phi_i\}$ needed to construct the lowest energy possible product-state wavefunction (equation 2.44)

$$\hat{H}_{\mathrm{s}}^{H}\phi_i = \varepsilon_i\phi_i, \tag{2.45}$$

where $\hat{H}_{\mathrm{s}}^{H}$ is a functional of the charge density

$$\hat{H}_{\mathrm{s}}^{H}[n] = \hat{K}_{\mathrm{s}} + \hat{V}_{\mathrm{ext}} + \hat{V}_{\mathrm{H}}[n], \tag{2.46}$$

$V_{\mathrm{H}}[n]$ is called the Hartree potential and is a functional of the density

$$V_H[n](x) = \int_{\forall} U(x, x')n(x')dx'. \tag{2.47}$$

These equations can be solved self-consistently; firstly a guess is made for the orbitals $\{\phi_i\}$ and thus the charge density n. This allows us to compute the single-particle Hamiltonian using equations 2.46 and 2.47. Then we solve the eigenequation 2.45 to give a new set of orbitals. This is then repeated until convergence is reached.

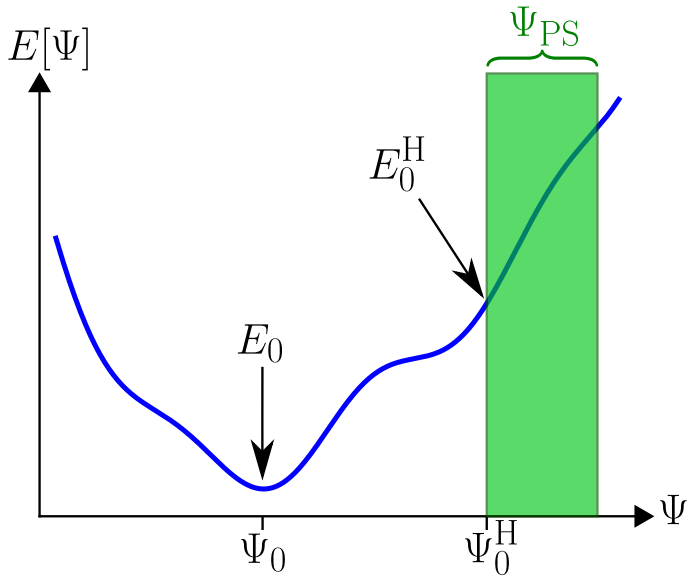

Figure 2.6: Illustration of minimizing the functional $E[\Psi]$, showing the reduction of the wavefunction space when restricted to a product state (PS), along with the Hartree approximation to the total energy E_0^{H} and wavefunction Ψ_0^{H}

The physical interpretation of this method is that our system is treated as a system of non-interacting electrons, and that each feels a mean field potential due to the Coulomb potential of all other electrons in the system (including itself). This potential is the same for all electrons in the system. This approximation has three key failings:

1. As the Hartree potential is local (is simply multiplied by the orbital in the eigenequation) every electron must feel the same potential. This means that each electron feels its own Coulomb potential, as well as the other electrons in the system. This error is termed the self-interaction error (SIE).

2. As we assume the wavefunction takes the form of a product state, it does not obey the Pauli exclusion principle (PEP), and thus the Pauli repulsion between the electrons is neglected entirely.[9]

3. Our electrons are treated as moving independently to each other in a mean field. In reality each electron affects the energetics of the surrounding electrons due to the Coulomb repulsion, this *correlation* of the motion of the electrons is also entirely neglected.

We now move onto a substantially better approximation, that ameliorates some of these serious flaws.

2.3.2 The Hartree-Fock approximation and exchange

We will now go beyond the Hartree approximation by directly addressing issue 2, and extend the approximation to obey the PEP. This problem stemmed from us constraining the wavefunction to be a product state. We will now instead limit the wavefunction to taking the form of a Slater determinant

$$\Psi_{\mathrm{SD}}(x_1, x_2, \ldots, x_n) = \frac{1}{\sqrt{N!}} \begin{vmatrix} \phi_1(x_1) & \phi_2(x_1) & \ldots & \phi_n(x_1) \\ \phi_1(x_2) & \phi_2(x_2) & \ldots & \phi_n(x_2) \\ \vdots & \vdots & \ldots & \vdots \\ \phi_1(x_n) & \phi_2(x_n) & \ldots & \phi_n(x_n) \end{vmatrix} \tag{2.48}$$

this gives us a much wider region of wavefunction space to search over. If we then apply this to the variational principle to determine that Slater determinant that gives us the minimum total energy we obtain a new single-particle Hamiltonian (now termed the 'Hartree-Fock' Hamiltonian $\hat{H}_{\mathrm{s}}^{HF}$) whose eigenfunctions are the $\{\phi_i\}$ needed to construct the lowest energy possible Slater determinant wavefunction (equation 2.48). These are obtained by solving the Hartree-Fock Hamiltonian's eigenequation,

$$K_{\mathrm{s}}\phi_i(x) + V_{\mathrm{external}}\phi(x) + V_{\mathrm{H}}[n](x)\phi_i(x) + \int_{\forall} \Sigma_{\mathrm{x}}[\{\phi_i\}](x, x')\phi_i(x')dx' = \varepsilon_i\phi_i. \tag{2.49}$$

where $\Sigma_{\mathrm{x}}[\{\phi_i\}](x, x')$ is called the exact non-local exchange potential (or sometimes the Fock operator[10]) and is a functional of the *occupied* single-particle orbitals. This potential is called non-local due to the way it acts on the eigenfunctions: it is not simply a direct multiplication (like in the Hartree potential case) but is integrated over the orbital. This allows each electron in the system to feel a different effective

[9] When the self-consistent Hartree method is used in practice, it is useful to choose to occupy each (like-spin) electron in each single-particle orbital. And once self-consistency is reached, construct the wavefunction from a Slater determinant (SD) of these Hartree orbitals. This ensures that the PEP is obeyed. Although the PEP is obeyed this is not the optimal SD that gives us the minimum energy, and hence this can be though of as only an approximate Pauli repulsion felt by non-interacting particles. Computing the optimal SD is discussed in the next section.

[10] When called the Fock operator, the symbol F is usually used instead of Σ_{x}

potential, whereas a local potential is felt by every electron identically. This additional freedom came from us not restricting the wavefunction to a product state, but instead a Slater determinant. As this exact exchange potential is non-local it depends explicitly on the orbitals, rather than the density and is given by

$$\Sigma_x[\{\phi_i\}](x,x') = -\sum_n^{\text{occ}} \phi_n(x)\phi_n^*(x')U(x,x'). \tag{2.50}$$

These equations can be solved self-consistently in the same way as the Hartree equations, except the exchange operator is included in the Hamiltonian, and is constructed from the occupied orbitals in the previous iteration.

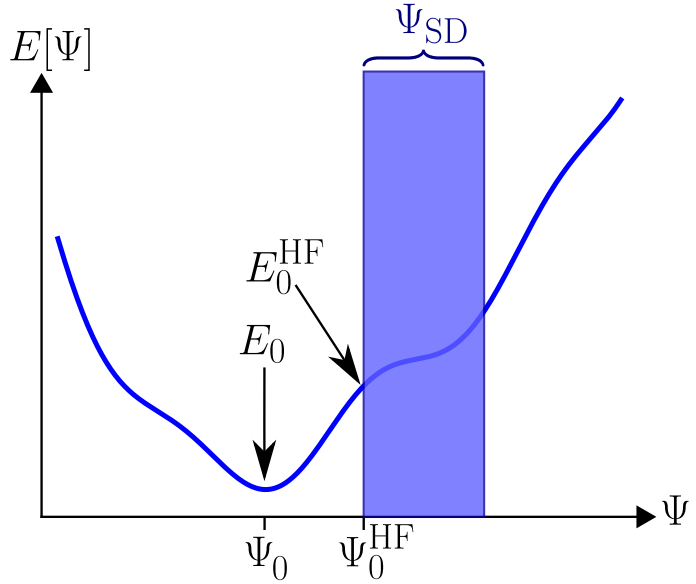

Figure 2.7: Illustration of minimising the functional $E[\Psi]$, showing the reduction of the wavefunction space when restricted to a Slater determinant (SD), along with the Hartree-Fock approximation to the total energy E_0^{HF} and wavefunction Ψ_0^{HF} as can be seen in comparison to figure 2.6, this allows a much more accurate wavefunction and gives an energy much closer to the exact energy.

The physical interpretation of the exchange potential is firstly, that the electrons now correctly obey the PEP, and experience a Pauli repulsion that is the closest possible[11] to that as felt by the interacting electrons. This is not exact, as in reality the electrons cannot be treated as independent particles and thus experience a *screened* Pauli repulsion as each electron causes the surrounding electrons to become excited out of their single particle lowest states[12]. Secondly, as each electron is now able to feel a separate potential, the self interaction error present in the Hartree approximation is corrected, as each electron now in the exchange term, removes the part of the Hartree potential that was due to its own presence. We can now summarize to what extent the Hartree-Fock approximation has corrected three key failings from the previous section:

1. The self-interaction error is entirely corrected. This is because the exchange potential is non-local and thus each electron sees an effective exchange potential, part of which acts to cancel out the part of the Hartree potential due to its own presence.

[11] Given we are restricted to a Slater determinant wavefunction
[12] This is beyond what can be captured by a Slater determinant wavefunction

2. The electrons now correctly obey the Pauli exclusion principle.

3. The electrons are still treated as moving independently to each other, which is incorrect. In order to correctly take account of the screening of the Pauli repulsion, and thus correlation of the electrons we must move beyond an independent particle picture, and beyond limiting the wavefunction to a single Slater determinant.

2.3.3 Full configuration interaction and correlation

We will now go beyond the single-particle picture, in order to take account of the correlation of the electrons. If we consider the Hartree-Fock wavefunction, it is the Slater determinant of the *lowest energy* single-particle orbitals. For example, for a two electron like-spin system with occupied single particle orbitals ϕ_1 and ϕ_2 the wavefunction is

$$\Phi_{12}(x_1, x_2) = \frac{1}{\sqrt{2}} \begin{vmatrix} \phi_1(x_1) & \phi_1(x_2) \\ \phi_2(x_1) & \phi_2(x_2) \end{vmatrix}. \tag{2.51}$$

If we consider the general Slater-determinant Φ_{nm}, it forms a complete set of functions. Therefore *any* exchange-antisymmetric function can be written as an infinite weighted sum of this set, including our many-body ground-state wavefunction[13]:

$$\Psi_0(x_1, x_2) = \sum_{nm} c_{nm} \Phi_{nm}(x_1, x_2). \tag{2.52}$$

This equation is at the heart of describing correlation, as it states that *the ground-state of a interacting system of electrons, can be treated as an excited state of a system of non-interacting electrons*. The full configuration interaction method involves choosing a basis set of Slater determinants (usually Hartree-Fock, as its lowest energy state Slater determinant is the closest as possible to the many-body wavefunction.) and then minimizing the total energy by varying the set of probability amplitudes. This method is in principle exact, although it is computationally very costly. The physical interpretation of this method is that the system of non-interacting electrons is in an excited state, as each electron effects the dynamics of the rest, due to their respective Coulomb repulsion. This now yields a method that corrects the remaining issue 3. This method of going beyond a single-particle picture is onerously expensive. An alternative approach to accounting for electron correlation is the Green's function based *GW* method, which can be feasibly used to compute the correlation effects of large scale systems.

[13] for a general N electron system this would be a function of $(x_1, x_2, \ldots, x_N)$ and the sum would be over $nm \ldots$.

2.4 Many-body perturbation theory

2.4.1 The many-body Green's function

The central concept in many-body perturbation theory is the many-body Green's function G. $G(x, x', t, t')$ is the probability amplitude that, if one electron is added to a many-body system at time t and removed at time t' it has propagated from position x to position x'. That is, the probability that when we added the electron at t it localized at x, and when we removed it at t' is was found at x'. This quantity describes the charged, one-body excitations[14] of a many-body system; the energy to add and remove single electrons, and how a systems responds to such perturbations. As we are only considering the system's external potential to be fixed in time, it is time-symmetric and hence the Green's function only depends of the difference in time between electron addition and removal, and so is written $G(x, x', t' - t)$.

We will investigate the Green's function of a system of non-interacting electrons first, this is called the non-interacting Green's function and is denoted G_0. Let us consider two non-interacting like-spin[15] electrons in a model atom, illustrated in Figure 2.8.

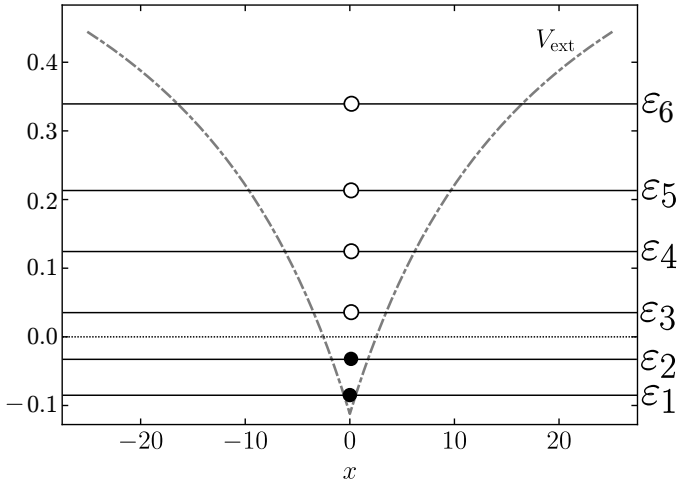

Figure 2.8: Illustration of the two non-interacting electron model atom. The external potential has the form of the 1D softened Coulomb interaction. The single-particle eigenvalues of this system ε_i are shown, with a solid or hollow dot indicating whether the orbital is occupied or unoccupied respectively. The energy scale is defined such that the chemical potential (dotted line) is at zero.

If at a time t we now add an electron to this system it may only fill a currently unoccupied state due to the Pauli exclusion principle. Lets consider it fills unoccupied state m, the probability amplitude that the added electron was added to the system at point x is[16]

$$\phi_m(x)e^{-i\varepsilon_m t}. \tag{2.53}$$

[14] excitations due the addition or removal of *one* electron.

[15] so each orbital only contains at maximum one electron for simplicity.

[16] From here on in we will choose to use Hartree atomic units (a.u.) $\hbar = e = m = \frac{1}{4\pi\varepsilon_0} = 1$, where e is the charge of the electron, m is the mass of the electron and ε_0 is the permittivity of free space.

If we then remove the electron at time t' the probability amplitude that it is found at x' is

$$\phi_m^*(x')e^{i\varepsilon_m t'}. \tag{2.54}$$

Therefore, the total probability amplitude of propagation of the added electron from space-time point (x,t) to (x',t') is the product of these two probability amplitudes. In this case we chose unoccupied orbital m to be the orbital the added electron fills, in reality however we must take account of the fact it could occupy any of these orbitals, and so we must perform a sum over all possible unoccupied orbitals to give

$$\sum_n^{\text{unocc}} \phi_n(x)\phi_n^*(x')e^{i\varepsilon_n(t'-t)}. \tag{2.55}$$

Now we consider what this means for $t' < t$. This means that the electron was removed before it was added. This can be thought of as adding a hole to the system, and measuring the probability amplitude of it's propagation. In reality this means we removed an electron at time t' and added it at t. This means that the sum for $t' < t$ must be over *occupied* states, as it is only those state holes may be added.

$$\sum_n^{\text{occ}} \phi_n(x)\phi_n^*(x')e^{i\varepsilon_n(t'-t)}. \tag{2.56}$$

These then give the non-interacting Green's function of this system to be[17]

$$G_0\left(x,x',t'-t\right) = \begin{cases} i\sum_n^{\text{occ}} \phi_n(x)\phi_n^*(x')e^{i\varepsilon_n(t'-t)} & t' \leq t \\ -i\sum_n^{\text{unocc}} \phi_n\left(x\right)\phi_n^*(x')e^{i\varepsilon_n(t'-t)} & t' > t \end{cases} \tag{2.57}$$

An illustration of an added electron propagating through the system is shown in Figure 2.9.

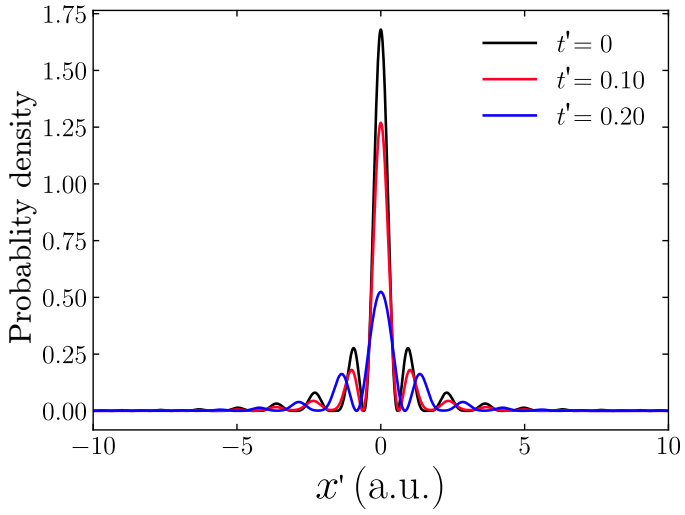

Figure 2.9: Illustration of an added electron propagating through the two non-interacting electron model atom. At $t = 0$ an electron is added to the system and it localizes at $x = 0$. Over time, the probability density of the added electron being found at x' is shown to spread out from the point the electron is added, as it propagates through the system.

If we now consider the case where $x = x'$ and $(t' - t) = 0^-$, this can be thought of the probability of removing and re-adding an electron at point x. It is intuitive that

[17]The i and $-i$ have been added in order to be compatible with the physics propagator convention.

this is counting the number of electrons at point x, and hence is the charge density at point x. We can show this is the case by substituting $x = x'$ and $(t' - t) = 0^-$ to equation 2.57, to yield

$$-iG_0\left(x, x, 0^-\right) = \sum_n^{\text{occ}} \phi_n(x)\phi_n^*(x) \tag{2.58}$$

$$= n(x). \tag{2.59}$$

Let us now consider the interacting Green's function G. We begin with the operators that act on the wavefunction of our system to to add or remove electrons at a particular space-time point. These are called creation $\hat{\psi}^\dagger(x,t)$ and annihilation $\hat{\psi}(x,t)$ field operators[18]:

$$\hat{\psi}^\dagger(x,t) = \sum_k \phi_k^*(x)\,\hat{a}_k^{\dagger H}(t) \tag{2.60}$$

$$\hat{\psi}(x,t) = \sum_k \phi_k(x)\,\hat{a}_k^{H}(t) \tag{2.61}$$

The Green's function is then simply the expectation value of adding an electron at (x,t) and removing it at (x',t') when you system is in the ground-state Ψ. In terms of these operators one would expect it to be

$$G\left(x, x', t' - t\right) = -i\langle\Psi|\hat{\psi}\left(x', t'\right)\hat{\psi}^\dagger(x,t)\,|\Psi\rangle. \tag{2.62}$$

But this will not make causal sense if $t' < t$. The correct definition requires the same account for time ordering as discussed earlier, when $t' < t$ we must remember to perform the removal of an electron first, then the addition. The correct form of the Green's function is therefore

$$G\left(x, x', t' - t\right) = i\theta\left(t' - t\right)\langle\Psi|\hat{\psi}\left(x', t'\right)\hat{\psi}^\dagger(x,t)\,|\Psi\rangle \tag{2.63}$$

$$- i\theta\left(t - t'\right)\langle\Psi|\hat{\psi}^\dagger(x,t)\,\hat{\psi}\left(x', t'\right)|\Psi\rangle, \tag{2.64}$$

where θ is the Heaviside step function. This can be written in a more condensed form using the time-ordering operator T, that is defined such that the addition and removal is done in such a way to not violate causality

$$G\left(x, x', t' - t\right) = -i\langle\Psi|T\left[\hat{\psi}\left(x', t'\right)\hat{\psi}^\dagger(x,t)\right]|\Psi\rangle. \tag{2.65}$$

This is then the definition for the Green's function of the interacting system of electrons with ground-state wavefunction Ψ. If we choose the wavefunction to be a Slater-determinant of the system's non-interacting single-particle orbitals Φ we yield the non-interacting Green's function for the system

$$G_0\left(x, x', t' - t\right) = -i\langle\Phi|T\left[\hat{\psi}\left(x', t'\right)\hat{\psi}^\dagger(x,t)\right]|\Phi\rangle. \tag{2.66}$$

By explicitly applying the operators equation 2.57 is yielded.

It is common to Fourier transform the Green's function of a system into the momentum k and energy ω[19] domain $G(k,\omega)$. From this quantity the spectral function is defined as

$$A(k,\omega) = -\frac{1}{\pi}\text{Im}\left[G(k,\omega)\right]. \tag{2.67}$$

[18] where $\hat{a}_i^\dagger$ and $\hat{a}_i$ are the creation and annihilation operators. Σ_i is defined as the sum of all orbital numbers before the operation

[19] As $E = \hbar\omega$ and in atomic units $\hbar = 1$

This describes the probability of an electron in our system with energy ω to have a momentum k. This can be measured experimentally; if we consider illuminating a system with light of frequency ω, the spectral function is the probability that an electron will be emitted with momentum k[20], as illustrated in figure 2.10.

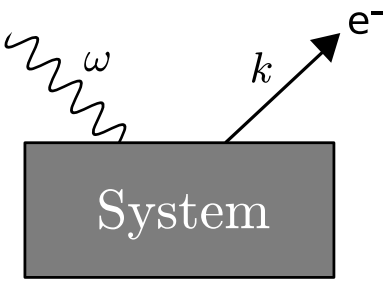

Figure 2.10: Illustration of the spectral function. $A(k,\omega)$ is the probability that, if light of frequency ω illuminated a system, an electron of momentum k is ejected from the system.

If we want to see the probability that *any* electron has an energy ω, we integrate over all possible momentum, and obtain the density of states

$$D(\omega) = \int_{\forall} A(k,\omega)dk. \tag{2.68}$$

This describes the probability that if we illuminate the system with light of frequency ω, an electron of any momentum is ejected from the system.

2.4.2 The self-energy

As in practice we do not know the many-body wavefunction Ψ, we next look at how to compute the interacting Green's function from the non-interacting Green's function. The non-interacting Green's function G_0 can be written in terms of the inverse of the single-particle Hamiltonian H_0:[21]

$$\begin{aligned} \left(H_0 - i\frac{\partial}{\partial t}\right) G_0 &= -I \\ \left(K_\mathrm{s} + V_\mathrm{ext} - i\frac{\partial}{\partial t}\right) G_0 &= -I \end{aligned} \tag{2.69}$$

We now define some new Hamiltonian H, that contains a potential Σ. This is defined in such a way that its inverse is the correct interacting Green's function:

$$\begin{aligned} \left(H - i\frac{\partial}{\partial t}\right) G &= -I \\ \left(K_\mathrm{s} + V_\mathrm{ext} + \Sigma - i\frac{\partial}{\partial t}\right) G &= -I. \end{aligned} \tag{2.70}$$

[20]This process is called photoemission and describes the case when $\omega > 0$. The case of $\omega < 0$ corresponds to inverse photoemission: light of frequency ω being emitted from the system due to an incident beam of electrons of momentum k.

[21]where K_s is the single-particle kinetic energy and I is the identity operator, here we are using fairly compact notation for simplicity.

Rearranging equations 2.69 and 2.70 we obtain the Dyson equation. In order to write it down in a compact from we introduce the following notation:

$$Q\left(x, x', t'-t\right) \rightarrow Q\left(12\right)$$
$$R\left(x, x', t'-t\right) = \int_{\forall} Q\left(x, x'', t''-t\right) P\left(x'', x', t'-t''\right) dx''dt'' \rightarrow$$
$$R\left(12\right) = \int Q\left(13\right) P\left(32\right) d3$$

In this more compact notation the Dyson equation is given by

$$G(12) = G_0(12) + \int G_0(13)\Sigma(34)G(42)d34 \tag{2.71}$$

The potential Σ is termed the self-energy of the system. It is the potential felt by an added electron or hole as it propagates through the system, where the system itself has changed in response to the presence of the added electron or hole. As well as being non-local in space, the exact self-energy is energy-dependent and hence non-Hermitian. It is this property that allows the model of our system to go beyond the single-particle picture. If a Hermitian (and so energy-independent) self-energy was used in equation 2.71, the resulting G would be able to be written in terms of single-particle orbitals. If the self-energy is energy-dependent (as the exact is) the resulting G *cannot* be written in terms of single-particle orbitals, hence accounting for the correlation of the electrons.

Equation 2.71 can be intuitively understood using a Feynman diagram:

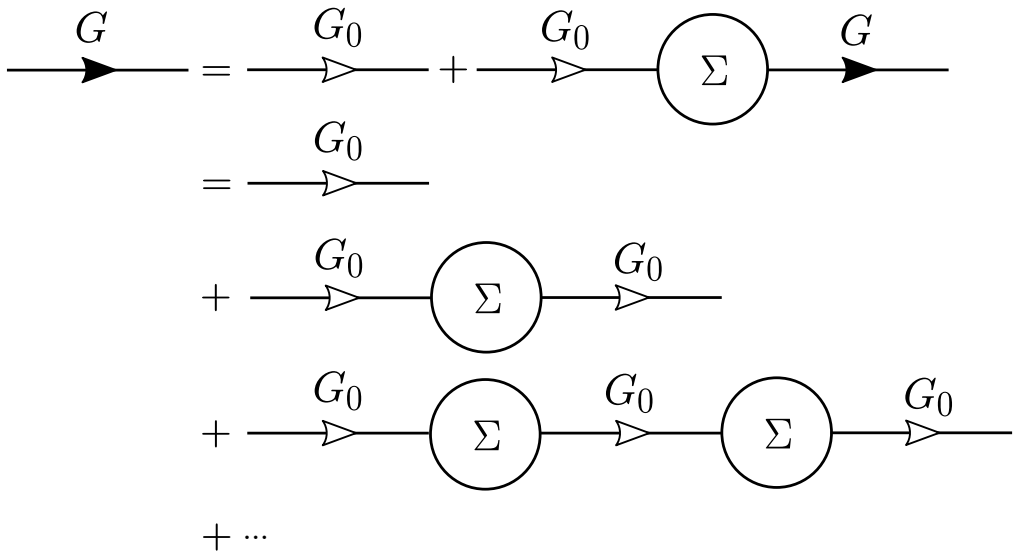

As shown, by substituting G recursively the equation becomes an infinite sum of scattering events. This describes the following: The probability amplitude of an added electron propagating from point 1 to 2 is the probability amplitude it propagates from 1 to 2 without interacting, plus the probability amplitude it propagates from point 1 to 2 where between points 3 to 4 it is scattered by the electrons in the system once, plus the probability amplitude it is scattered twice, and so on.

One example of an energy-independent self-energy is the Hartree-Fock case, whose

self energy is, in the time domain[22]:

$$\Sigma(12) = V_{\mathrm{H}}(1)\delta(12) + \Sigma_{\mathrm{x}}(12) \tag{2.72}$$

$$\Sigma(12) = \int v(13)G(33^{-})\delta(12)d3 + iG(12)v(12) \tag{2.73}$$

This can also be written as the following Feynman diagram [23]:

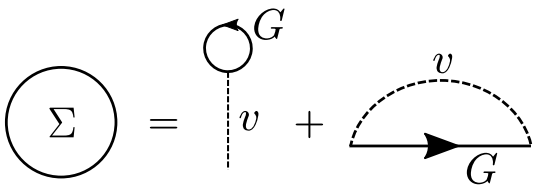

The physical interpretation of this is that the potential the added electron feels is the Hartree potential and exchange potential, but it does not cause the electrons to become excited out of their single-particle ground states. In the next section we will show how the exchange potential can be 'screened', in order to take account of the correlation of the electrons.

2.4.3 The screened Coulomb interaction

A fundamental quantity in the theory of screening is the polarizability of the system. This describes how easily the electrons become excited due to an external perturbation. When this excitation happens, an electron moves to a higher energy state, and leaves a hole behind, and this electron and hole then move through the system, and eventually recombine. Therefore, the polarizability of the system is defined by the probability amplitude of an added electron-hole pair from point 1 to point 2. Therefore, the larger the polarizability, the more easily electron-hold pairs can be created and move through the system. Hence this describes how readily the electrons become excited due to some external perturbation.

One of the simplest models of the polarizability is that the electron-hole pair do not interact. This approximation is called the 'Random Phase Approximation' (RPA) [40, 41, 42]. This is simply given by the probability amplitude of an electron propagating from point 1 to point 2, multiplied by the probability amplitude of an hole propagating from point 1 to point 2:

$$P(12) = -iG(12)G(21). \tag{2.74}$$

This can be illustrated using a Feynman diagram[24]:

[22] substituting the form of G (the form is actually of G_0 as this is within the single-particle picture) and $v(12) = U(x, x')\delta(t' - t)$ gives the formula for the Hartree-potential and exchange operator as shown in equations 2.47 and 2.50 respectively. Using our more condensed notation $\delta(12) = \delta(x_2 - x_1)\delta(t_2 - t_1)$.

[23] Note the diagram for the density, as $n(3) = G(33^{-})$

[24] It is conventional to draw the propagation of a hole as going in the opposite direction to an electron

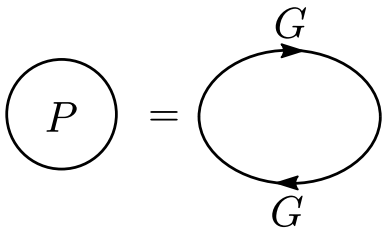

This illustrates an electron-hole pair propagating from point to point without interacting.

When we add an electron to a system, the electrons respond by repelling away from the added charge. The extent to which they can respond is directly determined by the polarizability. This gives rise to a screened Coulomb interaction, as felt by the added electron. The screened interaction W can be computed from the polarizability P via the Dyson like equation

$$W(12) = v(12) + \int v(13)P(34)W(42)d34, \tag{2.75}$$

as illustrated by the corresponding Feynman diagram:

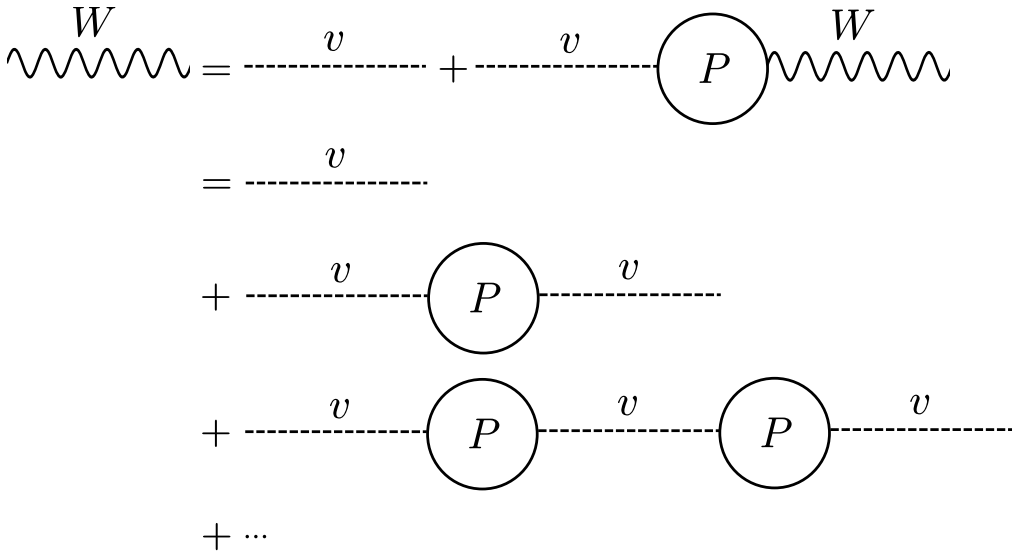

This describes that the interaction between points 1 and 2 is the bare Coulomb interaction v, plus a modification due to one electron-hole pair being created, plus a further modification due to two electron-hole pairs being created and so on.

This interaction is then used to screen the exchange interaction of the Hartree-Fock method, thus moving beyond the single-particle picture, approximately accounting for the correlation between the electrons:

$$\Sigma(12) = V_{\mathrm{H}}(1)\delta(12) + \Sigma_{\mathrm{xc}}(12) \tag{2.76}$$

$$\Sigma(12) = \int v(13)G(33^{-})\delta(12)d3 + iG(12)W(12) \tag{2.77}$$

This approximation to the self-energy is therefore called the 'GW' approximation, and is represented by the Feynman diagram:

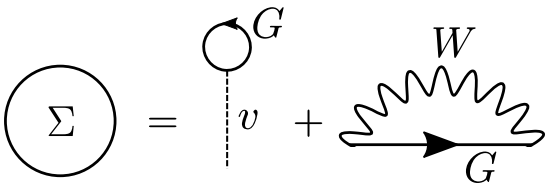

It is worth noting that the Hartree-Fock self-energy is recovered if the electrons are forced into their single-particle ground states by choosing $P = 0$.

The effect of moving beyond the single-particle picture on the spectral function is illustrated in figure 2.11.

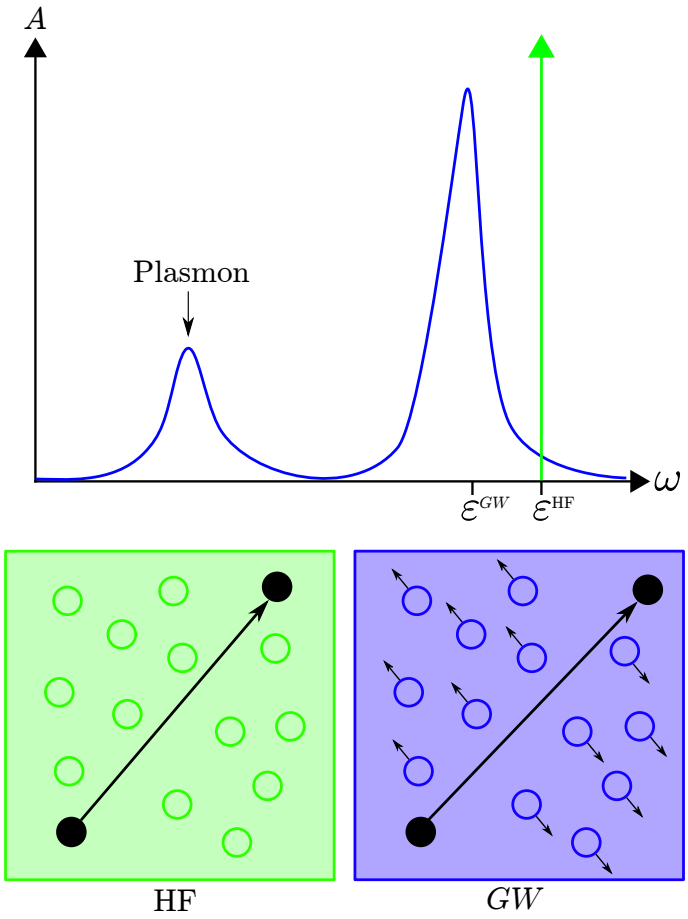

Figure 2.11: Illustration of the correlation described by the *GW* approximation. In the Hartree-Fock (HF) case (green), as an added electron propagates through the system, no electron-hole pairs are created (as $P = 0$) and hence the particles remain in their single-particle ground states. Therefore, the spectral function is simply a spike at the single particle energies, one such energy is shown here ($\varepsilon^{\mathrm{HF}}$). In contrast, in the *GW* case (blue), the electrons in the system screen the propagation of an added electron, as P is non-zero (approximated using the RPA). The effect this has on the spectral peak is to move the position of the peak, and for the peak to be broadened, which illustrates the non-single-particle nature of accounting for correlation (these broadened peaks are termed the quasi-particle peaks). In addition there is a satellite plasmon peak, which encapsulates the collective electron oscillations.

2.4.4 The *GW* equations

The Dyson equations for the Green's function and the screened interaction, the RPA model of polarizability, and the *GW* approximation to the self-energy form the set of self-consistent *GW* equations:

$$P(12) = -iG(12)G(21) \tag{2.78}$$

$$W(12) = v(12) + \int v(13)P(34)W(42)d34 \tag{2.79}$$

$$\Sigma(12) = V_{\mathrm{H}}(1)\delta(12) + iG(12)W(12) \tag{2.80}$$

$$G(12) = G_0(12) + \int G_0(13)\Sigma(34)G(42)d34 \tag{2.81}$$

These equations are solved self-consistently:

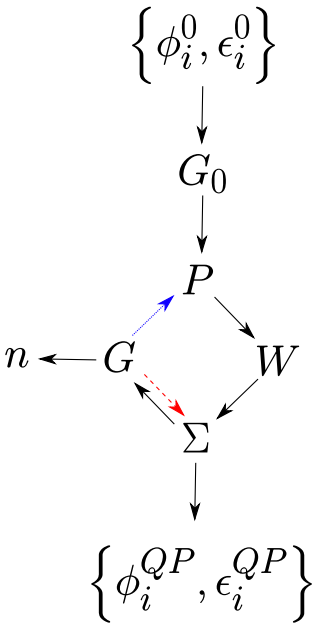

Figure 2.12: Flow-chart describing the *GW* method. The method begins with a set of non-interacting orbitals, from this the description of the propagation of an added electron or hole G_0 is constructed. From this we can then compute the propagation of an added electron-hole pair P. This can then be used to compute how the bare Coulomb interaction is screened, yielding W. This is then used to construct the energy-dependent potential Σ, that a added electron would feel as it propagates through the system. This potential is then used to compute the interacting Green's function G. This process is repeated until self-consistency is reached (blue arrow). The ground-state density and quasi-particle orbitals are then computed from G and Σ respectively. An alternative approach is to only compute G and Σ self-consistently (red arrow, termed the GW_0 or semi-self consistent method), or to simply perform only one-iteration, from some reasonably starting orbitals (black arrows only, termed the G_0W_0 or one-shot method).

When describing the single-particle excitation properties of a system, the *GW* method is the most common method of choice, but it is not exact as it neglects terms to the polarizability and self-energy. The computation of the exact quantities requires 'vertex corrections'.

2.4.5 Hedin's equations and vertex corrections

The *GW* equations are an approximate case of Hedin's equations [13], the solution of which yields the exact ground-state and single-particle excitation properties:

$$P(12) = -i \int G(13)G(41)\Gamma(342)d34 \tag{2.82}$$

$$W(12) = v(12) + \int v(13)P(34)W(42)d34 \tag{2.83}$$

$$\Sigma(12) = V_{\mathrm{H}}(1)\delta(12) + i \int G(13)W(14)\Gamma(342)d34 \tag{2.84}$$

$$G(12) = G_0(12) + \int G_0(13)\Sigma(34)G(42)d34 \tag{2.85}$$

$$\Gamma(123) = \delta(12)\delta(13) + \int \frac{\delta\Sigma(24)}{\delta G(16)} G(45)G(76)\Gamma(573)d4567 \tag{2.86}$$

Where the equations for the polarizability and self-energy now contain the vertex function Γ. Solving these equations in practice is totally intractable, which is why approximations must be made. The *GW* approximation is recovered from these equations using

$$\frac{\delta\Sigma}{\delta G} = 0 \tag{2.87}$$

It is however useful to consider the diagrams beyond the *GW* approximation, as in some case these help illustrate what physical phenomena are neglected. For example some of the terms of the exact polarizability are given by the diagrams:

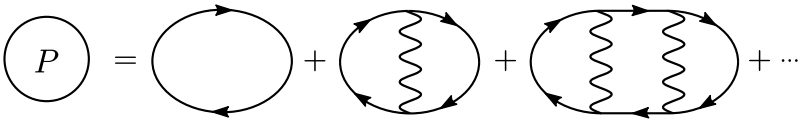

This adds in some of the electron-hole interaction neglected by the RPA, as the pair now interact by the static screened Coulomb interaction. An expansion of this type can be obtained using

$$\frac{\delta\Sigma}{\delta G} = iW \tag{2.88}$$

and is called the Bethe-Salpeter equation [43], which is a common type of beyond-*GW* many-body perturbation theory, often used to compute optical absorption properties. Some of the diagrams of the exact self energy are:

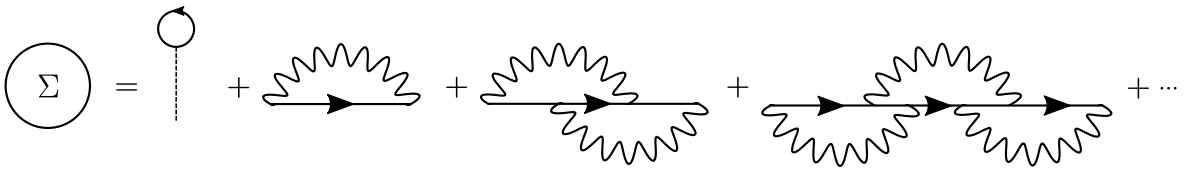

These terms beyond the Hartree and screened exchange describe the self-interaction correction to the *GW* method [44]. Neglecting such terms gives rise to the *GW* approximation exhibiting the *self-screening* error [22]. In chapter 5 we investigate this error in detail along with proposing a correction.

2.5 Density functional theory

2.5.1 The Hohenberg-Kohn theorem

We now introduce density functional theory (DFT), which is a method to compute the ground-state properties of a system of interacting electrons. This approach is in principle exact, although approximations must be made if it is to be applied to large-scale systems. The key property of this method is that it does not focus on the wavefunction or Green's function as in the previous methods, but instead on the ground-state density

$$n(x) = Ne\rho(x), \tag{2.89}$$

whose integral is the total charge between points A and B in system

$$Q\left(A,B\right) = \int_{A}^{B} n\left(x\right) dx. \tag{2.90}$$

Where $\rho(x)$ is the electron probability density:

$$\rho(x) = \int_{\forall} \cdots \int_{\forall} |\Psi(x, x_2, \ldots, x_N)|^2 dx_2 \ldots dx_n. \tag{2.91}$$

The Hohenberg-Kohn theorem [29] states that for a given Hamiltonian the external potential is, up to an additive constant, a unique functional of the electron density. Hohenberg and Kohn proved that the total energy of the system can be written as a functional of the ground-state density[25]:

$$E\left[n\right] \tag{2.92}$$

The value of E obtained from equation 2.92 for a guessed density n' will always be greater that the true ground state energy E_0, therefore n_0 and E_0 can be obtained by minimizing the functional

$$\delta E\left[n\right] = 0. \tag{2.93}$$

The total Hamiltonian can be split into three parts

$$E\left[n\right] = K\left[n\right] + v_{\text{external}}\left[n\right] + U\left[n\right] \tag{2.94}$$

The form of the external potential function is known to be:

$$v_{\text{ext}}\left[n\right] = \int V_{\text{external}}\left(x\right) n\left(x\right) dx \tag{2.95}$$

So E can be written in terms of the universal functional $F = K + U$ and the known functional:

$$E\left[n\right] = F\left[n\right] + \int V_{\text{external}}\left(x\right) n\left(x\right) dx \tag{2.96}$$

In principle, inserting the exact ground-state density into this functional will yield the exact ground-state energy. The most common approach to determining this density is the Kohn-Sham approach.

[25] from here on in we use density to mean charge density, not probability density unless otherwise stated.

2.5.2 The Kohn-Sham ansatz

The Kohn-Sham approach to DFT [45] considers a fictitious system of non-interacting electrons whose ground-state density is exactly the same as the many-body system. This fictitious system is defined by a new external potential, termed the Kohn-Sham potential V_{KS}. This is illustrated in figure 2.13.

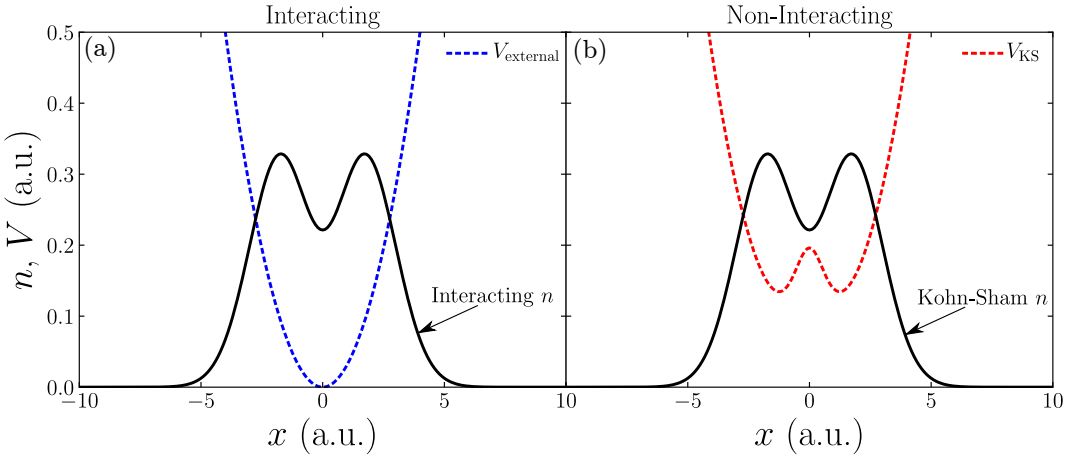

Figure 2.13: Illustration of the Kohn-Sham concept. We consider a system of two electrons in a model 1-dimensional quantum harmonic oscillator. In panel (a) we show the external potential of the system V_{external}. We then solve the many-body Schrödinger equation for this system to obtain the interacting ground-state density. This density shows each electron is pushed away from the center of the system due to the Coulomb repulsion. In panel (b) we show the corresponding Kohn-Sham system. The exact Kohn-Sham potential V_{KS} is the potential that represents the fictitious system of non-interacting electrons, that yields exactly the same density as the real interacting system. In this case the exact Kohn-Sham potential contains a central bump, that accounts for the effect of the electron repulsion present in the real system.

This Kohn-Sham potential is often split into three distinct parts:

$$V_{\mathrm{KS}}(x) = V_{\mathrm{ext}}(x) + V_{\mathrm{H}}(x) + V_{\mathrm{xc}}(x) \tag{2.97}$$

$V_{\mathrm{ext}}(x)$ is the external potential of the real system, and $V_{\mathrm{H}}(x)$ is the previously defined Hartree potential. $V_{\mathrm{xc}}(x)$ is the Kohn-Sham exchange-correlation potential, which is the potential that allows the fictitious Kohn-Sham system to reproduce the same density as the real system, despite the fact that exchange and correlation are neglected in this single-particle picture. This potential, along with the Hartree potential, are functionals of the density, and therefore so is the Kohn-Sham Hamiltonian:

$$H_{\mathrm{KS}}[n] = K_s + V_{\mathrm{KS}}[n]. \tag{2.98}$$

If one has the exact exchange-correlation functional, the Kohn-Sham equations can be solved self-consistently. Firstly, a guess is made for the single-particle orbitals $\{\phi_i\}$ and thus the charge density n. This allows us to compute $V_{\mathrm{KS}}[n]$ and hence $H_{\mathrm{KS}}[n]$ using equations 2.97 and 2.98. Then we solve for the Hamiltonian's eigenstates to give a new set of orbitals. This is then repeated until convergence is reached. In practice though, the exact exchange correlation functional is not known, and must be approximated. The power of DFT lies in the fact that the exchange-correlation potential is small compared to the whole Kohn-Sham potential, therefore relatively crude approximations can yield surprisingly accurate results.

2.5.3 The local density approximation

If approximations can be made to the exchange-correlation potential, the Kohn-Sham potential can be approximated, and DFT can be applied to physical systems. One such approximation is the local density approximation (LDA), where the functional only depends locally on the density, that is, the exchange-correlation potential at point x only depends on the density at point x. The LDA exchange-correlation energy is given by

$$E_{\mathrm{xc}}^{\mathrm{LDA}}[n] = \int \varepsilon_{\mathrm{xc}}(n)\, n(x)\, dx, \tag{2.99}$$

where $\varepsilon_{\mathrm{xc}}(n)$ is the exchange-correlation energy per electron of the homogeneous electron gas. This functional can be used to construct the LDA exchange-correlation potential:

$$V_{\mathrm{xc}}^{\mathrm{LDA}}[n](x) = \frac{\delta E_{\mathrm{xc}}^{\mathrm{LDA}}}{\delta n} \tag{2.100}$$

Figure 2.14 illustrates the LDA applied to our model system of figure 2.13. This fictitious system of non-interacting electrons only *approximately* reproduces the density of the interaction system, although surprisingly accurate given its simplicity.

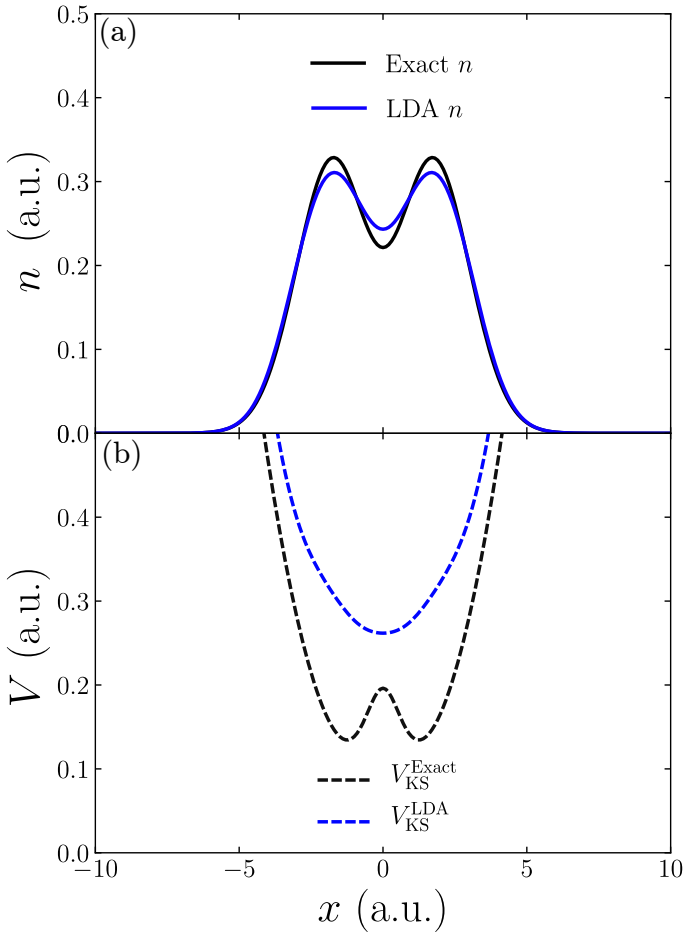

Figure 2.14: Here we show the performance of the LDA for the model system presented in figure 2.13. As shown in panel (a) the LDA yields a reasonably accurate density for this system. Panel (b) shows the corresponding Kohn-Sham potentials.

2.5.4 Time-dependent density functional theory

The Runge-Gross theorem [35] extends density functional theory to the case where the system is now driven out of its ground-state with a perturbation $V_{\text{ptrb}}(x)$. It proves that there is a one-to-one mapping between the time-dependent external potential and the time-dependent electron density up to an additive constant. As in the ground-state case we can invoke the Kohn-Sham Ansatz, and consider a time-dependent fictitious system of non-interacting electrons, that has exactly the same time-dependent density as the real system.

We can then define this time-dependent fictitious system by the time-dependent Kohn-Sham potential:

$$V_{\text{KS}}(x,t) = V_{\text{ext}}(x) + V_{\text{ptrb}}(x,t) + V_{\text{H}}(x,t) + V_{\text{xc}}(x,t), \tag{2.101}$$

where now the exchange-correlation potential is a functional of the density at the current time, and all previous times. It is for this reason the exact time-dependent exchange-correlation potential is said to contain 'memory effects'. This potential can then be used to determine the time-dependent density when inserted into the single-particle time-dependent Schrödinger equation. As in the ground-state case, this is in principle exact, but approximations must be made to the exchange-correlation term. In the time-dependent case, crude approximations such as the LDA perform very poorly [12].

Chapter 3

The interacting Dynamic Electrons Approach (iDEA)

3.1 Overview

The purpose of the iDEA (interacting Dynamic Electrons Approach) code is to test existing, and develop novel methods of solving the many interacting electron problem [46].

It is concerned with simple finite model systems for which the many-electron Shrödinger equation can be solved exactly, both for ground-state and time-dependent cases. We can therefore compute the exact many-electron wavefunction and from this, many properties of the system, such as charge density, ionization potential, electron affinity, quasiparticle gaps, total energies and Kohn-Sham potentials. In order for this to be computationally tractable we work with small 1-dimensional model systems containing a small number of electrons (1,2 or 3), whose properties can be determined exactly by performing an exact numerical solution to the Schrödinger equation on a real-space real-time grid. We model our systems to reproduce as closely as possible the physical effects that occur in real molecules and molecular junctions; such as atoms, unbonded and bonded atom pairs, and strongly bound electrons. We often choose the electrons to have like-spin[1] (unless otherwise stated) in order to more closely approach the exchange and correlation effects in large-scale systems for a given computational effort. As the systems are 1-dimensional, we use a softening parameter of 1.0 in the Coulomb interaction unless otherwise stated. This ensures we as closely possible reproduce the interaction of two charged disks in a nano-wire [46].

As well as the exact solution, iDEA also contains many implementations of commonly used approximate approaches. These include Kohn-Sham density functional theory (KS-DFT) approaches such as purely non-interacting electrons, the Local Density Approximation (LDA) [47] and the time-dependent adiabatic LDA. For this work, additional modules of iDEA were developed; in particular, many forms of many-body perturbation theory (MBPT) [28], such as the Hartree and Hartree-Fock methods, and many flavors of the GW approximation including; G_0W_0, GW_0, fully-self-consistent GW, as well as static forms such as COHSEX (these flavors are described in detail in chapter 4). This allows us to compute approximate densities and

[1] Achieved by enforcing the spatial part of the wavefuntion to be exchange-antisymmetric.

quasi-particle energies, as well as Green's functions and self-energies.

The goal of the iDEA approach is to compare various approximate methods against the exact case for these characteristic model systems and determine where, and for what reason, common approaches fail. This then allows us to investigate such failings in detail as all of the key quantities are explicitly available. From this we can formulate corrections and novel methods that yield more accurate results. The hope is that these improved methods can then be used in large-scale codes and thus improve the models, predictions and understanding of real molecules and molecular junctions.

3.2 Implementation

3.2.1 Exact solution

We first introduce the exact many-body module. This is used to compute the exact wavefunction, total energy and charge density of a ground-state system, as well as evolving charge and current densities for time-dependent systems. The process begins by finding the ground-state of a system by means of the Crank-Nicholson propagation [48] through imaginary-time.

The Crank-Nicholson method is used to propagate a given state of a system in time by representing the time-dependent Schrödinger equation as a set of linear equations. If we begin with the time-dependent form of an arbitrary wavefunction written in terms of the eigenfunctions of the many-body Hamiltonian ϕ_n:

$$\Psi(x,t) = \sum_n e^{-iE_n t} c_n \phi_n, \tag{3.1}$$

and then we move to imaginary-time via the substitution $\tau = it$

$$\Psi(x,\tau) = \sum_n e^{-E_n \tau} c_n \phi_n, \tag{3.2}$$

we can see that as we evolve over imaginary-time, the terms of the wavefunction exponentially decay with the energy of the associated eigenfunction. So as $\tau \to \infty$ the contributions from higher energy states will decay fastest. As long we keep renormalising the wavefunction at each time-step, any initial arbitrary antisymmetric wavefunction will tend to the system's ground state. Once this ground-state has been determined, a perturbing potential is applied to the system to cause the charge density to evolve with time. The time evolution is also computed using the Crank-Nicholson method, but now in the real time-domain. From this we can compute any required time-dependent property of the system.

3.2.2 Reverse-engineering

The purpose of the reverse engineering module is to determine the exact ground-state Kohn-Sham potential that corresponds to given charge density, as computed from the exact many-body module[2]. To obtain the ground state Kohn-Sham potential we begin with a guess (usually the external potential), and from this solve the single-particle Shrödinger to obtain a set of orbitals and a ground-state charge density n_{KS}. From this we update our guess of the Kohn-Sham potential using the difference in our Kohn-Sham density and the target density $n(x)$

$$V_{\mathrm{KS}} \to V_{\mathrm{KS}} + \mu \left(n_{\mathrm{KS}}(x)^p - n(x)^p \right). \tag{3.3}$$

Where μ is a stability parameter usually chosen to be 0.01, and the value of p is chosen to be 0.05 to focus the algorithm on the important low-density regions.

[2]This algorithm is also capable of finding the corresponding Kohn-Sham potential of *any* given density, such as that from MBPT approaches.

3.2.3 Non-interacting electrons

The non-interacting module is used to compute the charge density via the simplest possible approximation - the total neglect of the Coulomb interaction. This can be treated as an approximation to the KS-DFT Hartree exchange-correlation potential

$$V_{\mathrm{Hxc}}\left(x\right) = 0, \tag{3.4}$$

this ensures that the electrons are truly non-interacting:

$$V_{\mathrm{KS}}\left(x\right) = V_{\mathrm{external}}\left(x\right) + V_{\mathrm{Hxc}}\left(x\right) = V_{\mathrm{external}}\left(x\right). \tag{3.5}$$

While this approximation is very trivial in the framework of DFT, it is nevertheless a good reference approximation to ensure interaction is having a significant effect on the density for a given system. Although, this approximation does contain no self-interaction and so, in some special cases may perform better than Hartree theory. The charge density is then computed from the resulting N occupied orbitals

$$n\left(x\right) = \sum_{n=1}^{N} |\phi_n\left(x\right)|^2. \tag{3.6}$$

Where ϕ_n are calculated by diagonalising the non-interacting Hamiltonian of the system. To calculate the time-dependent current density, each of the orbitals is evolved separately in time using the time-dependent single-particle Schrödinger equation.

3.2.4 The local-density approximation

Next we present the LDA module. This is an implementation of the self-consistent KS equations using the LDA exchange-correlation functional. There are several variations of the functional available; those fitted from a series of one, two and three electron 1-dimensional density slabs[3], or via the usual Monte-Carlo calculations of the 3-dimensional homogeneous electron gas. We compute the LDA exchange-correlation potential from these exchange correlation functionals using

$$V_{\mathrm{xc}}^{\mathrm{LDA}}[n]\left(x\right) = \frac{\delta E_{\mathrm{xc}}^{\mathrm{LDA}}}{\delta n}. \tag{3.7}$$

This gives the LDA KS potential to be

$$V_{\mathrm{KS}}\left(x\right) = V_{\mathrm{external}}\left(x\right) + V_{\mathrm{H}}\left(x\right) + V_{\mathrm{xc}}^{\mathrm{LDA}}\left(x\right). \tag{3.8}$$

We use the following algorithm to solve the self-consistent Kohn-Sham equations:

[3]Described in detail in reference [47]

Algorithm 1 Self-consistent density functional theory with the Local Density Approximation

1: Start with an initial guess of V_{KS} (usually V_{external})
2: Solve the KS equations for the ground-state density n
3: Compute $V_{\text{H}}[n](x)$ and $V_{\text{xc}}[n](x)$ for this density
4: Compute the full V_{KS} using equation 3.8
5: Use linear stability mixing to update the KS potential: $V_{\text{KS}} = \alpha V_{\text{KS}}^{new} + (1 - \alpha)V_{\text{KS}}^{old}$. For optimal stability we choose $\alpha = 0.2$.
6: Repeat from step 2 until self-consistency with respect to the density is reached

3.2.5 The Hartree-Fock approximation

The next module we present is the Hartree-Fock (HF) module. This allows us to investigate the performance of one of the most widely used and simplest levels of MBPT, along with being an invaluable tool to quantitatively deduce the level of correlation in a given system. We solve the HF equations using the following self-consistent method:

Algorithm 2 Self-consistent Hartree-Fock

1: Start with an initial guess of the orbitals (usually the purely non-interacting orbitals of the external potential)
2: Construct the Hartree and exchange potentials
3: Use linear stability mixing to update the Hamiltonian: $H_{\text{HF}} = \alpha H_{\text{HF}}^{\text{new}} + (1 - \alpha)H_{\text{HF}}^{\text{old}}$. For optimal stability we choose $\alpha = 0.9$.
4: Diagonalise the HF Hamiltonian for an updated set of orbitals
5: Repeat from step 2 until self-consistency is reached

Along with the HF charge density total energy and quasiparticle energies, we can also explicitly observe the non-local exchange operator on our spatial grid.

3.2.6 The *GW* approximation

For this work we also created the Many-Body Perturbation theory module. This has the ability to solve the *GW* equations with various levels of self-consistency, starting orbitals and various approximations to the self-energy and polarizability. The module is used to compute the ground-state charge density of a given system, along with the quasi-particle energies, Green's functions, self-energies etc.

We implement the space-time method [49] to solve the self-consistent *GW* equations. The first step is to construct the non-interacting Green's function G_0 from a given set of single-particle orbital and energies[4]. In the space-time method this is constructed in the imaginary time-domain ($i\tau = t' - t$) as this allows the Green's function to be stored on an finite imaginary-time grid, as G_0 will decay instead of oscillate.

$$G_0\left(x, x', i\tau\right) = \begin{cases} i\sum_n^{\text{occ}} \phi_n(x)\phi_n^*(x')e^{-\varepsilon_n\tau} & \tau \leq 0 \\ -i\sum_n^{\text{unocc}} \phi_n\left(x\right)\phi_n^*(x')e^{-\varepsilon_n\tau} & \tau > 0 \end{cases} \tag{3.9}$$

[4]this determines the starting point of the calculation; we usually pick LDA or HF orbitals. The energies are defined on a scale that places the chemical potential at zero.

The imaginary part[5] of the non-interacting Green's function for a two-electron quantum harmonic oscillator (QHO) (from purely non-interacting orbitals) at imaginary time $i\tau = 0$ is shown in figure 3.1.

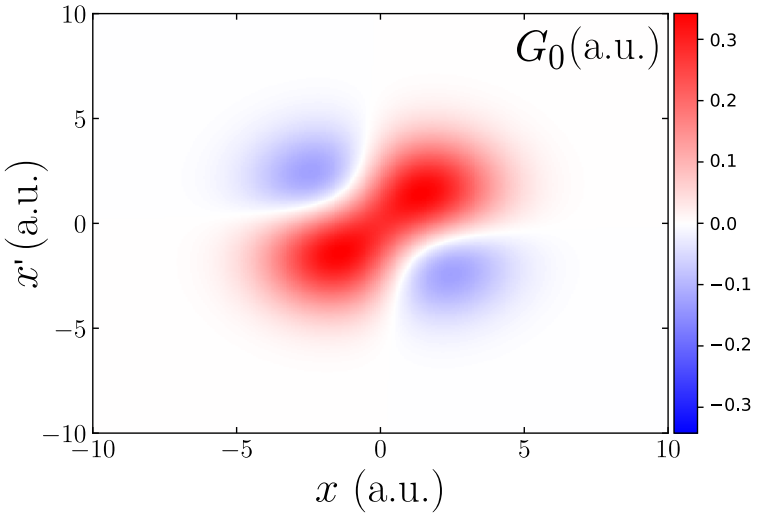

Figure 3.1: Imaginary part of the non-interacting Green's function at $i\tau = 0$ for the two-electron QHO ($\omega = 0.25$) constructed from purely non-interacting orbitals.

The initial guess for the interacting Green's function G is then taken to be this non-interacting Green's function.

The next stage is to construct the polarizablity P. In the imaginary time-domain this is constructed using the expression

$$P\left(x, x', i\tau\right) = -iG\left(x, x', i\tau\right) G\left(x', x, -i\tau\right) \tag{3.10}$$

$$P\left(x, x', 0\right) = -iG\left(x, x', 0\right) G^{ALT}\left(x', x, 0\right). \tag{3.11}$$

Where G^{ALT} is an alternative Green's function that treats $\tau = 0$ as an electron addition, rather than a hole addition, as is in the standard definition. Figure 3.2 shows the probability density of finding an electron-hole pair added to our illustrative QHO system at $x = 0$, an infinitesimal time after it was added.

[5]the real part is zero by definition, as in iDEA all the single-particle orbitals are chosen to be entirely real. This is possible as it is in one-dimension.

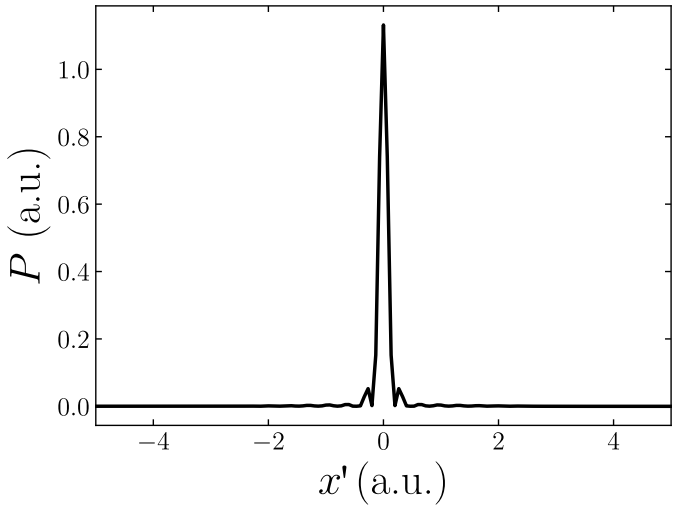

Figure 3.2: Probability density of finding an electron-hole pair added to the two-electron QHO at $x = 0$, an infinitesimal time after it was added. Computed from the imaginary part of $P(x = 0, x', i\tau = 0)$. Note the small amount of propagation through the system, which is due to the added pair having to obey the Pauli exclusion principle at the moment of addition.

Next, we construct the screened Coulomb interaction. From the *GW* equations we can see that W is written as a convolution in the imaginary time-domain, so if we appropriately Fourier transform the quantities into the imaginary frequency-domain we can write out the Dyson equation for W as a matrix equation [6]

$$W(i\omega) = v + vP(i\omega)W(i\omega), \tag{3.12}$$

which can be rearranged for the screened coulomb interaction[7]:

$$W(i\omega) = (I - vP(i\omega))^{-1} v. \tag{3.13}$$

This is then Fourier transformed back into the imaginary time-domain. We show the screened Coulomb interaction W in comparison to the bare Coulomb interaction v for the QHO system in figure 3.3. We show the interaction felt by a test charge at points $x = 0$ (panel (a)) and $x = 3.5$ (panel (b)). Note that the interaction is reduced in strength at short range, and increased at long range. This is due to the electrons in the system moving out of the vicinity of the test charge.

[6] Where $W(x, x', i\omega)$ is stored on a 2D spatial grid and 1D imaginary energy grid.
[7] Where I is the identity matrix.

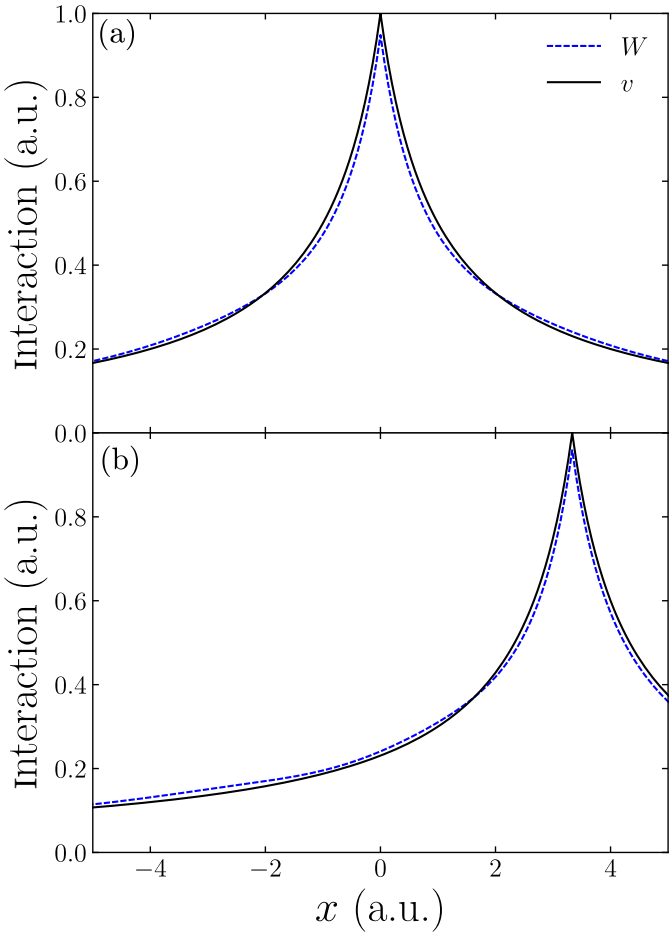

Figure 3.3: The screened Coulomb interaction W as felt by a test charge at points $x = 0$ (a) and $x = 3.5$ (b) in comparison to the bare Coulomb interaction v for the QHO.

Next, we construct the self-energy Σ in the imaginary time-domain. The exchange correlation term is simply given by

$$\Sigma_{xc}\left(x, x', i\tau\right) = iG\left(x, x', i\tau\right) W\left(x, x', i\tau\right). \tag{3.14}$$

This is then Fourier transformed back into imaginary frequency-domain. The exchange correlation self-energy for the QHO system is shown in figure 3.4.

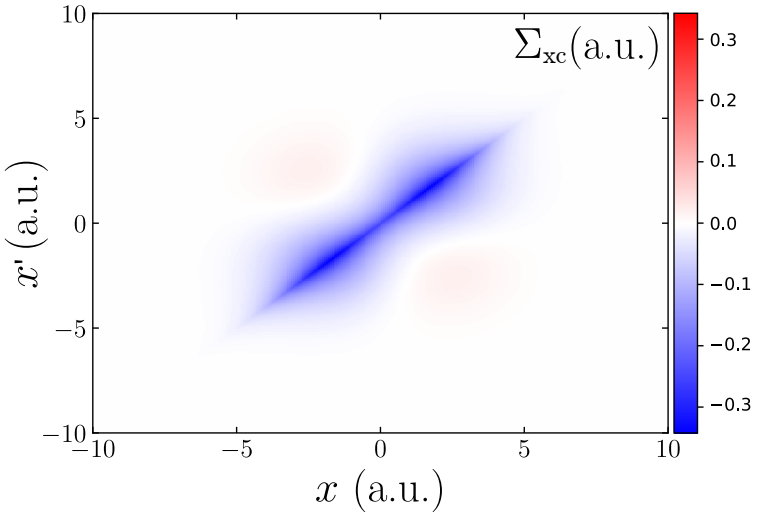

Figure 3.4: The exchange correlation part of the *GW* self-energy for the QHO system at $i\omega = 0$.

The Hartree term is then included by adding the Hartree potential along the diagonal of Σ. If we begin our calculation from a set of starting orbitals that are *not* purely non-interacting, in order to ensure we are not double-counting diagrams, we must also subtract the associated V_{Hxc}.

The final stage of an iteration is to update G using the current self-energy Σ using the Dyson equation for the Green's function in the imaginary frequency-domain:

$$G\left(i\omega\right) = G_0\left(i\omega\right) + G_0\left(i\omega\right)\Sigma\left(i\omega\right)G\left(i\omega\right). \tag{3.15}$$

Which can be rearranged for the interacting Green's function:

$$G\left(i\omega\right) = \left(I - G_0\left(i\omega\right)\Sigma\left(i\omega\right)\right)^{-1} G_0\left(i\omega\right) \tag{3.16}$$

As the chemical potentials of the input and output Green's function are different, we must shift our energy grid in order to ensure the number of electrons remains conserved. To do this the self-energy must be appropriately shifted in the imaginary frequency-domain, we term this the 'Hedin Shift'. This is implemented by adding the expectation value of the real part of the self-energy at the chemical potential to Σ in the imaginary frequency-domain:

$$\Sigma\left(i\omega\right) \rightarrow \Sigma\left(i\omega\right) - I\frac{\langle\phi_L|\Sigma\left(i\omega=0\right)|\phi_L\rangle + \langle\phi_H|\Sigma\left(i\omega=0\right)|\phi_H\rangle}{2}. \tag{3.17}$$

Where ϕ_H and ϕ_L are the HOMO and LUMO states respectively. We monitor the particle number at each iteration to ensure the effectiveness of this shift.

Once G is updated we can extract the charge density $n(x) = -iG(x,x,i\tau=0)$. Depending on the level of self-consistency required, we repeat the cycle until convergence is reached at the level of the density. We then output the density, quasiparticle energies as well as the quantities G,P,W and Σ.

3.3 A physical example: The covalent bond

We will now illustrate the exact many-body module of iDEA for a relevant physical example: a model covalent bond. We consider two 1-dimensional model hydrogen atoms separated by a distance d. This external potential is shown in figure 3.5

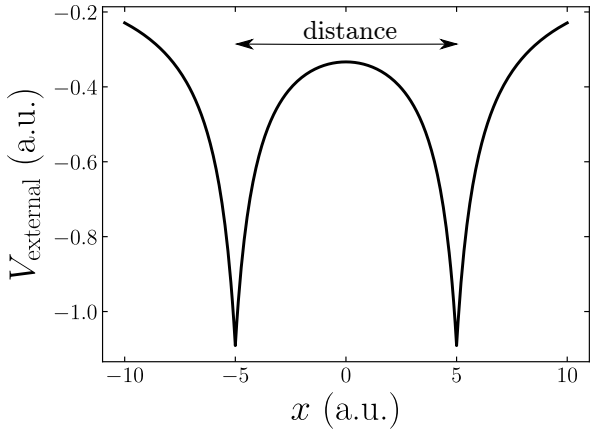

Figure 3.5: The external potential representing two 1-dimensional model hydrogen atoms separated by a distance d.

We employ the exact many-body module of iDEA to determine the total electron energy, we then add on the proton energy to yield the total energy for a given distance d. We then repeat this for a range of distances from 0 a.u to 8 a.u. We find the characteristic unbonded (when using like-spin), and bonding energy curve (when using opposite-spin) . These are shown in figure 3.6.

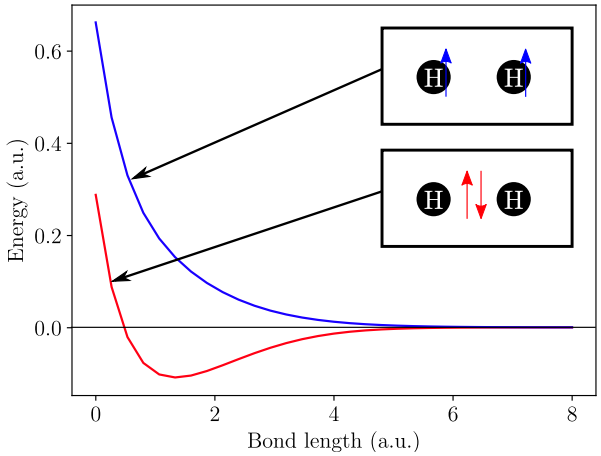

Figure 3.6: The total energy vs distance curves for our system containing two model hydrogen atoms. The blue curve shows the result when we treat the electrons as like-spin and as is expected no bond forms. The red curve shows the corresponding result for when the electrons are treated as having opposite-spin. We see the usual bonding curve characteristic of a covalent bond.

This is only one example of a large number of characteristic systems we model in iDEA, as we are free to choose any external potential to generate a model system that exhibits the required physical phenomena.

Chapter 4

Densities from existing and novel flavors of the *GW* approximation

Even though many-body perturbation theory (MBPT) is a popular method for calculating the properties of many-electron systems, little is known regarding the accuracy of the ground-state electron density obtained. In this chapter we assess the accuracy of the electron density and quasi-particle (QP) energies obtained via various flavors of the *GW* approximation. We vary the level of approximation used in both the self-energy and the polarizability. We also introduce a novel approximation to the polarizability, termed 'inertial screening'. Our approximation is most appropriate for our model systems with appreciable correlation; we find it yields more accurate electron densities compared against the standard dynamic and static screening methods within *GW* for all systems studied. Furthermore, the inertial screening approximation also yields accurate QP energies. Within the dynamic approximation to the polarizability, we find that one-shot methods are most appropriate, particularly when Hartree-Fock orbitals are employed as a starting point. We find that the densities and ionization potentials are adversely effected by the self-screening error, caused by neglect of vertex terms in the self-energy. We also show that the Kohn-Sham (KS) potentials, which correspond to our densities obtained via MBPT, capture aspects of the exact KS potential provided the level of approximation within *GW* is appropriate.

4.1 Introduction

In chapter 2 we showed how MBPT describes the response of a system to the addition or removal of electrons (or holes). For large scale systems it is most often used to compute exited-state properties of materials, such as optical absorption [50, 51], photoemission and inverse-photoemission spectra [52] and single-particle addition and removal energies [21]. While the exact one-body excitation properties of the system are in principle obtained by iteratively solving Hedin's equations [13, 14], in practice approximations must be made. One of the most common approximations used in practical calculations is the *GW* approximation. This approximation can be implemented in several ways (or flavours) by either controlling the level of self-consistency, i.e., solving Hedin's equation and updating Σ only once (termed one-shot or G_0W_0), or from one's choice of approximation to the polarizability, P. The most common flavour is a one-shot calculation with a single-particle starting point, such as a Kohn-Sham (KS) density-functional calculation within the local density approximation (LDA) [14].

The G_0W_0 approximation generally improves upon the band gap and all other single-particle energies from a density-functional calculation [19, 20], due to a cancellation of errors between the absent vertex corrections and the lack of self-consistency in the calculation [22]. In contrast, fully self-consistent *GW* (referred to as *GW*) has been found to overestimate the band gap [50], owing to the need for vertex corrections in a self-consistent calculation [22].

The accuracy of the *GW* ground-state electron density is not well known, in contrast to density functional theory (DFT) or the Hartree-Fock (HF) method. In principle, an exact solution of Hedin's equation yields an exact electron density. However, it is not understood what effect neglecting the vertex corrections has on the density, which flavor of *GW* gives the most accurate density, or, if necessary, what corrections to Σ are needed to obtain an accurate density from MBPT.

In this chapter we investigate the performance of MBPT for a set of one-dimensional model systems for which we can exactly solve the many-electron Schrödinger equation and therefore have access to the exact many-electron, fully-correlated wavefunction and thus the exact electron density. We choose our electrons for this investigation to be like-spin to more closely approach the exchange and correlation effects present in large scale systems. We compare the performance of various flavors of *GW* across several levels of approximation. We also 'reverse engineer' each electron density, using our reverse-engineering algorithm, to find the corresponding local effective KS potential. As we have access to the exact density, we can compute the exact KS potential and compare it to the KS potential obtained from MBPT. From our investigation, we gain a deeper insight into the strengths/failings of the *GW* approximation.

4.2 Flavors of the *GW* approximation

As shown in Chapter 2, the Dyson equation for G describes all of the ground-state properties as well as the one-body[1] charged excitations:

$$G = G_0 + G_0 \Sigma G, \tag{4.1}$$

where G_0 is the initial non-interacting Green's function constructed from a set of single-particle starting orbitals. The self-energy is given by $\Sigma = V_{\mathrm{H}} + iGW\Gamma$, where V_{H} is the Hartree potential and $\Gamma = I + \frac{\delta\Sigma}{\delta G} GG\Gamma$. The screened Coulomb interaction is expressed as $W = v + vPW$, where $P = -iGG\Gamma$. Within the GW approximation, $\frac{\delta\Sigma}{\delta G} = 0$ and thus the self-energy is given by $\Sigma = V_{\mathrm{H}} + iGW$. In this case the polarizability $P = -iGG$ – this is known as the random phase approximation (RPA) [40, 41, 42]. Together these approximations to Σ and P, and Eq. (4.1), are termed the GW equations.

These two approximations introduce systematic error into the method. Firstly, the RPA neglects the electron-hole interaction between the excited electron-hole pairs in the polarizability. This usually causes the GW approximation to perform poorly for optical properties [51]. In principle, this error can be removed by vertex corrections, such as the Bethe-Salpeter equation [43, 53]. Secondly, the GW approximation to the self-energy neglects the self-interaction correction, and gives rise to the self-screening error [25, 22], which is discussed in detail in Chapter 5. It is largely unknown what effect the neglect of vertex corrections has on the density.

The one-shot solution of the GW equations means that the exchange-correlation (xc) component of the self-energy can be written in terms of a non-interacting Green's function G_0, as such

$$\Sigma_{\mathrm{xc}} = iG_0W_0. \tag{4.2}$$

The screened interaction W_0 is computed from G_0. This is the self-energy felt by an electron or hole added to a system of non-interacting electrons, usually in some effective potential. As a result, G_0W_0 depends on the starting orbitals that describe the non-interacting system. In this work we use the single-particle orbitals from a density-functional calculation employing the LDA[2] (G_0W_0@LDA) and the orbitals from a HF calculation (G_0W_0@HF). These one-shot methods are usually the preferred way of performing GW calculations due to their relatively low computational cost. We also perform fully self-consistent GW calculations. In this case the xc self-energy is given by

$$\Sigma_{\mathrm{xc}} = iGW. \tag{4.3}$$

As the GW equations are solved self-consistently, the fully interacting G and W are updated at each iteration of the self-consistent procedure, hence this approximation does not depend on the starting orbitals used to construct G_0. Semi self-consistent solutions of the GW equations are also used (GW_0). In this case, G and Σ are updated until self-consistency is reached, while W_0 remains constructed from the starting orbitals. Therefore

$$\Sigma_{\mathrm{xc}} = iGW_0. \tag{4.4}$$

The flow chart in figure 2.12 illustrates the difference between these three levels of self consistency. The sections of the flow chart indicated with black solid ar-

[1] Excitation due to the addition or removal of *one* electron or hole.

[2] We use the LDA as construced from 1-dimensional density slabs as described in detail in reference [47].

rows show the path of G_0W_0 from a set of starting orbitals to a density and quasi-particle energies. The blue dotted arrow shows where the fully self-consistent GW method connects to the beginning of the cycle, which is repeated until convergence is reached and then the density and quasi-particle energies are calculated. The red dashed arrow illustrates the path of a semi self-consistent GW_0 calculation, as the screened interaction W is not updated.

The polarizability within the RPA can be implemented in several ways, depending on how one treats the energy dependence. The most computationally expensive is known as *dynamic* RPA,

$$P_{\text{dynamic}} = P^{\text{RPA}}(x, x', \omega). \tag{4.5}$$

This is the full RPA with all of its approximate dynamic correlation effects included. This choice for P takes GW beyond a single particle-picture, as the self-energy becomes energy-dependent and non-hermitian, and the single-particle addition and removal peaks become broadened. One can also choose a *static* RPA, which removes the energy dependence from the dynamic RPA by taking the value at zero energy:

$$P_{\text{static}} = P^{\text{RPA}}(x, x', \omega = 0). \tag{4.6}$$

In this case the self-energy is energy independent, meaning that the electrons are represented by a non-interacting Hamiltonian that is similar to that of HF but with a Fock term which is statically screened. When determining the self-energy for this form of P, the statically screened exchange (SEX) term must be accompanied by the Coulomb-hole (COH) term[3] in order to take account of the screening cloud adiabatically built-up around the added electron [14]. Using this form of the self-energy is called the COHSEX approximation.

In this work we also introduce the '*inertial*' RPA, which is also a static approximation to the screening, but instead of enforcing the static behavior in the energy domain, we do so in the time domain, hence

$$P_{\text{inertial}} = P^{\text{RPA}}(x, x', t = 0). \tag{4.7}$$

One may consider this approximation as fixing the screening from the moment the electron or hole is added to the system, opposed to the total screening over all time, as in the COHSEX case. Hence, we would expect that this approximation is more suitable for systems with stronger correlation, as systems of this type have a narrow screening distribution in the energy domain, and hence a broad distribution in the time domain. We term this 'inertial screening' as it can be thought of as increasing the effective mass of the collective electron oscillations in the COHSEX case, making them respond much slower. This increase in inertia could act to cancel the over-screening error in the COHSEX approximation while maintaining the beneficial simplicity of a static approximation to P.

[3] $\Sigma_{\text{COH}} = \frac{1}{2}\delta(x, x')W_{\text{c}}(x, x', \omega = 0)$.

4.3 Performance for model systems

We model a set of our one-dimensional model systems using the exact many-body method, DFT, the HF method, and various flavours of *GW*. Furthermore, we reverse-engineer each of these densities to obtain their corresponding KS potential. This allows us to see how well important aspects of exact KS-xc is captured by *GW* in order to aid the development of more advanced approximations within DFT. In addition to investigating the accuracy of the electron density from MBPT, we compare the quasi-particle (QP) energies, specifically the ionization potential (IP), electron affinity (EA) and fundamental gap (IP minus EA). These quantities are important, e.g., in quantum chemistry and material science [21, 19]. Furthermore, we investigate any correlation between the accuracy of the electron density and the QP energies for our various approximations.

In this chapter we study two types of system which we term 'exchange-dominated' and 'correlated'. We define an exchange-dominated system to be that which is accurately described by HF. For our exchange-dominated systems, we use the external potential of the quantum harmonic oscillator (QHO), $V_{\text{ext}}^{\text{QHO}}(x) = \frac{1}{2}\omega^2 x^2$, which strongly confines the electrons when $\omega = 0.25$. We study three QHOs containing 1, 2 and 3 electrons in turn. Systems which are termed correlated are systems for which the density and energies are *not* well represented by HF. For these systems we use an 'atom-like' potential which acts to weakly confine the electrons and hence include significant correlation effects. The external potential for our correlated systems is the atom-like potential $V_{\text{ext}}^{\text{Atom}}(x) = (a|x| + 1)^{-1}$, where, $a = 0.05$ for our one- and two-electron atoms and $a = 0.02$ for our three-electron atom.

4.3.1 Overview of the performance of the *GW* approximation

First we show the general performance of the *GW* approximation for various flavors and levels of approximation. Figure 4.1 shows the accuracy of the electron density across all our exchange-dominated and correlated systems (described above and investigated in detail below). As shown, the density error[4], particularly in the correlated atom-like systems, is highly dependent on the flavour of *GW* used. As can be seen by the three sets of columns, inertial screening preforms much better than dynamic and COHSEX for all of the system studied, which will be analyzed in detail in Section 4.3.3. The first five columns show that when performing dynamic *GW* calculations, the level of self-consistency chosen and the starting orbitals has a huge effect on the density, and in general the G_0W_0@HF flavor is the best across all systems, which will be investigated in detail in Section 4.3.2.

Figure 4.2 shows the accuracy of the quasi-particle energies[5] across all our exchange-dominated and correlated systems. As with the density, the error in quasi-particle energies[6], particularly in the correlated atom-like systems, is highly dependent on

[4]The density error is defined as the integrated absolute difference between the approximate and exact densities.

[5]For dynamic screening the quasi-particle energies are computed using the first order expansion $\epsilon_i^{\text{QP}} = \epsilon_i^0 + \langle \phi_i^0 | \Sigma(\omega = 0) | \phi_i^0 \rangle$ and COHSEX and inertial are simply computed from the single-particle eigenvalues (as these are both static methods).

[6]The quasi-particle energy error is defined as the absolute difference between the approximate and exact quasi-particle energies.

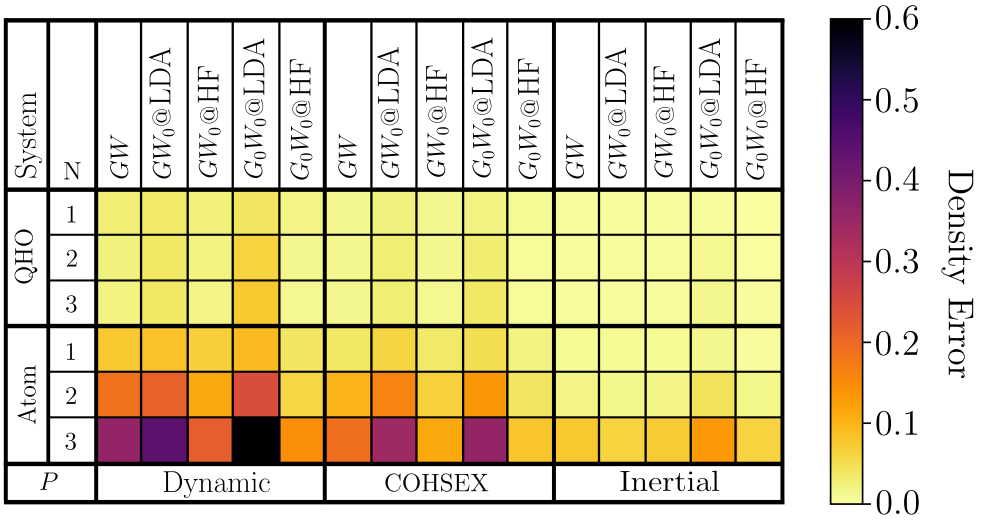

Figure 4.1: Color-chart showing the accuracy of the electron density for a range of exchange-dominated and correlated systems. The rows are the six systems under investigation: the one-, two- and three-electron QHO and the one-, two- and three-electron atom-like systems (described in detail in Section 4.3). The three sets of columns represent the approximation to the polarizability, P. Within each of these, the five columns correspond to the approximation to the xc self-energy, Σ_{xc}, as determined by the level of self-consistency (described in detail in Section 4.2 by Eqs. 4.2-4.7). The color in each case represents the error in the density (given by $n_{\text{error}} = \frac{1}{N}\int \left|n_{\text{exact}}(x) - n_{\text{approx}}(x)\right| dx$). A lighter color indicates a more accurate density; the maximum density error for all systems is 2.0, which would correspond to no overlapping of the densities.

the flavour of *GW*. First, looking at the first set of rows corresponding to the IPs, the inertial screening preforms the best. This is expected, as inertial screening performs significantly better than dynamic screening and COHSEX for the density and the decay of the density far from any system depends directly on the IP. As anticipated [13], the COHSEX in general performs worse than dynamic screening for the IPs. The next set of rows shows the performance of the EA; in general the COHSEX method outperforms inertial and dynamic, and is generally very accurate for all flavors of *GW*. Inertial screening performs very similarly to dynamic *GW*. For the fundamental gap, we find that the performance is highly sensitive to the flavor of *GW* in the dynamic and COHSEX case, with COHSEX generally performing worse. In contrast, the inertial screening generally performs well for the gap, independent of the flavor used.

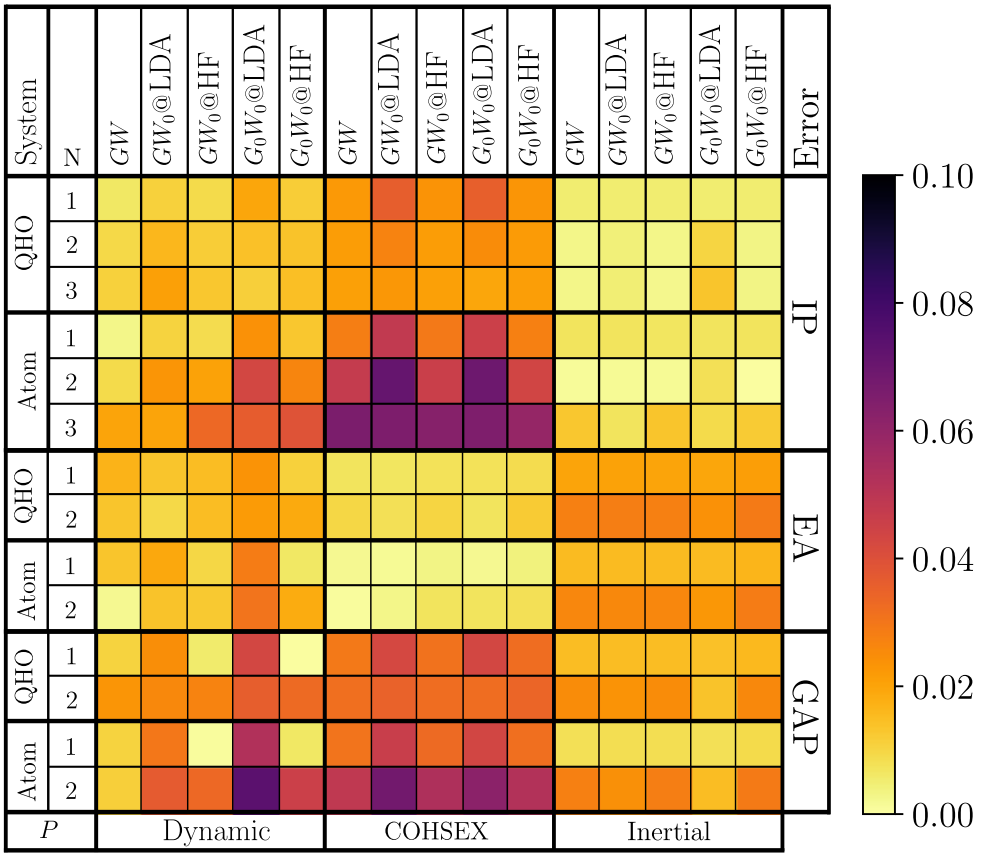

Figure 4.2: Color-chart showing the accuracy of the quasi-particle energies, namely the ionization potential (IP), electron affinity (EA) and the fundamental gap (GAP) for a range of exchange-dominated and correlated systems. The three sets of rows are the different quasi-particle energies, within each of these sets, the rows are the six systems under investigation: the one-, two- and three-electron QHO and the one-, two- and three-electron atom-like systems (described in detail in Section 4.3). The three sets of columns represent the approximation to the polarizability, P. Within each of these, the five columns describe the approximation to the xc elf-energy Σ_{xc} as determined by the level of self-consistency (described in detail in Section 4.2 by Eqs. 4.2-4.7). The color in each case describes the error in the quasi-particle energy (given by $\epsilon^{QP}_{\text{error}} = |\epsilon^{QP}_{\text{exact}} - \epsilon^{QP}_{\text{approx}}|$). A lighter colors indicates a more accurate quasi-particle energy.

4.3.2 Approximations to the self-energy

We now analyze in detail the effect various approximations to Σ has on the electron density, and hence the corresponding KS potential, in some specific cases of interest. As we vary our approximation to Σ we keep our approximation to P fixed, which in this case is chosen to be the dynamic RPA as it is the most commonly used.

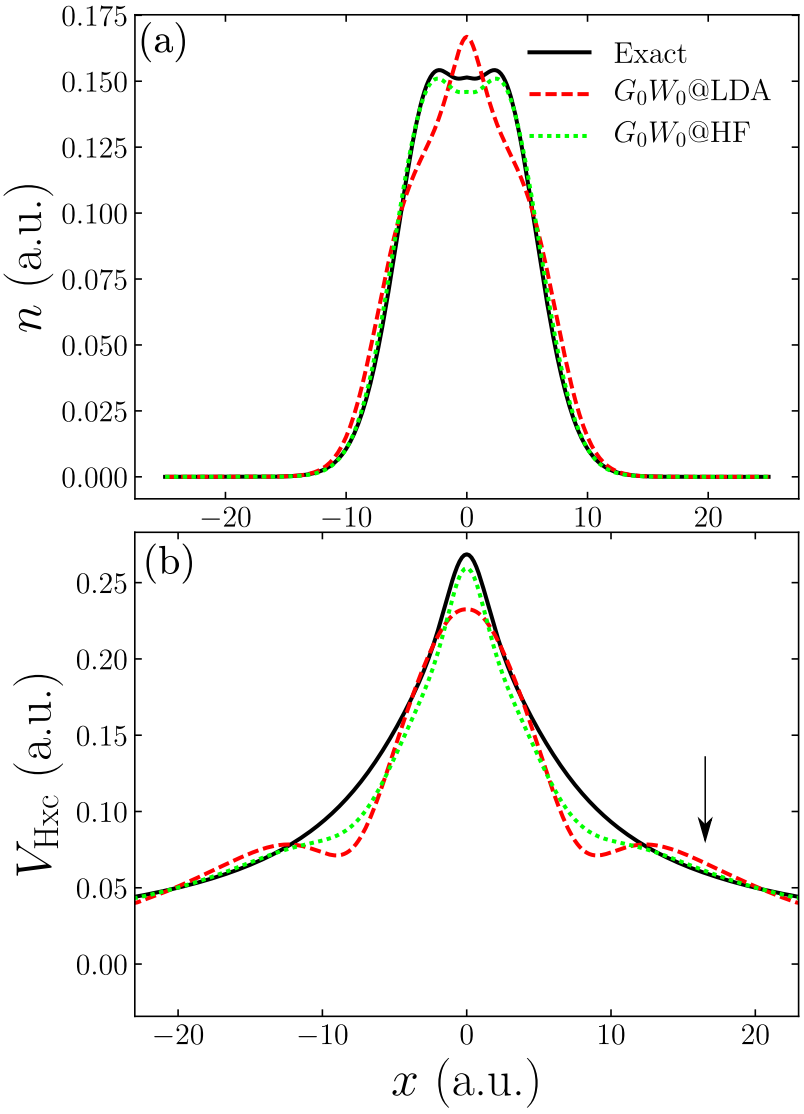

Figure 4.3: Comparison of G_0W_0 with LDA and HF starting orbitals for the correlated two-electron atom. (a) Exact, one-shot from LDA (G_0W_0@LDA) and one-shot from HF (G_0W_0@HF) density. The G_0W_0@LDA density is poor: both the central bump and the decay of the density are incorrect. The G_0W_0@HF density is much more accurate, especially the decay. (b) Exact, G_0W_0@LDA and G_0W_0@HF KS-Hxc potential. The G_0W_0@HF $V_{\mathrm{Hxc}}(x)$ is much more accurate than the G_0W_0@LDA V_{Hxc}: its asymptotic decay (arrow) and shape in the central region are correct; whereas G_0W_0@LDA V_{Hxc} has incorrect oscillations and an incorrect asymptotic decay.

Initially we investigate the performance of one-shot GW. We begin with a correlated system: 2 electrons in the atom-like potential (described above)[7]. Figure 4.3(a)

[7]This system is termed 'correlated' due to the poor performance of HF for the density and total energy; the HF density for this system is shown in figure 4.5(b).

shows the density calculated by one-shot GW with the LDA (G_0W_0@LDA) and HF (G_0W_0@HF) starting orbitals, and the exact for comparison. G_0W_0@LDA yields a poor density: there is a spurious central bump in the center of the system and an incorrect decay from the center. By comparison, the G_0W_0@HF density is accurate: it has the correct shape of the density in the center of the system and a highly accurate decay.

Figure 4.3(b) shows the KS-Hartree exchange-correlation (Hxc) potential ($V_{\text{Hxc}}(x) = V_{\text{KS}}(x) - V_{\text{ext}}(x)$) corresponding to each density. The G_0W_0@HF KS-Hxc potential is accurate, and possesses the correct asymptotic decay (arrow). The G_0W_0@LDA KS-Hxc potential is poor as it consists of incorrect oscillations and an incorrect asymptotic decay, as expected by the poor decay seen in the density.

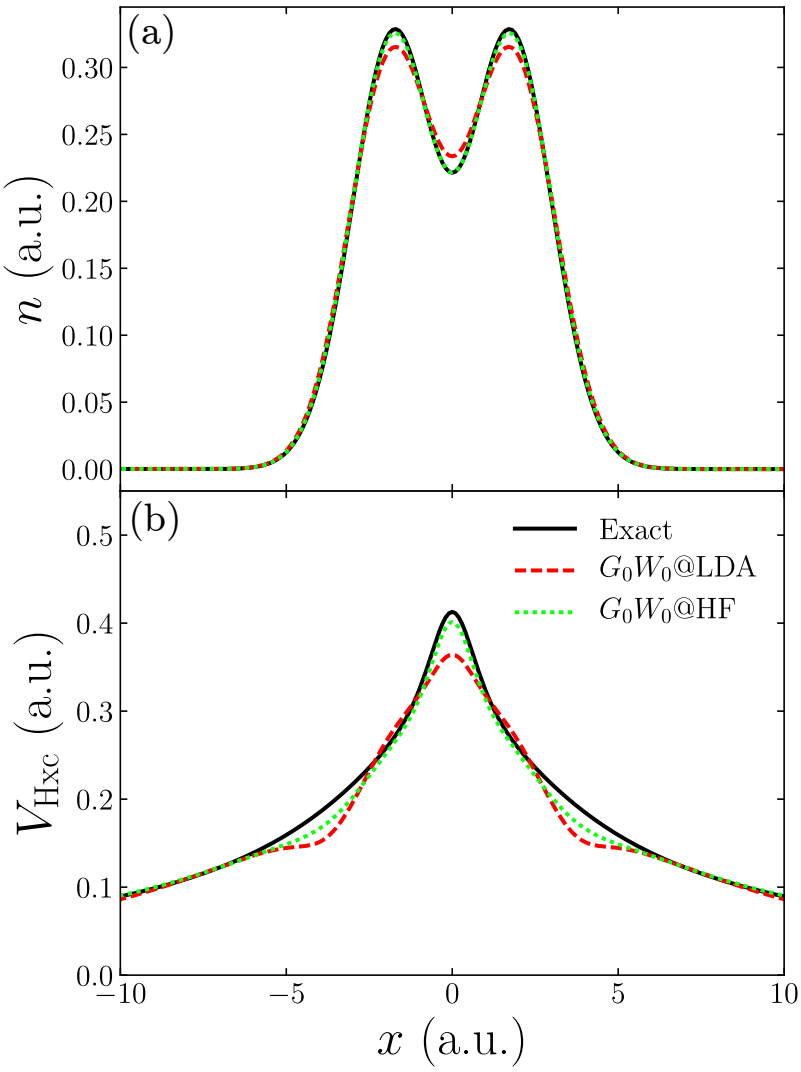

Figure 4.4: Comparison of G_0W_0 for the LDA and HF starting orbitals for the exchange-dominated two-electron QHO. (a) Exact, G_0W_0@LDA and G_0W_0@HF density. The G_0W_0@LDA density is generally accurate, although the magnitude of the 'peaks' are slightly incorrect. G_0W_0@HF is almost exact. (b) Exact, G_0W_0@LDA and G_0W_0@HF KS-Hxc potential. G_0W_0@LDA and G_0W_0@HF both exhibit the correct asymptotic decay of the Hxc potential although the G_0W_0@LDA potential contains incorrect spacial oscillations like for the correlated system; see figure 4.3(b).

We now investigate the performance of G_0W_0 calculation for an exchange-dominated system: the two-electron QHO. As shown in figure 4.4(a), the G_0W_0@HF density is

extremely accurate. Therefore, systems for which HF yields an almost exact density, a one-shot *GW* calculation retains the proper description of exchange already achieved by HF; this is common across all of our tested exchange-dominated systems, as seen in figure 4.1. As well as the density, the KS-Hxc potential is accurate, with a highly accurate asymptotic decay as shown in figure 4.4(b). G_0W_0@LDA performs relatively well for this system, yielding a density with the correct shape, although the 'peaks' are of incorrect height; see figure 4.4(a). Thus again demonstrating that HF orbitals are a better starting point for yielding an accurate density from a one-shot *GW* calculation than the LDA orbitals. As shown in figure 4.4(b), the G_0W_0@LDA also gives a substantially worse KS-Hxc potential in comparison to starting from HF orbitals. As with the correlated system, it contains incorrect oscillations. Despite this, the asymptotic decay far from the center of the system is accurate in this case.

A density-functional calculation employing the LDA is a common starting point for G_0W_0. However, we find this to be poor for yielding an accurate density, in particular as correlation becomes significant. We find that starting from HF orbitals yields strikingly accurate densities, as one may expect owing to HF's proper treatment of exchange – this is common across all the model systems we investigated; see figure 4.1. We show in figure 4.2 that G_0W_0@HF also outperforms G_0W_0@LDA for the IP, EA and fundamental gap, across all of our model systems. This is expected due to HF's exact treatment of exchange.

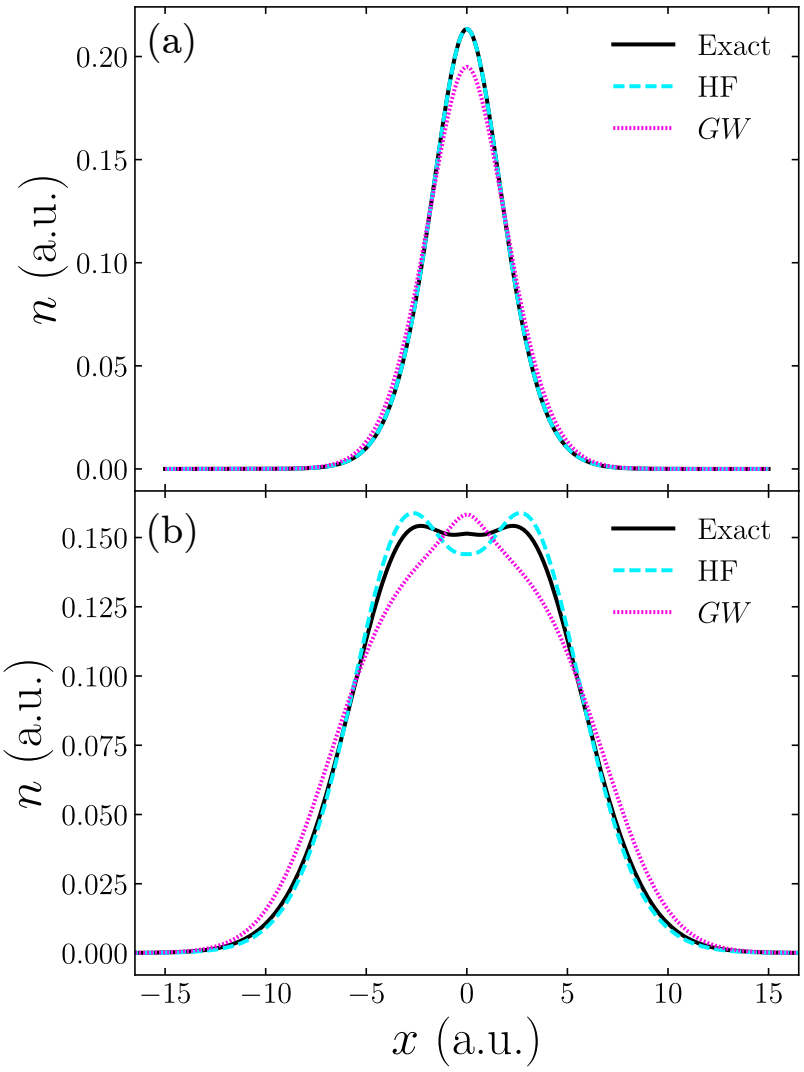

Figure 4.5: Comparison of fully self-consistent *GW* and HF for a one- and two-electron atom. (a) Exact, *GW* and HF density for the one-electron atom. The HF density is exact as it is free from the SIE. The *GW* density is more diffuse as the electron screens its own presence introducing the self-screening error. (b) Exact, *GW* and HF density for the two-electron atom. The HF density is largely incorrect due to the lack of screening as the electrons are incorrectly pushed away from the center of the well. The *GW* density is also largely incorrect due to over-screening of the bare Coulomb interaction, and the electrons are incorrectly pushed towards the center of the well.

Next we investigate the accuracy of fully self-consistent *GW*. We compare the performance of the density against HF for the one- and two-electron atoms. The one-electron atom is shown in figure 4.5(a). For any one-electron system, the HF density is exact owing to the cancellation between the non-local exchange operator and the self-interaction error (SIE) introduced by the Hartree potential. The *GW* density on the other hand is broadened relative to the exact, this is due to the screening of the exchange potential resulting in the reduction of the self-interaction correction; this error is termed the 'self-screening error' [22, 25, 54] and is due to the neglect of vertices in Σ. We investigate this error in more detail and develop a novel correction in chapter 5.

The two-electron atom is shown in figure 4.5(b). HF performs poorly for this system due to the lack of electron screening which is required to model the electron correlation; this causes the electrons to be artificially pushed away from the center of the atomic potential. *GW* also performs relatively poorly for this system: the electron interaction appears to be over-screened, causing the electrons to incorrectly fall into the center of the atom. This failure of fully self-consistent *GW* stems from the absent vertex corrections [23, 55].

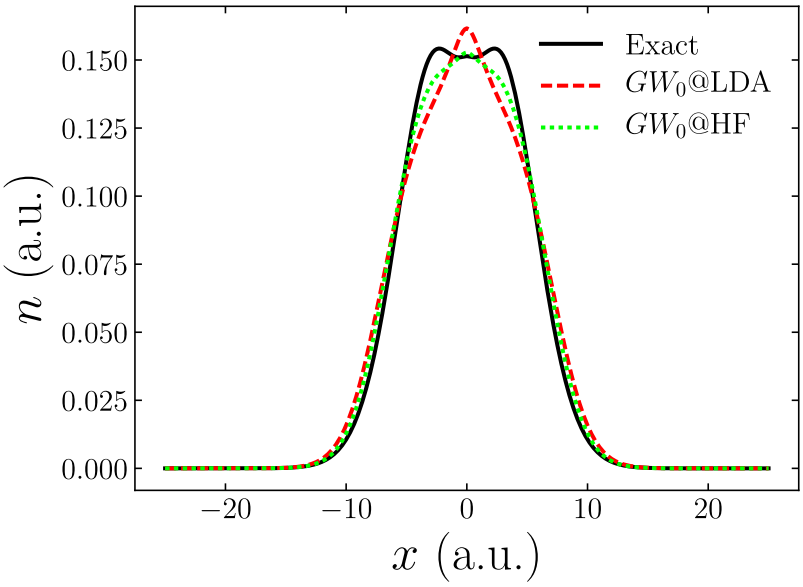

Figure 4.6: Comparison of semi self-consistent GW_0 for LDA and HF starting orbitals for the two-electron atom. GW_0@LDA preforms poorly for the density, failing to predict the correct shape or decay rate; it is similar in performance G_0W_0@LDA (figure 4.3(a)). Thus, adding the Green's function self-consistency is not sufficient to improve the method when starting from LDA orbitals. GW_0@HF performs much better than GW_0@LDA as it yields an accurate decay, but unlike G_0W_0@HF has the incorrect shape in the highly delocalized central region.

Next, we analyze the performance of semi self-consistent GW_0. As shown in figure 4.6, GW_0@LDA performs poorly in a similar fashion to G_0W_0@LDA (see figure 4.3(a) above). Therefore, it not the lack of self-consistency in the Green's function which is causing the poor performance, but the model of the *screening*. It is clear that the LDA KS orbitals provide a poor starting point for *GW* calculations in terms of predicting an accurate density (a trend we observe throughout this investigation), and starting from HF orbitals is much more accurate, even in the case of a self-consistent *G*. This can be seen across all our model systems in figure 4.1. One should note that although HF orbitals are more computationally expensive to compute than those from

a KS-LDA calculation, this is a relatively small cost in comparison to performing the GW calculation itself.

Figure 4.1 shows the performance of all flavors of GW for the correlated systems studied above and also the exchange-dominated QHO. It shows clearly that fully and semi self-consistent GW perform poorly for the density for correlated systems, and poorer than G_0W_0 starting from HF orbitals. We attribute this poor performance to the missing vertex corrections to Σ and P. We propose that alternative models for the polarizability, P, could yield a more accurate density in the case of full self-consistency GW. Specifically, we suggest energy-independent models of the screening – various examples of which are investigated in detail in Section 4.3.3 – as modifications of this type are substantially cheaper than including explicit vertex corrections.

The KS-Hxc potentials shown in Figs. 4.3 and 4.4, which correspond to the densities from one-shot GW, demonstrate the ability of MBPT to recreate features of the exact KS potential. We find this to be the case for all our densities obtained via MBPT; in general, the features of the exact potential are captured, however, when the density is poor it naturally corresponds to a poor KS potential. Therefore, our focus for the remainder of this chapter is on obtaining accurate densities from MBPT in order to also obtain accurate KS potentials.

4.3.3 Approximations to the polarizability

We now investigate how the accuracy of the density is affected by different approximations to the polarizability, P, namely the treatment of the energy dependence which determines the correlation part of the self-energy. We consider three methods as described in Section 4.2, specifically dynamic, static (COHSEX) and our proposed form of static screening, 'inertial screening'.

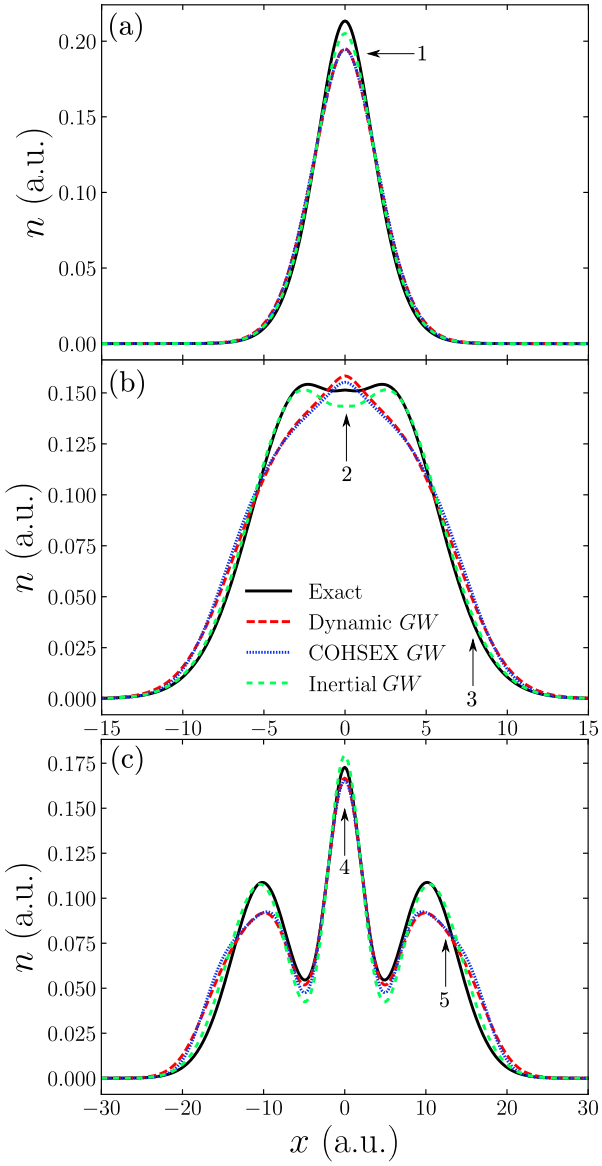

Figure 4.7: Comparison of dynamic, static (COHSEX) and inertial *GW* for the one-, two- and three-electron correlated atom. (a) Exact, dynamic, COHSEX and inertial density for the one-electron atom. The COHSEX density is remarkably similar to the dynamic density being overly diffuse, thus exhibiting a similar self-screening error. The inertial density performs much better than dynamic, reducing the diffusion by about 50% (arrow 1). This demonstrates that the inertial screening method lessens the self-screening error, yielding a more accurate one-electron density. (b) Exact, dynamic, COHSEX and inertial density for the two-electron atom. Again, the COHSEX density is remarkably similar to the dynamic with the same shape and decay rate. On the other hand, the inertial density is much more accurate: the decay is remarkably accurate (arrow 3) as well as the overall shape. The only noticeable error is in the central region where the electrons are strongly delocalized (arrow 2). (c) Exact, dynamic, COHSEX and inertial density for the three-electron atom. Again the COHSEX and dynamic density are almost indistinguishable. The inertial density is again highly accurate in the decay (arrow 5), and with a very accurate overall shape. However, an appreciable error in the central region of strong delocalization persists (arrow 4).

We begin by comparing the usual dynamically-screened *GW* (dynamic *GW*) and static screening *GW* (COHSEX) when iterated to full self-consistency. As shown in figure 4.7(a), the COHSEX density is remarkably similar to that of dynamic *GW* (the same as shown in figure 4.5(a)) this shows that the COHSEX approximation also experiences the self-screening error, thus it would require vertex corrections along with self consistency if it were to yield accurate densities, as the decay of the density is highly dependent on self-screening [28]. This can be seen in figure 4.7(b) and (c) as the decay of the COHSEX density is as poor as the dynamic *GW* case. Another property that is also highly dependent on the self-screening error is the ionization potential, and as can be seen in figure 4.2, the COHSEX, just like dynamic *GW*, also yields poor ionization potentials. Figure 4.7(b) and (c) show that in correlated systems of multiple electrons this trend continues: the COHSEX density is remarkably similar to the dynamic *GW* density. This shows that the COHSEX approximation captures well in its frequency-independent correlation potential the relevant effects of the dynamic correlation potential. However, these effects ultimately yield a poor density for correlated systems.

We now turn our attention to our inertial *GW* method for these correlated systems. Figure 4.7(a) shows how inertial *GW* outperforms the dynamic *GW* density: it has a reduced broadening (arrow 1), thus reducing the error in the density in comparison to dynamic *GW* by about 50%. This shows that the inertial method is affected less by the self-screening error due to the reduction in screening inherent in the method relative to the over-screening within the COHSEX approach. This is supported in figure 4.7(b) and (c), which show that the inertial *GW* method predicts highly accurate decay rates (arrows 3 and 5). This is also reflected in figure 4.2 which shows that the inertial method gives much more accurate ionization potentials for these correlated systems.

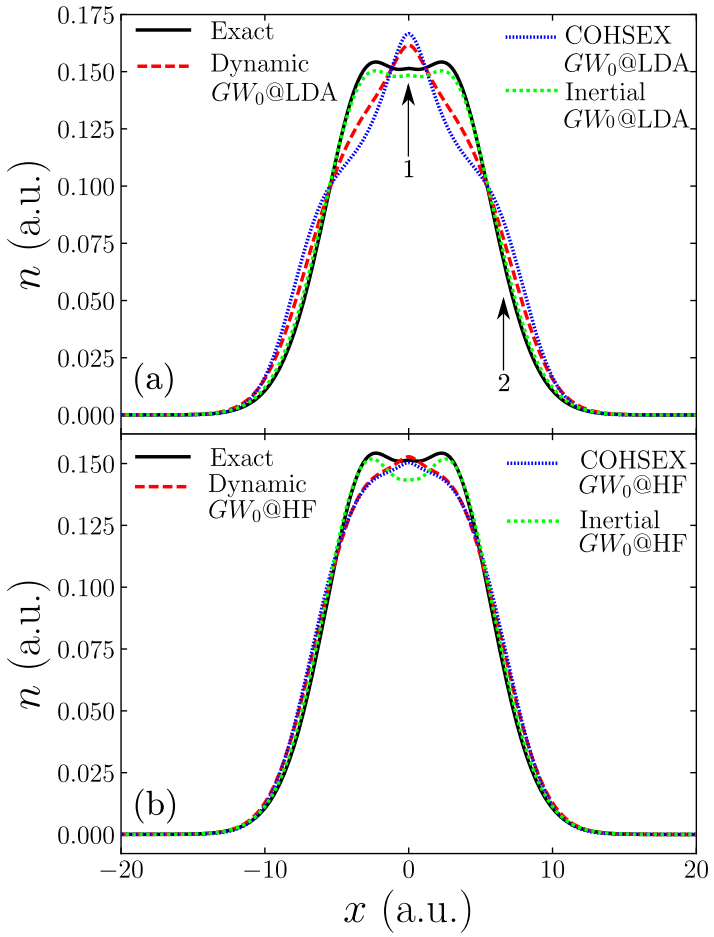

Figure 4.8: Comparison of semi self-consistent dynamic, static (COHSEX) and inertial GW_0 for the two-electron correlated atom. (a) Exact, dynamic, COHSEX and inertial GW_0 density for the two-electron atom starting from LDA orbitals. In the semi self-consistent case, the COHSEX GW_0@LDA density is slightly less accurate than dynamic: the decay rate (arrow 2) is poor and the density contains a large spurious bump in the central region (arrow 1). Inertial GW_0 shows significant improvement, yielding an extremely accurate density over the entire system, with a correct shape in the usually challenging strongly delocalized central region (arrow 1) and highly accurate decay (arrow 2). (b) Exact, dynamic, COHSEX and inertial GW_0 density for the two-electron atom starting from HF orbitals. The COHSEX GW_0@HF density is again in very good agreement with the dynamic GW_0@HF density, being overall poor, although with a reduced incorrect bump in the central region in comparison to GW_0@LDA. Thus again showing the greater performance in general when starting from HF orbitals. The inertial GW_0@HF density is again accurate for the decay and overall shape.

We now analyze the different models of screening in the semi self-consistent case. As shown in figure 4.8(a) the COHSEX GW_0@LDA density is slightly less accurate in comparison to the dynamic and still features the incorrect bump in the central region (arrow 1). Furthermore, it predicts an even poorer decay compared to dynamic. The COHSEX GW_0@HF still performs poorly. Again its yielded density is very similar to that from dynamic GW_0@HF; see figure 4.8(b).

For the semi self-consistent case, the inertial screening method again performs exceptionally well. As shown in figure 4.8(a), the inertial GW_0@LDA is almost exact. It has the correct shape across the entire system, including the highly delocalized central region (arrow 1), and an extremely accurate decay rate (arrow 2). This large improvement which comes from employing inertial screening in a semi self-consistent calculation is observed for all our model systems; see figure 4.1.

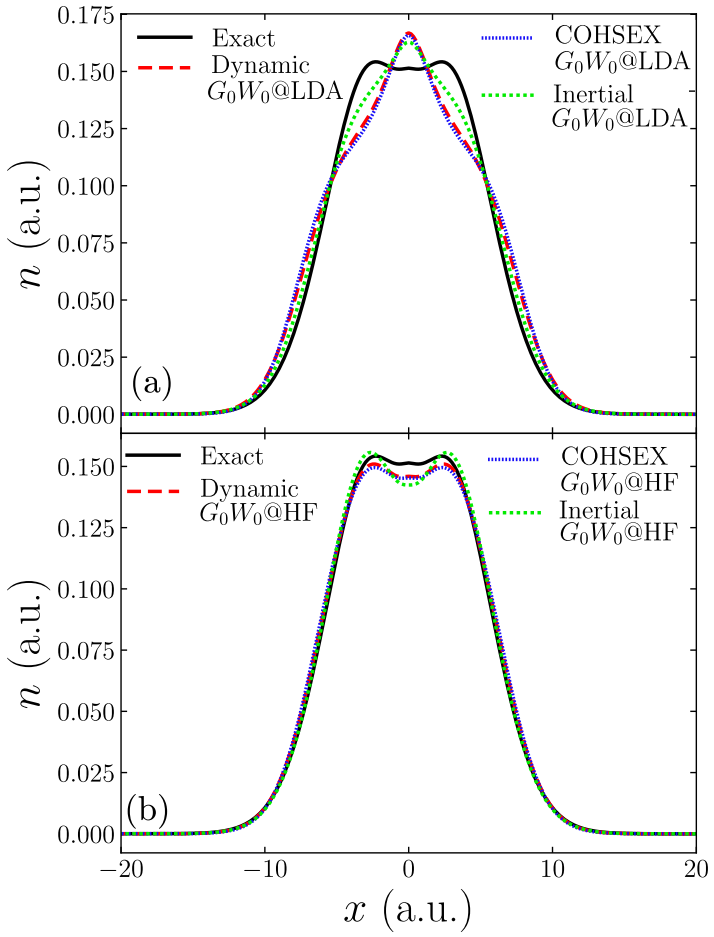

Figure 4.9: Comparison of semi self-consistent dynamic, static (COHSEX) and inertial G_0W_0 for the two-electron correlated atom. (a) Exact, dynamic, COHSEX and inertial G_0W_0 density for the two-electron atom starting from LDA orbitals. The COHSEX G_0W_0@LDA density is again remarkably similar to the dynamic. inertial G_0W_0 in this case only shows minor improvement, although more vastly improving the decay rate of the density. (b) Exact, dynamic, COHSEX and inertial G_0W_0 density for the two-electron atom starting from HF orbitals. The COHSEX G_0W_0@HF density is again in very good agreement with the dynamic GW_0@HF density, giving a very accurate density for this system and a much better density than when starting from LDA orbitals. The inertial G_0W_0@HF density is also just a minor improvement to dynamic G_0W_0@HF although again yielding a highly accurate decay.

Finally, we find that the density yielded from the COHSEX approximation is almost indistinguishable from the full dynamic RPA for G_0W_0, and hence this is a trend common among all systems studied. Figure 4.9(a) and (b) shows that the COHSEX GW_0@LDA density is only slightly less accurate than the dynamic GW_0@LDA density, albeit largely inaccurate with an inaccurate central bump. We find in the one-shot case that the inertial RPA still gives an improvement over the usual dynamic RPA, but not as significant as in the self-consistent cases. This is again the case for all of our model systems; as shown in figure 4.1 our inertial screening method always yields an accurate density, but this is a slightly reduced effect in the one-shot case, especially when starting from LDA orbitals. Although in all cases we still find it yields a very accurate ionization potential as shown in figure 4.2.

We emphasize that the accurate densities shown above have corresponding to KS potentials which capture features of the exact KS potential. Hence, in general, densities obtained employing our inertial screening, yield the most accurate KS potentials.

4.4 Summary

In this chapter, we have assessed the accuracy of the electron density and quasi-particle energies yielded from a variety of flavours of the *GW* approximation. We studied finite systems consisting of few electrons for which the many-electron Schrödinger equation can be solved exactly thus allowing us to compare densities and energies obtained from MBPT to the exact quantities. We vary approximations to the polarizablity as well as the self-energy. We also introduce our own static approximation to the polarizablity, which we term inertial screening as it may be thought of as increasing the mass of the electrons in the system in order to reduce the over-screening inherent in the usual COHSEX static approximation.

In general, we find the accuracy of the density depends highly on the flavor of *GW* used. However, in terms of the polarizablity, our inertial screening approximation outperforms the standard dynamic and COHSEX approximations for all flavors of *GW* for both the density and quasi-particle energies save a slightly worse performance for the electron affinity. Employing the commonly used dynamic screening, we find that one-shot methods perform best, due to the cancellation of errors between neglecting vertex corrections and lack of self-consistency in the calculation. In this case we find Hartree-Fock orbitals are always a more successful starting point, owing to their treatment of exact exchange. We find that the self-screening error, caused by the neglect of vertex terms in the self-energy, is responsible for inaccuracies is the *GW* density and ionization potential. We investigate this in more detail in the next chapter, along with proposing a novel correction to ameliorate the effects of this error.

We find that the electron density obtained from many-body perturbation theory (MBPT), in principle, corresponds to a Kohn-Sham (KS) potential which captures features of the exact KS potential. However, depending on the level of approximation used within MBPT, the accuracy of the yielded density varies largely, thus influencing the accuracy of the corresponding KS potential.

Chapter 5

Correcting the *GW* self-screening error with a local density functional

In chapter 4 we showed that densities and ionization potentials calculated using the *GW* approximation are adversely effected by the self-screening error. The self-screening error is the part of the self-interaction error that would remain within the *GW* approximation if the exact dynamically screened Coulomb interaction, *W*, were used, causing each electron to artificially screen its own presence. In this chapter we propose a simple, computationally efficient correction to *GW* calculations in the form of a local density functional, obtained using a series of finite training systems; in tests, this eliminates the self-screening errors in the electron density and ionization potential [28].

5.1 Introduction

In chapter 4 we showed that commonly used flavours of the *GW* approximation give very poor densities and ionisation potentials. It is vital that we improve upon such limitations if we are to accurately predict the properties systems with appreciable correlation. Higher-order terms beyond *GW* include a self-screening correction [22] related to the self-interaction familiar in density-functional theory (DFT) [**?** 45]. Attempts to correct the entirety of the self-interaction error via explicit vertex corrections have proved challenging [23, 27]. We adopt a physically more direct approach to the self-screening correction. In large-scale calculations, a *GW* calculation normally takes a DFT calculation as its starting point. The goal is to improve the quantities calculated from DFT, such as the ionization potential (IP) [20]. However, the self-screening error is known to have an adverse effect on the IP. In this chapter we focus on the computation of the electron density from the Green's function and IP. Again, we use the space-time method to solve Hedin's equations [49]. We identify the self-screening error inherent in all *GW* calculations via the use of an effective potential. We then propose a simple and computationally inexpensive correction term that is a local potential added to the self energy and applicable to any *GW* calculation. Finally we test our self-screening correction (ssc) by comparing the *GW*+ssc electron density and IP to the exact quantities from systems of few electrons in 1D where the many-electron Schrödinger equation (SE) can be solved exactly. For these test systems we find that the spurious effects of the self-screening error on the density and the IP are removed.

5.2 Investigating the self-screening error

Within *GW* the screened interaction *W* amounts to dynamically adjusting the strength of the bare Coulomb interaction between electrons. One merit of the exchange operator of Hartree-Fock theory is that it exactly corrects the self-interaction error introduced by the Hartree potential. If the Coulomb interaction in the Hartree-Fock exchange operator were screened using the exact irreducible polarizability P, Hartree-Fock's self-interaction correction would be improperly reduced, so that part of the self-interaction error – the self-screening error – remains uncorrected. It may be thought of as each electron artificially screening its own presence. It follows that the self-screening error is largest when screening, and therefore correlation, is strong [22].

The only source of error in a *GW* calculation of the hydrogen atom (H) is self-screening because H is a one-electron system, and the RPA screening is exact for one electron (or strongly localized electrons) as no electron-hole interactions are present. This is apparent if one looks at the correlation part of the self-energy for this system, which should be zero. Instead, it consists of the spurious self interaction [25].

We now employ a simple one-dimensional, one-electron model to investigate the self-energy of a *GW* calculation. In this chapter the electrons are again treated as like-spin to more closely approach the nature of exchange and correlation in systems of many electrons, hence each electron occupies its own distinct orbital. First we model *one* electron in a 1D atomic potential, $V_{\text{ext}} = -1.0/(\alpha|x| + 1)$ where $\alpha = 0.05$. The potential loosely confines the electron, which clearly displays the adverse effect of the self-screening error on the *GW* density and energy (described above); see fig-

ure 5.1(a). We observe the effect self-screening has on the density by comparing the *GW* density to the exact. As in this one-electron system, the screening has been accurately described by the RPA; the self-screening error is the only error present in the system, thus allowing us to investigate the effect of self-screening on the correlation part of the self energy.

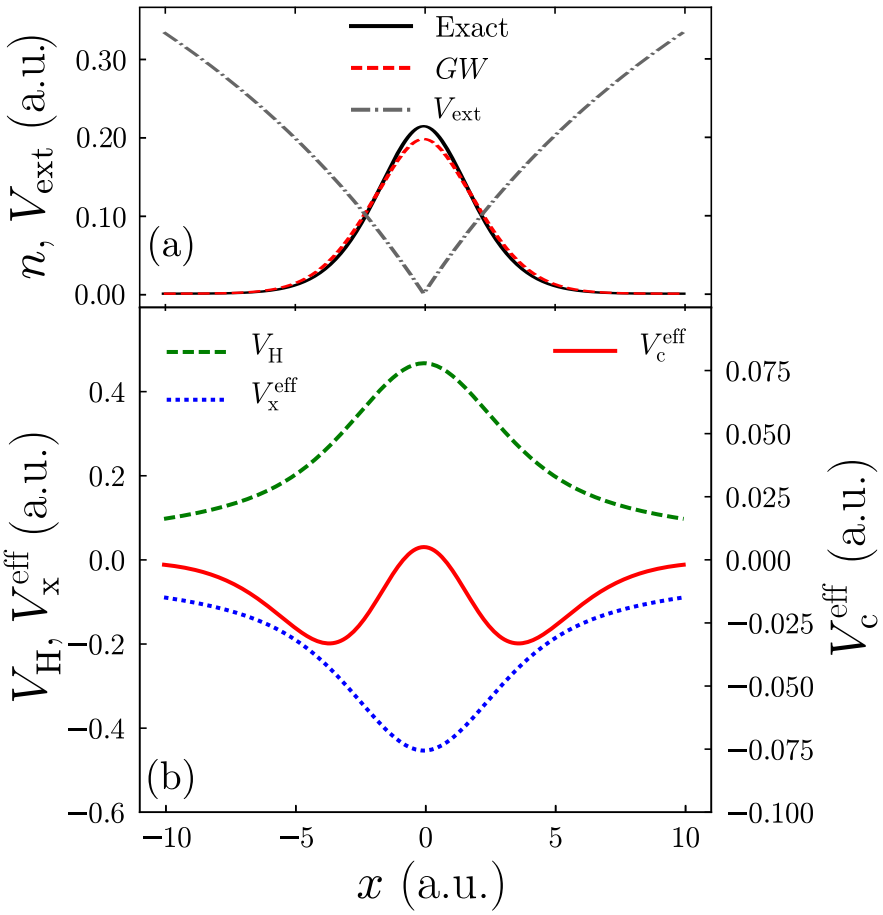

Figure 5.1: *GW* self-screening error for a one-electron atom. (a) The exact density, fully self-consistent *GW* density, and the external potential. The *GW* density is more diffuse as the electron screens itself; the decay rate of the density towards the edge of the system is wrong. (b) The self-consistent *GW* Hartree and effective exchange potentials (left scale), and effective correlation potential (right scale) (see Eq. 5.1). The Hartree and effective exchange potentials cancel out, but there is a spurious non-zero effective correlation potential that results in the artificial spreading of the density away from the center of the system (a). This effective correlation potential is responsible for the entire self-screening error.

Figure 5.1(a) shows the *GW* and exact electron densities. Compared to the exact, the *GW* density is more diffuse and its exponential decay is incorrect far from the center. If these inaccuracies in the density are a result of the self-screening, the correlation part of the self-energy will be non-zero. First we split the self-energy (Σ) into its separate contributions: $\Sigma = V_H + \Sigma_x + \Sigma_c$, the Hartree potential (V_H), exchange term (Σ_x), and the correlation part (Σ_c). Σ_x and Σ_c are non-local, and Σ_c is energy dependent. To get a clear picture of what effect a particular part of the self-energy is having on our only occupied orbital (ϕ), we define an effective local potential, akin to DFT:

$$V_{Hxc}^{eff}(x) = \frac{1}{\phi(x)} \int \Sigma(x, x', \varepsilon)\, \phi(x')\, dx', \tag{5.1}$$

where ε is the corresponding eigen-energy [1]. The three parts V_{H}, $V_{\mathrm{x}}^{\mathrm{eff}}$, $V_{\mathrm{c}}^{\mathrm{eff}}$, defined in this way, may be examined separately.

Figure 5.1(b) shows the Hartree, effective exchange and correlation potentials for our one-electron atom. The *GW* Hartree and effective exchange potentials completely cancel, as expected. However, there is a small correlation potential that is solely responsible for the error in the *GW* density. We call this potential the self-screening potential V_{ss} which is present in all *GW* calculations of any number of electrons (N). Examining the shape of V_{ss} we see this potential acts to draw the density away from the center of the system.

5.3 Developing the local self-screening correction

References [56, 57, 58, 59] note that a self-interaction error arises in the RPA total energy owing to the lack of a vertex in P. However, our preference is to focus on developing an effective vertex in the self-energy Σ, in order to retain the exact polarizability of a one-electron system.

Reference [44] proposes to correct the self-screening error via an orbital- and spin-dependent screened interaction and is applicable to methods in which the Green's function is constructed from normalized single-particle orbitals. Our proposed self-screening correction, because it consists simply of a spatially local potential, is applicable to all flavors of *GW*.

We define a potential $V_{\mathrm{ssc}}[n](x)$, that, when added to the *GW* self-energy, Σ_{GW}, strives to yield a self-energy with self-screening removed:

$$\Sigma_{GW+\mathrm{ssc}} = \Sigma_{GW} + V_{\mathrm{ssc}}[n](x), \tag{5.2}$$

where the density is obtained from the Green's function G.

We construct a local density approximation for $V_{\mathrm{ssc}}[n](x)$. To do so we choose a set of finite, centrally homogeneous one-electron 'density slabs', as used in reference [47] to construct local-density approximations to the overall exchange-correlation functional of DFT [2]. We use one-electron slabs because, as we have established, in a one-electron system the self-screening is the only source of error in a *GW* calculation. The density of each slab is chosen to be $n_0 e^{-mx^{12}} + 10^{-4} \cdot e^{-0.007|x|}$, where n_0 is the height of the slab, and m follows from normalization; see, e.g., figure 5.2(a). Our set of slabs have a range of plateau densities $0.03 \leq n_0 \leq 0.58$. For each of these densities we apply the single orbital approximation (SOA) [60, 61], which is exact for one electron, to obtain the external potential that defines this slab density. We then use our set of external potentials to calculate the corresponding exact total energy (E) for each slab density in turn via the single-particle SE.

[1] As we use the space-time method we have access to the self-energy in the imaginary frequency domain, so for the purposes of Eq. 5.1 we approximate $\Sigma(\varepsilon) \approx \Sigma\left(\varepsilon_f\right)$ where ε_f is the Fermi energy. To check this is a good approximation, once we have constructed the total effective potential, we solve the single-particle SE using $V_{\mathrm{Hxc}}^{\mathrm{eff}}$ to ensure this potential gives the same density as the *GW* calculation.

[2] These 'density slabs' are systems with uniform density within a finite region, resembling the homogeneous electron gas, and decaying to zero outside this region. Local approximations may therefore be constructed from results for a set of such slabs spanning a range of densities.

Next we perform a fully-self consistent *GW* calculation for each slab system using the corresponding external potential to obtain the total *GW* energy (E_{GW}). We choose to calculate E_{GW} via the effective potential experienced by the single electron using Eq. (5.1) – note this is not the only means of calculating E_{GW}. To calculate E_{GW}, we construct an effective potential ($V^{\text{eff}} = V_{\text{ext}} + V^{\text{eff}}_{\text{Hxc}}$). We then solve the single-particle SE to find the lowest eigenvalue of this one-electron system, which is E_{GW} [1]. Finally, we define the self-screening energy per electron as $\varepsilon_{\text{ss}} = E_{GW} - E$.

Figure 5.2(a) shows an example of one of our slabs with height $n_0 = 0.22$. The *GW* density shows the effect of the self screening, and hence is not homogeneous in the central region whereas the exact is. Figure 5.2(a) also shows the effective self-screening potential. Figure 5.2(b) shows the self-screening energy as a function of the density $\varepsilon_{\text{ss}}(n)$ for our whole range of slab systems (crosses)[3]. We require that $\varepsilon_{\text{ss}}(n)$ must be zero when $n = 0$ as there is no self-interaction, and therefore no self-screening error. We then apply a fit to this data yielding a functional form of the self-screening energy per electron:

$$\varepsilon_{\text{ss}}(n(x)) = -an(x)e^{-bn(x)^c}, \tag{5.3}$$

where $a = 4.09268$, b=9.20609 and c=0.53652.

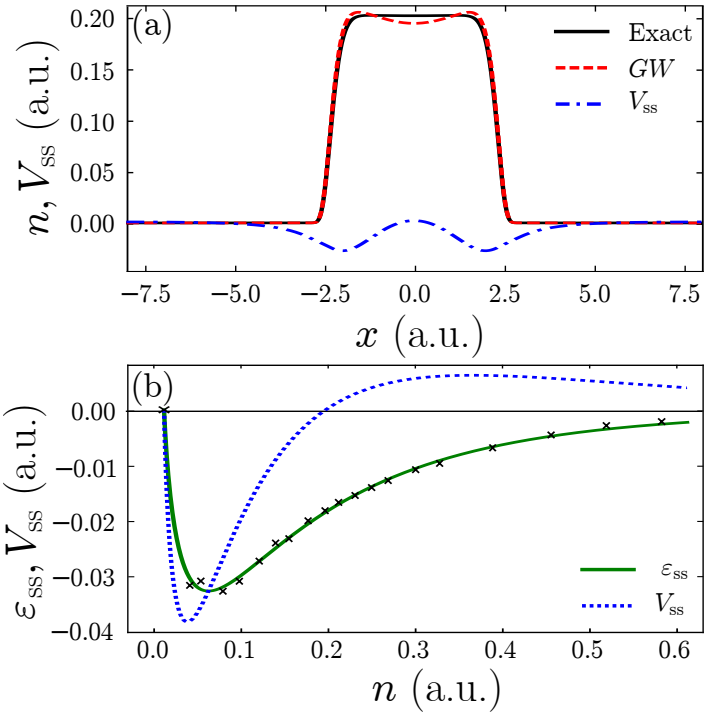

Figure 5.2: (a) An example one-electron finite, homogeneous density of height $n_0 = 0.22$, compared to the density produced by a self-consistent *GW* calculation with the same external potential. The self-screening error causes the slab to curve as the electron screens itself. This is illustrated by the self-screening potential. (b) The crosses show the computed self-screening energy ε_{ss} per electron of each of the slab systems, with a cross added for $\varepsilon_{\text{ss}}(n = 0) = 0$. A fit for ε_{ss} is applied to these points. The corresponding self-screening potential V_{ss} is computed as the functional derivative of ε_{ss} (Eq. (5.4)).

[3]Due to the increasingly large imaginary energy grids required, the data points become more sparse as we approach $n = 0$.

Next we compute the local functional derivative, as follows [4]

$$V_{\mathrm{ss}}(n) = \varepsilon_{\mathrm{ss}}(n) + n\frac{d\varepsilon_{\mathrm{ss}}}{dn}, \tag{5.4}$$

in order to determine the local self-screening potential functional $V_{\mathrm{ss}}(n)$; shown in figure 5.2(b). It follows that $V_{\mathrm{ssc}}[n](x) \approx -V_{\mathrm{ss}}(n(x))$, in order for our correcting potential V_{ssc} to cancel the spurious self-screening of the electrons. Thus, our final local-density functional for correcting the *GW* self-screening error is

$$V_{\mathrm{ssc}}(n(x)) = ane^{-bn^c}\left(2 - bcn^c\right), \tag{5.5}$$

where a, b and c are given above. When we apply the *GW* calculation with our local self-screening correction (*GW*+ssc) method to the training slabs via the self-energy:

$$\Sigma_{GW+\mathrm{ssc}} = \Sigma_{GW} + V_{\mathrm{ssc}}(n(x)), \tag{5.6}$$

we obtain the exact energy [5].

5.4 Effectiveness of the local self-screening correction

We test the effectiveness of our self-screening correction (Eq. (5.5)) by employing it for *GW* calculations of various flavors (including self-consistent *GW*) for the one-electron atom described above, where self-screening is the only source of error. Figure 5.3 shows the same one-electron model system as in figure 5.1; now the fully self-consistent *GW*+ssc is also shown. The *GW*+ssc density is in excellent agreement with the exact density, with the peak height and decay matching. (We show below that the IP predicted by the *GW*+ssc is also very accurate.) Figure 5.3 also shows our local self-screening correction potential V_{ssc} and the *GW* effective correlation potential $V_{\mathrm{c}}^{\mathrm{eff}} = V_{\mathrm{ss}}$; they cancel out very well thus removing the self-screening error, hence showing the success of correcting the self-screening error with a local potential. Here we only show the density calculated from self-consistent *GW*. However, we also find that the our self-screening correction is equally successful when applied to all of our flavors of *GW* for this system.

[4] The total self-screening energy, E_{ss}, is approximated to depend on the self-screening energy per electron as follows: $E_{\mathrm{ss}} = \int n(x)\,\epsilon_{\mathrm{ss}}(n)\,dx$

[5] But not the exact density, since the density of each slab system is extremely sensitive to the potential.

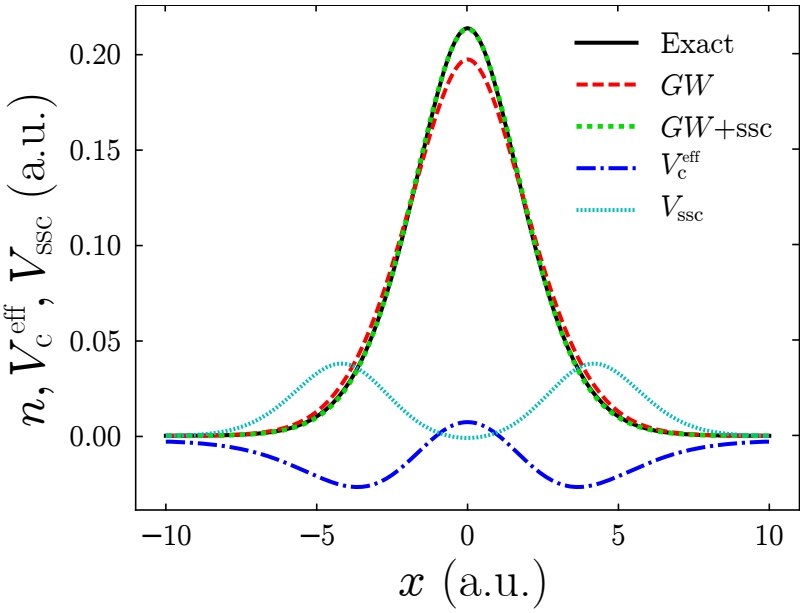

Figure 5.3: Applying our self-screening correction to the one-electron atom of figure 5.1. The *GW* density is broadened relative to the exact due to the self-screening error, which is the only error present in the one-electron system. The self-screening-corrected *GW* density is in excellent agreement with the exact, thus demonstrating the success of our functional. We can see that our self-screening correction potential successfully acts to cancel the self-screening potential present in the self-consistent *GW* calculation, this also has the effect of correcting the decay of the effective xc potential far from the finite system.

We also investigate two- and three- electron atoms using the same form of external potential as the one-electron atom (above), with $\alpha = 0.05$ for two electrons and $\alpha = 0.02$ for three electrons. Figure 5.4(a) shows that our self-screening correction significantly improves the *GW* density for the two-electron atom; it corrects the decay rate of the density, thus improving the predicted IP (see Table 5.1). The density maintains the incorrect central feature due to the electron-hole interaction neglected by the RPA in this delocalized region, which could in-principle be corrected by vertex corrections to P [43].

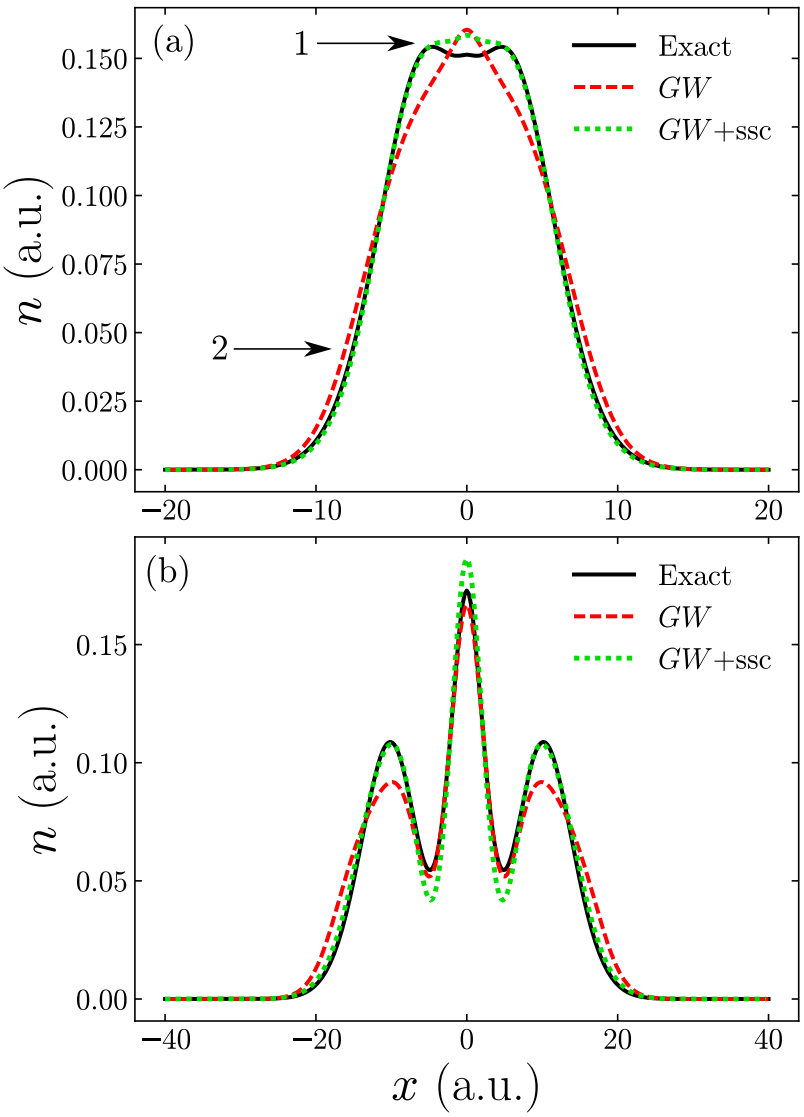

Figure 5.4: (a) Applying our self-screening correction to the two-electron atom. The *GW* density is again dispersed compared to the exact. The self-screening corrected *GW* density is in excellent agreement with the exact in region 2, where the electrons are strongly localized as the HOMO orbital is dominant in this region, and so the RPA gives a good account of the screening. Furthermore, the decay of the density is corrected, thus improving the IP of the system. In region 1 the density is less accurate owing to the delocalization of the electrons leading to electron-hole interactions present that are neglected in the RPA. Vertex correction to the polarizablity would be required to correct the density in this region [43]. (b) Applying our self-screening correction to the three-electron atom. The *GW* density is once again diffuse compared to the exact. The self-screening corrected *GW* density is in better agreement with the exact, it corrects the decay rate and overall shape of the density, again improving the IP of the system. The height of the central peak remains incorrect, again due to the electron-hole interactions in this region neglected by the RPA.

Figure 5.4(b) shows the effectiveness of our self-screening correction for the three-electron atom. Again, we find the self-screening-corrected GW density is in better agreement with the exact; it corrects the decay rate of the density far from the center of the system, again improving the predicted IP (see Table 5.1), and the overall shape of the density. The height of the central peak remains incorrect, which again suggests a failing of the approximation to the polarizability P and *not* the presence of self screening.

This ssc also improves G_0W_0 calculations. In this case the ssc is applied in the same way as above: the local potential is added to the self-energy via Eq. 5.2. When applied to G_0W_0 starting from a conventional LDA calculation, the density errors are reduced by $16-50\%$ for these model systems.

Table 5.1 shows the IPs predicted by GW via two different methods for all three of our atoms, with and without our self-screening correction. Our first method extracts the IP from the density, which in principle can be done by determining the decay rate of the density far from the center of the system: $\lim_{|x|\to\infty} I = \frac{1}{4}\left(\frac{\partial \ln(n)}{\partial x}\right)^2$. In practice, we find it less computationally onerous to determine the exact KS potential corresponding to the GW density for each atom in turn using the algorithm of reference [46] and obtain the highest occupied KS eigenvalue which is the negative of the IP. When calculated in this way, the GW+ssc IP is strikingly accurate. (Similar results are obtained for non-self-consistent versions of GW.) We expect our ssc to similarly correct the IP for any N-electron system as localization becomes absolute far from the center of the system. Hence, in this region, the HOMO orbital is dominant and the RPA gives a good account of the screening. Therefore, the decay rate of the GW+ssc density is very accurate and thus so is the IP. This can be seen in figure 5.4 (region 2 in (a)). Second, we calculate the IP via the quasiparticle (QP) energies. In contrast to the HOMO energy, these QP energies are affected by the electron-hole interactions present in the two- and three-electron atoms, hence the predicted IPs are not as accurate relative to extracting the IP from the density, but are generally improved by the ssc; see Table 5.1.

Table 5.1: The IPs predicted by GW, and GW with our self-screening correction, against the exact for the one, two and three electron atoms. IPs extracted via the KS potential and QP energies are shown.

	N	GW	GW+ssc	Exact
KS	1	0.908	0.900	0.900
	2	0.624	0.610	0.611
	3	0.662	0.641	0.642
QP	1	0.908	0.900	0.900
	2	0.577	0.577	0.611
	3	0.675	0.654	0.642

5.5 Summary

In conclusion, we propose a simple self-screening correction which is a local potential added to the self-energy of any *GW* calculation. The correcting potential is a local functional of the electron density. We find that the self-screening error is removed from our *GW* calculations of various test systems when our correction is employed. The electron density is significantly improved for all systems studied. In one-electron systems, and regions of high localization in many-electron systems, the density is almost exact. Beyond our self-screening correction, electron-hole corrections to the screening would be required in the delocalized regions. Furthermore the IPs predicted by *GW* are improved by our correction.

Chapter 6

Advantageous nearsightedness of many-body perturbation theory

For properties of large-scale interacting electron systems, Kohn-Sham (KS) theory is often favored over many-body perturbation theory (MBPT) owing to its low computational cost. However, the exact KS potential can be challenging to approximate, for example in the presence of localized subsystems where the exact potential is known to exhibit pathological features such as spatial steps [62]. By modeling two electrons, each localized in a distinct potential well, we illustrate that the step feature has no counterpart in MBPTs (including Hartree-Fock and *GW*) or hybrid methods involving Fock exchange because the spatial non-locality of the self-energy renders such pathological behavior unnecessary. We present a quantitative illustration of the orbital-dependent nature of the non-local potential, and a numerical demonstration of Kohn's concept of the nearsightedness [32, 63] for self-energies, when two distant subsystems are combined, in contrast to the KS potential. These properties emphasize the value of self-energy-based approximations in developing future approaches within KS-like theories.

6.1 Introduction

When considering the multiple approaches to the many-electron problem it is key to compare and contrast their respective strengths and weaknesses. Many-body perturbation theory (MBPT) is widely used for computing the electronic structure and properties of materials and molecules [55, 13, 64, 24, 49, 15, 52, 65, 50], yet approximate Kohn-Sham density functional theory (KS-DFT) is often favored owing to its accuracy at a low computational cost [**?** 45, 66, 31, 67]. The price for the computational efficiency is the difficulty in developing advanced approximations to the spatially local exchange-correlation (xc) potential of KS theory, $V_{\text{xc}}(\mathbf{r})$ [68]. It has been noted that some modern approximate density functionals tend to focus on calculating accurate energies from empirical data to the detriment of the density [69]. In finite systems, reproducing the exact many-electron density requires $V_{\text{xc}}(\mathbf{r})$ to contain pathological features [70, 62, 71], which common approximations fail to capture [60]. Thus practical calculations can be less reliable, e.g. for systems with strong localization such as molecules [12]. In MBPT, on the other hand, exchange and correlation are described using a spatially non-local and energy-dependent potential, the self-energy operator. Generalized Kohn-Sham approaches [72] have much in common with MBPT and are known to avoid some of the pathological aspects of KS theory insofar as quasiparticle energies are concerned [73, 74].

We describe the many-electron density in both *exact* KS-DFT and two examples of MBPT for two interacting[1] electrons in a 1D asymmetric double-well external potential (figure 6.1(a)) for which a spatial step is known to be present in the exact KS potential [62]. As in previous chapters, we use like-spin electrons in order to more closely capture the nature of exchange and correlation in larger systems. We calculate the exact KS potential for this system by first solving the many-electron Schrödinger equation using the iDEA code [46, 28] in order to find the exact ground-state many-electron density. Then we reverse-engineer the KS equations to find the corresponding exact KS potential for this system, $V_{\text{KS}}(x)$.

6.2 The exact Kohn-Sham potential

Figure 6.1(a) shows the exact many-electron density for our double-well system. The Coulomb repulsion between the electrons forces each electron in the system to localize in a distinct potential well. (In the absence of the Coulomb repulsion, both electrons would occupy the right well of the external potential as the lowest two non-interacting single-particle states of this system are localized in this well.) Figure 6.1(a) shows the KS potential which yields the exact density for this system: a spatial step is present in the potential[2]. The step acts to raise the right well by a constant relative to the left well. In doing so, the lowest energy state of the left well is made lower than the first excited energy state of the right well, and thus one occupied KS orbital is localized in the left well and the other is localized in the right well. This step feature has a non-local dependence on the density and is therefore beyond the capability of any common approximations [62, 60] to the KS-xc potential,

[1] We again use a softened Coulomb repulsion $(|x - x'| + 1)^{-1}$ as is appropriate in one dimension.

[2] While the KS potential shown yields the exact density to within computational precision, the localized nature of the two subsystems places a numerical limitation on the exact height of the step. However, analysis [62] shows that it must be at least 0.03 a.u.

such as the LDA [45] or GGAs [75].

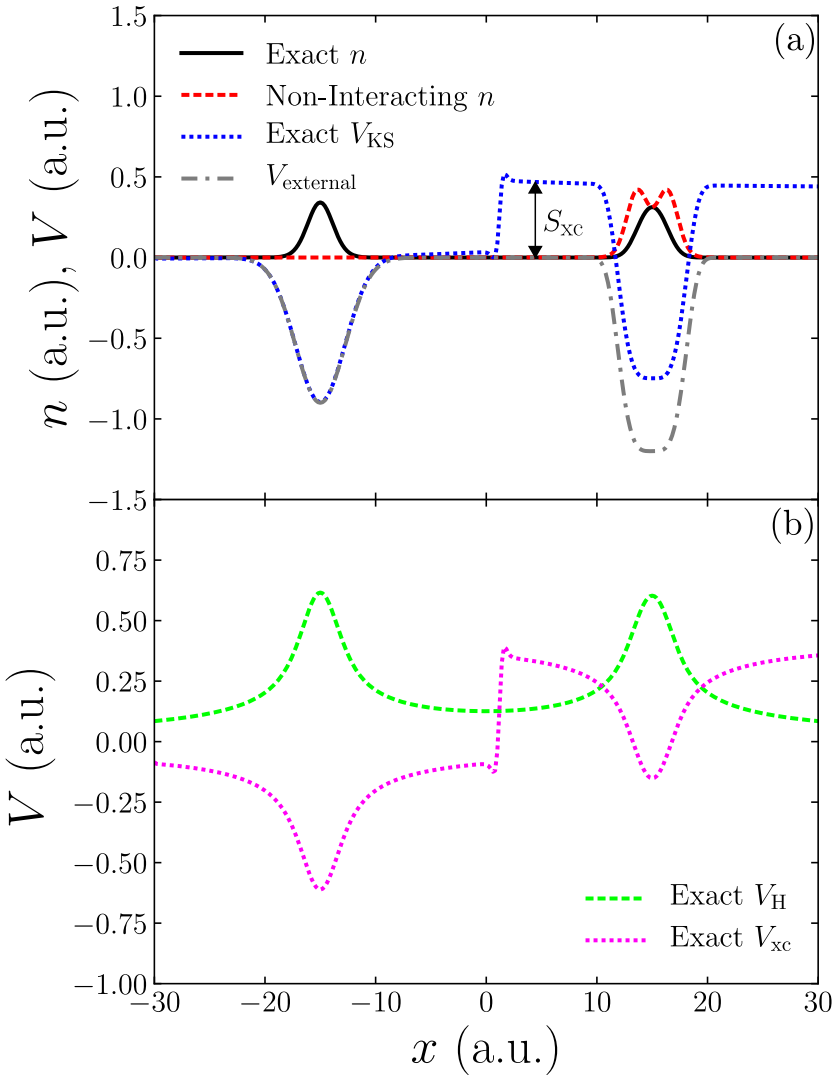

Figure 6.1: Exact many-electron density for two electrons in a 1D asymmetric double well and the corresponding exact KS system. (a) The exact many-electron and non-interacting density, the external potential and the exact KS potential. The external potential consists of two wells. The exact many-electron density corresponds to one electron in each well. Both of the non-interacting electrons occupy the right well. The exact KS potential for this system contains a step feature which raises the energy of the right subsystem by a constant, ensuring the correct distribution of electrons between wells. (b) The Hartree potential consists of two repulsive bumps centred one on each well, and the KS-xc potential is essentially the negative of the Hartree potential plus the step.

The step in the KS potential is sharp owing to the large spatial separation of the potential wells in our system, which in turn means that the electrons are strongly localized. The step forms at the point in the density where the local effective ionization potential (IP) changes [62]. This change occurs at the interface between the two individual potential wells (subsystems).

6.3 The exact self-energy for the ground-state density

We now turn to the Hartree-Fock (HF) description of this system, the lowest level of MBPT. The HF ground-state density is extremely precise as expected for what is essentially two distant one-electron subsystems, this is shown in figure 6.2.

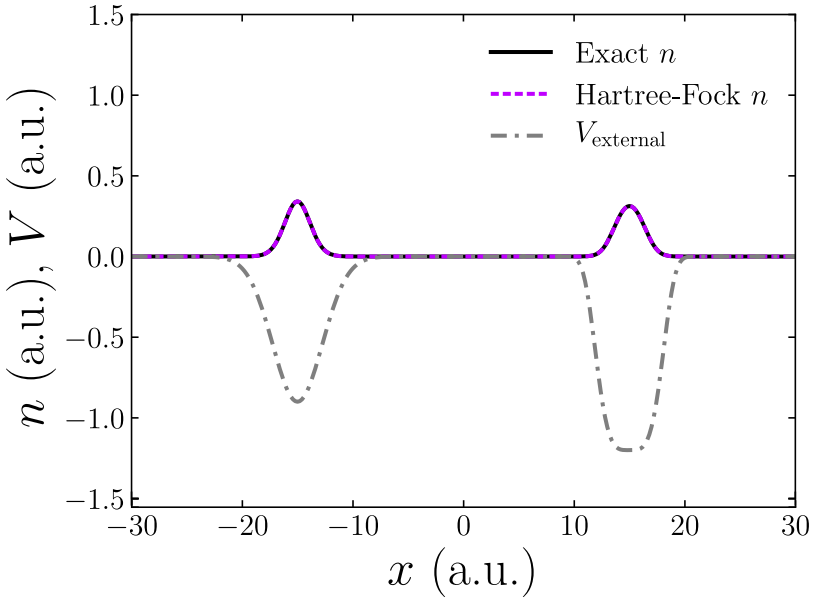

Figure 6.2: The double well ground-state density from by HF theory. As this system is composed of two separate subsystems a large distance apart, there is negligible overlap between the left and right orbitals and therefore negligible correlation. Therefore we see that HF yields an almost exact density.

In figure 6.3(a) we show the Fock operator for this system: no features corresponding to the step in the KS potential are visible and the operator appears to have an approximately local dependence on the density. F is seen to be non-local on the length scale of the subsystem, but *not* of the overall system. Our analysis of the nearsightedness of the Fock operator below constitutes a quantitative confirmation of these observations.

6.4 The nearsightedness of many-body perturbation theory

Our concept of an effective orbital-dependent local potential introduced in chapter 5 is illustrative here. For a particular orbital, the mathematical effect of a non-local potential is exactly equivalent of an effective local potential; in the case of the exchange operator this is

$$V^{\text{eff}}_{\text{x},m}(x) = \frac{1}{\phi_m(x)} \int F(x,x')\phi_m(x')dx'. \tag{6.1}$$

It is key to note that this effective potential is different for every orbital, in contrast to KS theory in which every electron feels the same local effective potential.

Figure 6.3(b) shows the effective potentials felt by $\phi_1(x)$ in HF theory[3]. This orbital is localized in the left well. It feels the external potential and the Hartree potential of the *whole* system, which consists of two large positive bumps; one is in the region of the left well and the other the right well. In addition, ϕ_1 feels its effective local exchange potential, which acts to cancel out the Hartree potential on the left, i.e., the self-interaction correction (SIC), but is negligible on the right; see figure 6.3(b). Figure 6.3(c) shows the resulting net potential felt by ϕ_1: the left electron feels the Coulomb repulsion due to the right electron, ensuring that each electron occupies its own well in accordance with the many-electron picture. Thus, for weakly correlated system, such as this one, HF successfully localizes electrons. For systems comprising more complex separated subsystems, further vertex corrections beyond *GW* can be significant, but nearsightedness should remain assured by the self-energy diagrams' analytic dependence on the single-particle orbitals, with terms connecting the two systems going to zero at large separations.

It is straightforward for the Fock operator to remove the self-interaction (SI) part of the Hartree potential *for each electron separately* owing to to its spatial non-locality. In contrast, the spatially local exact xc potential does not have such freedom, and must remove the SI part of the Hartree potential for all electrons simultaneously, this acts to essentially cancel the *whole* Hartree potential; see figure 6.1(b). Thus, without each electron experiencing the Hartree potential due to the other electron, the KS potential must instead include a spatial step at the interface between the electrons.

[3]To handle the singularity arising from the node in $\phi_1(x)$ which occurs in the vicinity of the right well, a careful numerical treatment of the denominator of Eq. 6.1 is necessary.

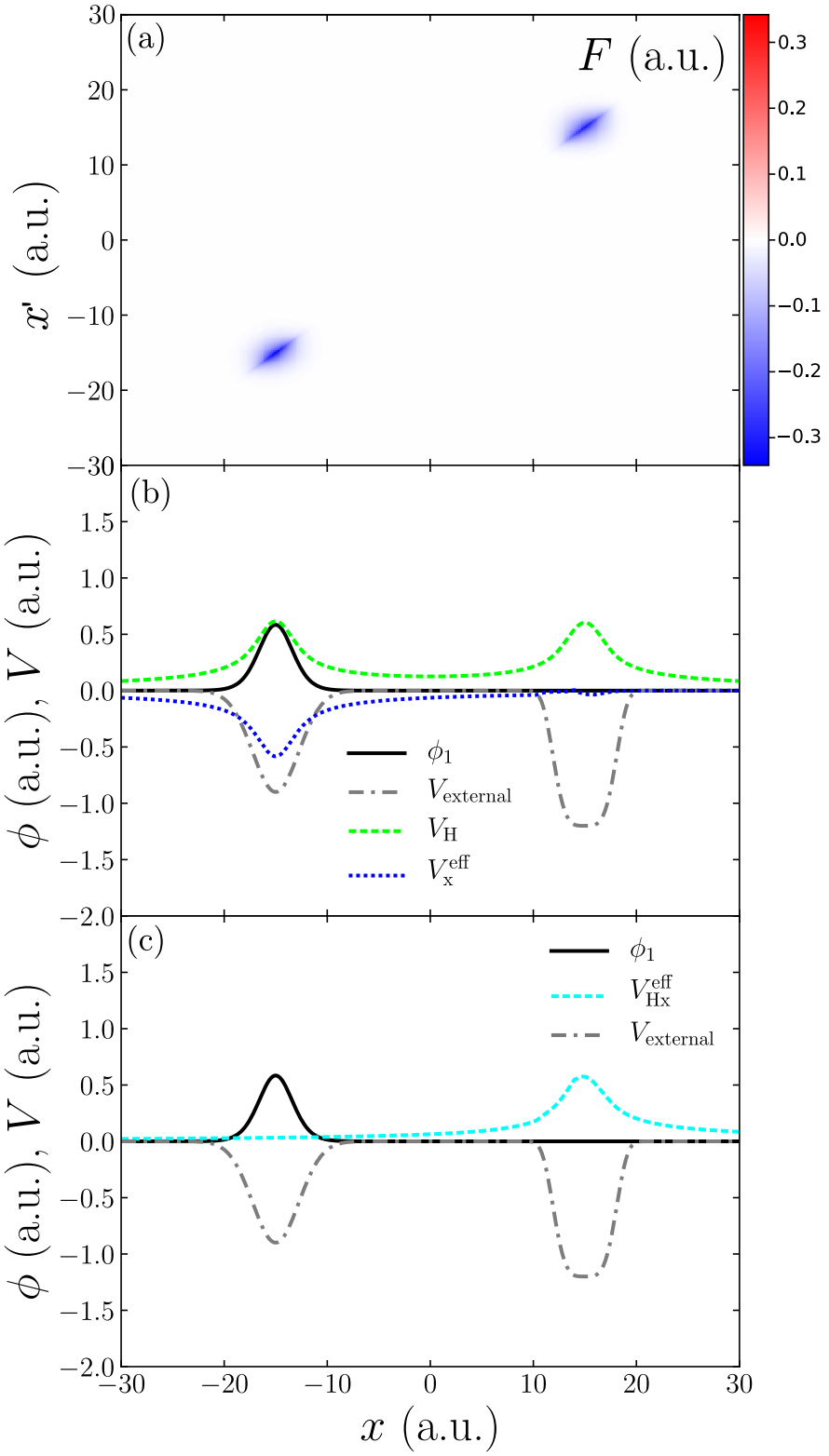

Figure 6.3: The double well described by HF theory. (a) The Fock operator, which as shown in figure 6.2 yields a highly accurate density. The pathological features in the exact KS potential are absent. (b) Effective potentials (see text) experienced by ϕ_1. It 'feels' the external potential $V_{\text{ext}}(x)$, the Hartree potential $V_{\text{H}}(x)$ of the whole system, which consists of a repulsion bump from both orbitals (ϕ_0 and ϕ_1) and its own effective exchange potential $V_{\text{x},1}^{\text{eff}}(x)$ that acts to cancel the Hartree potential due to its own presence (SIC). (c) The overall effective Hartree-xc potential felt by orbital ϕ_1 – the electron in the left well feels the repulsion of the electron in the right well and vice-versa resulting in a density corresponding to one electron in each well as per the many-electron density.

To demonstrate that the Fock operator of the *whole* double-well system consists of the SIC for each electron and *no additional features* we calculate the Fock operator for each one-electron subsystem completely independently (F_L and F_R). For the case shown in figure 6.3[4], $F_L + F_R$ reproduces the Fock operator for the composite system to high accuracy as shown in figure 6.4: ~ 0.03 a.u. ($\sim 2\%$ of the scale on which F varies)[5], i.e.,

$$F(x, x') = F_L(x, x') + F_R(x, x'). \tag{6.2}$$

Equation 6.2 becomes exact in the limit that the subsystems are infinitely separated. This property of F (and more generally the self-energy in MBPT) is an example of Kohn's 'nearsightedness' principle [76], in which the physical properties of one subsystem are blind to those of another, distant, subsystem. In contrast, this is *not* the case for the exact KS potential. The exact $V_{\text{xc}}(x)$ for the left subsystem is simply the negative of the Hartree potential, and the same for the right subsystem. Therefore their sum does not reproduce the KS potential for the whole system as this contains the step at the interface between the subsystems, i.e.,

$$V_{\text{xc}}(x) = V_{\text{xc}}^L(x) + V_{\text{xc}}^R(x) + S_{\text{xc}}(x). \tag{6.3}$$

This highlights the straightforward nature of a non-local potential compared to a local potential.

[4]The plots show the non-local Fock operator on our spatial grid, and hence in our spatial basis.

[5]The density calculated from employing $F_L + F_R$ in the HF equations for the whole system yields a density which is very similar to the true HF density for this system: ~ 0.01 a.u. ($\sim 2\%$ of the scale on which n varies). This value approaches zero as the wells are separated.

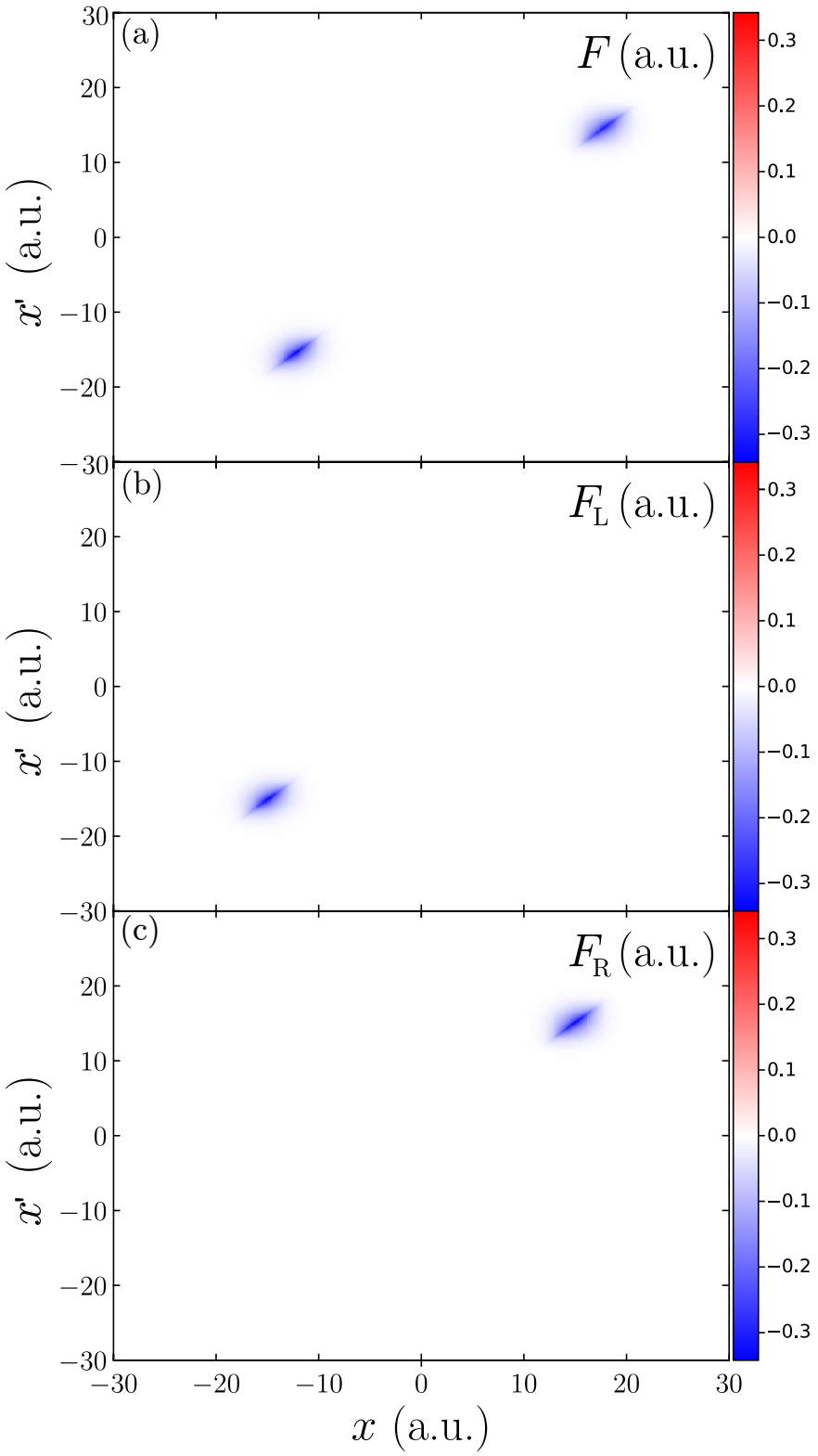

Figure 6.4: Demonstration that the sum of the Fock operators of the left and right subsystems yields the Fock operator of the composite system.

6.5 Orbital swapping in the *GW* method

We now move onto the *GW* approximation, the next level of MBPT. First, we demonstrate that the density from a one-shot (G_0W_0) calculation is surprisingly accurate even when starting from a set of orbitals which yield a very poor initial density. In our case we choose to start from the non-interacting orbitals of the external potential which yield a density that is quantitatively different from the many-electron density; see figure 6.1(a). As shown in figure 6.5(a), the G_0W_0 correctly gives one electron in each well in contrast to its starting point, but the shape of the density in the subsystems is broadened relative to the exact. We find that the self-energy swaps occupied and unoccupied starting orbitals[6] when the Dyson equation is solved as shown in figure 6.5(b). As the G_0W_0 case has a non-local potential these orbitals can be moved independently and thus the self-energy needs no step feature. This is in contrast to the KS case where all of the orbitals in the right well are shifted simultaneously by the magnitude of the step in order to get the correct occupation of KS electrons. This swapping mechanism implies that the accuracy of G_0W_0 depends on the features of the unoccupied as well as the occupied starting orbitals.

[6] We use first order perturbation theory when computing the updated quasi-particle energies from the self-energy.

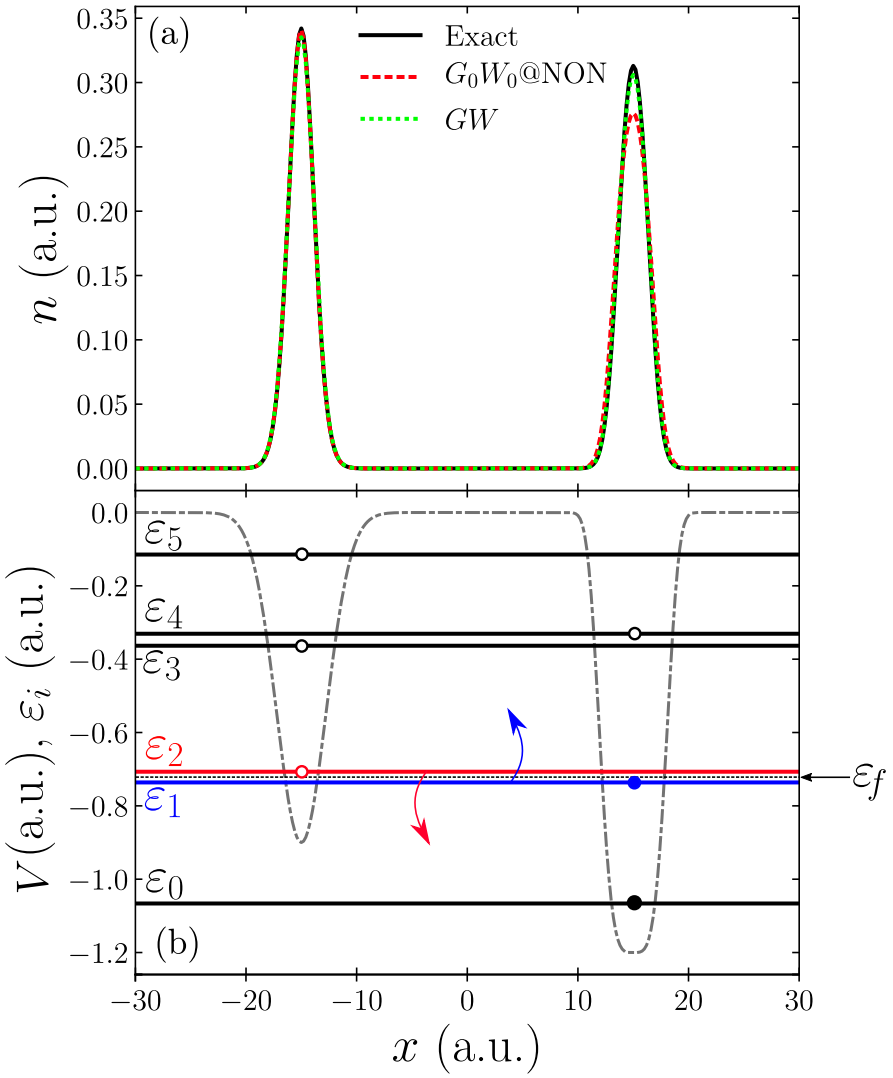

Figure 6.5: *GW* calculations for the double-well system. (a) One-shot G_0W_0 density starting with non-interacting (NON) orbitals yields a surprisingly accurate density, although the shape of the density in each well is broadened relative to the exact. The fully self-consistent *GW* density is much more accurate, as this broadening is significantly reduced. (b) Orbitals are swapped in the one-shot case. The horizontal lines (ε_0 and ε_1) indicate the non-interacting single-particle starting energies, where the circle on the line indicates in which of the two wells a particular orbital occupies – a filled circle indicates an occupied state and a hollow circle represents an unoccupied state. Initially both of the occupied orbitals are localized in the right well, thus giving the non-interacting density; see figure 6.1(a). In the first iteration of both *GW* calculations the orbitals of the self-energy are swapped; the HOMO orbital (blue) is raised above the Fermi energy, and the LUMO (red) is brought below. This means that after the swap one electron occupies the left well and the other the right, as required.

Second, we perform a fully self-consistent *GW* calculation for this system. The fully self-consistent *GW* density is very accurate, albeit slightly worse than HF. This small error in this density is due to the self-screening error [25, 44, 54, 27, 44, 27], which arises from a spurious non-zero correlation part of the self-energy as shown in figure 6.6.

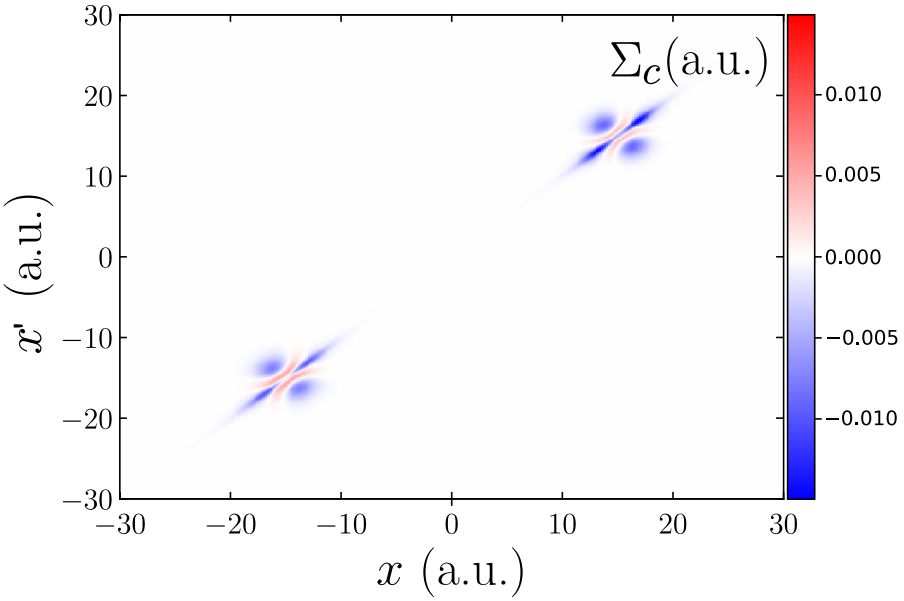

Figure 6.6: The self-screening potential for the double well system of the fully-self consistent *GW* method at $i\omega = 0$. This is the spurious part of the non-zero correlation self-energy.

We showed in chapter 5 that the self-screening error may be accurately corrected by a local-density-type expression which therefore retains Σ_{xc}'s nearsighted character within each well.

6.6 Relationship to the derivative discontinuity

We also consider an open system, connected to an electron reservoir, allowing a fractional number of electrons. The exact KS potential experiences a jump by a spatially constant shift Δ when the number of electrons, N, in the system infinitesimally surpasses an integer [70]. This is known as the 'derivative discontinuity' as it is a result of the discontinuity in the derivative of the total energy as a function of N. It is essential in KS theory if one wishes to determine the electron affinity (EA) from the single-particle KS energies of a system alone, yet it is not reproduced at all by common approximations [77, 68].

We now model only the right-hand well of our double-well system; see figure 6.7(a). We investigate what happens to the non-local potential of HF when $\delta = 10^{-4}$ of an electron is added to a one-electron system. First we calculate the exact density for the $1 + \delta$-electron system and the corresponding exact KS potential; see figure 6.7(a). When δ is small but finite, the shift Δ is a no longer uniform throughout all space but a plateau – it is uniform in the center but at each side has a step in the potential; see figure 6.7(a). The height of these steps is the discontinuity Δ. In the limit that $\delta \to 0^+$, these steps form further and further away from the well and hence the plateau becomes a spatially uniform shift [78].

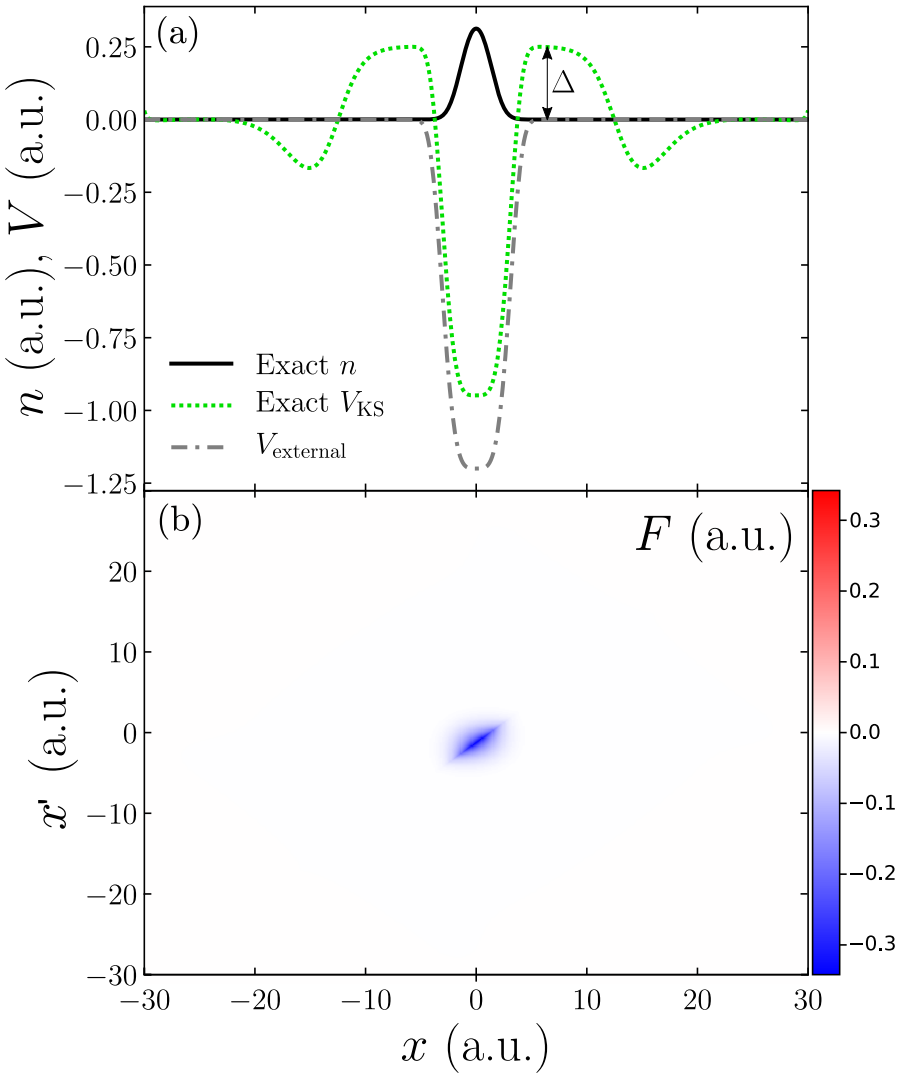

Figure 6.7: (a) The right-hand well of our double-well system with 1.0001 electrons. The exact electron density is indistinguishable from the HF density. The exact KS potential has a plateau in the vicinity of the well with height Δ. This plateau occurs in the KS system as a result of the derivative discontinuity. (b) The corresponding Fock operator contains no features which correspond to the steps in the KS potential.

The Fock operator corresponding to the $1 + \delta$-electron system is shown in figure 6.7(b). The steps in the KS potential do not correspond to any features in this Fock operator, and thus do not occur in the effective exchange potentials either. Instead, when δ of an electron is added to the HF system it experiences a different effective potential to the one felt by the whole electron which already occupies the well. The additional fraction of an electron experiences essentially just the Hartree potential of the whole electron originally in the system plus the external potential; whereas the whole electron in the system feels effectively no Hartree potential from δ. Thus δ has a higher energy than the other electron in the system which in turn determines the system's new IP without the need for any discontinuous change to the Fock operator. This reasoning also applies to the case for hybrid density functionals (which combine the Fock operator with a usually local xc potential) [79, 34, 80] and other schemes within generalized KS theory [72, 74] as well as the *GW* approximation, all of which are known to yield improved values for the fundamental gap (IP minus EA) compared to (approximate) Kohn-Sham gaps [79, 34].

6.7 Summary

In conclusion, a quantitative analysis of orbital-dependent effective potentials and the nearsightedness of the self-energy operator shows that the crucial pathological features of the exact Kohn-Sham exchange-correlation potential – beyond the capability of common approximations – are not required in the non-local potential of many-body perturbation theory: in effect, each electron is able to experience a different local potential. This emphasizes the potential value of constructs from self-energy methods in developing future approaches within KS-like theories.

Chapter 7

An alternative approach to the screened exchange potential: Koopmans-compliant hybrid functionals

In this chapter we consider an alternative approach to the *GW* screened exchange potential as a way of moving beyond Hartree-Fock theory; Koopmans-compliant hybrid functionals [81]. We evaluate the accuracy of electron densities and quasi-particle energy gaps given by hybrid functionals by directly comparing these to the exact quantities obtained from solving the many-electron Schrödinger equation. We determine the admixture of Hartree-Fock exchange to approximate exchange-correlation in our hybrid functional via one of several physically justified constraints, including the generalized Koopmans' theorem[47]. We find that hybrid functionals yield strikingly accurate electron densities and gaps in both exchange-dominated and correlated systems. We also discuss the role of the screened Fock operator in the success of hybrid functionals.

7.1 Introduction

A key measure of success for any electronic-structure theory is its ability to yield accurate electron densities and energies for many-electron systems. For example, Kohn-Sham (KS) density functional theory (DFT) [29, 30] is in principle exact, but the use of an approximate exchange-correlation (xc) potential, such as the local density approximation (LDA) [82] or the generalized gradient approximation (GGA) [75], is associated with a self-interaction error which can cause the spurious delocalization of localized charge [83] and incorrect dissociation behavior for molecules [84]. Recently, hybrid functionals that mix Hartree-Fock (HF) exchange with a (semi-)local approximation (such as the LDA or GGA) [79] have become popular as an alternative approach to xc. However, hybrids introduce at least one additional parameter, the mixing parameter α. This is often determined empirically, e.g., via experimental data, or through the adiabatic connection [85]. We determine α using a group of more physically justified constraints, including the generalized Koopmans' theorem [86, 87, 88, 89, 81]. While it has been shown that this constrained hybrid approach results in ionization energies and band gaps close to experimental values [86, 88], to date the electron density of this approach has not been directly compared to the exact density.

As Medvedev *et al.* [69] argue, progress in the accuracy of electronic structure calculations requires improvements in both energies *and* densities. Srebro *et al.* indirectly assessed densities obtained via hybrid functionals using the electric field gradient at the nucleus [90]. Reference [91] obtained densities from popular empirical hybrid functional parameterizations and found sensitivity to the value of the various mixing parameters.

In order to address the density more directly, we consider our set of model systems where the many-body problem can be solved exactly using the iDEA code, allowing for a direct comparison of densities, energy gaps and ionization potentials (IPs) obtained from the constrained hybrid approach to the exact values. We show that an *ab initio* determination of α results in hybrid functionals yielding extremely accurate densities and gaps.

7.2 Koopmans' compliant hybrid functionals

The exact total energy E (of a many-electron system) is piecewise linear with respect to the number of electrons, N [70, 92]. In exact KS DFT, the slope of each straight-line segment $\partial E/\partial N$ is shown by Janak's theorem to equal the highest (partly) occupied molecular orbital (HOMO) eigenvalue [93]. The usual approximate density functionals (LDA and GGAs), and HF, exhibit nonzero curvature $\partial^2 E/\partial N^2$, which can lead to qualitatively wrong physical behavior [10, 12, 68]. The curvatures are of opposite signs which means that hybrid approximations benefit from a partial cancellation of these errors[86, 87]. An illustration of the curvature is shown in figure 7.1

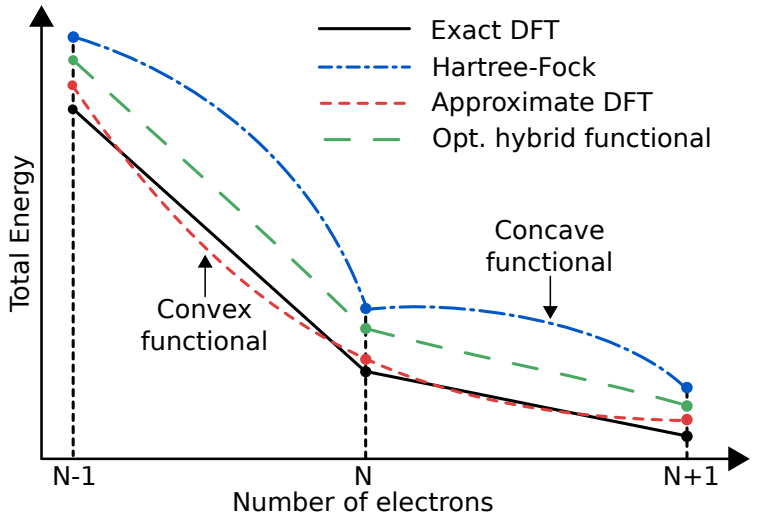

Figure 7.1: Illustration of the deviation from the piecewise linear behaviour of the energy against electron number curve for various approximations. Note the opposite curvature of the LDA and HF methods can be cancelled in a hybrid approach.

The exact total energy difference $E(N-1) - E(N)$ is both the ionization energy of the N–electron system, $I(N)$, and the electron affinity of the $(N-1)$–electron system, $A(N-1)$. In HF, the equivalent of Janak's theorem [94] shows that the slope $(\partial E/\partial N)_{N-\delta}$ is equal to the HOMO eigenvalue, and $(\partial E/\partial N)_{N+\delta}$ to the LUMO eigenvalue. In exact KS and exact generalized KS DFT, the LUMO eigenvalue differs from $A(N-1)$ by a discontinuity, Δ, in the xc potential [70]. Thus all three quantities $\varepsilon_N(N-1) + \Delta$ [1], $\varepsilon_N(N)$ and $E(N) - E(N-1)$ should, in principle, be equal, where Δ is non-zero for exact DFT methods. But for approximate methods such as hybrids where exchange and correlation are explicitly analytical functionals of the single-particle orbitals and therefore exhibit zero derivative discontinuity Δ, the first quantity becomes $\varepsilon_N(N-1)$ [94, 95, 72]. We may therefore identify three conditions,

(A) $\varepsilon_N(N-1) = -A(N-1) \equiv E(N) - E(N-1)$,

(B) $\varepsilon_N(N-1) = \varepsilon_N(N)$,

(C) $\varepsilon_N(N) = -I(N) \equiv E(N) - E(N-1)$,

which may be used to constrain a hybrid calculation by enforcing internal consistency. In practice, the parameter α of the basic hybrid approach provides a single degree of freedom and so can be used to impose (A) the LUMO-A condition *or* (B) the LUMO-HOMO condition *or* (C) the HOMO-I condition, or generalized Koopmans' theorem (GKT).

A key point regarding the hybrid approach is that the derivative discontinuity Δ in the xc potential not only *is* zero, but also *should be* zero. This is most clearly seen by noting that the description of exchange and correlation in the hybrid approach includes a reduced-strength Fock operator, essentially mimicking the screened exchange operator that is at the heart of the well-known GW approximation to the self-energy operator [13, 14, 96], plus LDA exchange and correlation reduced in strength. This identification of the hybrid approach's 'self-energy' as a screened-exchange approximation to the exact self-energy Σ_{xc}, as noted by other authors

[1] $\varepsilon_N(N-1)$ denotes the N^{th} eigenvalue for the $(N-1)$–electron system.

[97, 98], means that Σ_{xc} would yield exact electron addition and removal energies through its one-electron eigenvalues that then acquire the significance of quasiparticle energies. Hence in both the N and $(N-1)$–particle systems both the HOMO and LUMO energies may be regarded as fairly sophisticated approximations to the ionization potential and electron affinity, and therefore require no Δ correction.

The hybrid functional that we use for our main tests straightforwardly mixes HF with an LDA xc potential:

$$V_{xc}^{HYB}(\alpha) = \alpha V_x^{HF} + (1-\alpha) V_{xc}^{LDA}, \tag{7.1}$$

where V_{xc}^{HYB}, V_{xc}^{LDA} and V_x^{HF} denote the hybrid and LDA xc potentials [2] and the non-local HF exchange potential, respectively. This has the advantage of focusing more on the variational power of HF for exchange-dominated systems and accommodating better the cross-over between exchange and correlation when the LDA is applied to inhomogeneous systems. We also explore the retention of the full LDA correlation potential, mixing only the exchange terms, in common with other hybrid functionals such as PBE0 [79]:

$$V_{xc}^{HYB}(\alpha) = \alpha V_x^{HF} + (1-\alpha) V_x^{LDA} + V_c^{LDA}. \tag{7.2}$$

We assess hybrid functionals (in the form of equation 7.1 unless otherwise stated) for a range of both exchange-dominated and correlated systems. The exact many-body wavefunction (used to compute the exact density) is obtained by direct solution of the many-body Schrödinger equation using the iDEA code [46]. As in previous chapters, the electrons interact via the softened Coulomb interaction and are treated as like-spin.

[2] The LDA used in this work is parameterized from finite slabs [47]; our testing has shown these give indistinguishable results compared to homogeneous electron gas (HEG)-based LDAs.

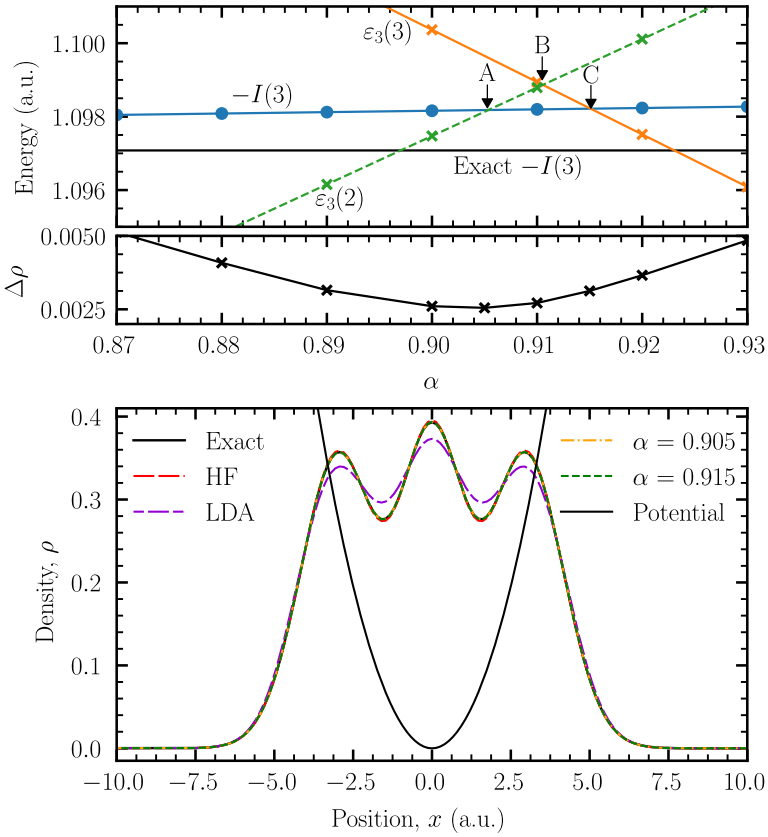

Figure 7.2: (Upper) The variation in hybrid ionization energy $I(3)(= A(2))$, exact $I(3)(= A(2))$, $\varepsilon_3(3)$ and $\varepsilon_3(2)$ with α are illustrated for three electrons in an harmonic oscillator with $\omega = 0.25$, an exchange-dominated system. Energies are in Hartree atomic units. There are three 'crossing points': (A) A-LUMO, (B) HOMO-LUMO and (C) I-HOMO. (Center) The integrated absolute error in the density $\Delta\rho$ is shown for each value of α. This is defined as $\int |\rho^{\mathrm{EXT}}(x) - \rho^{\mathrm{HYB}}(x)| dx$ where the ρ^{EXT} and ρ^{HYB} correspond to the exact and hybrid densities. (Lower) The densities for crossings (A) and (C) are benchmarked against the exact, LDA and HF cases; the hybrid, HF and exact curves lie close together.

7.3 Performance for model systems

7.3.1 Exchange-dominated systems

In figure 7.2 we demonstrate for the harmonic well with angular frequency $\omega = 0.25$ (an exchange-dominated system) that application of any of the conditions (A)–(C) yields an α very close to pure HF, i.e., $\alpha \approx 1$, as expected. Other exchange-dominated systems we tested yield similarly good results from the constrained hybrid.

Conditions (A)–(C) correspond to three 'crossing points', as shown in figure 7.2. Using the argument laid out previously, the self-energy should satisfy all three of these conditions. Generally, (A)–(C) correspond to different conditions that specify where the HOMO, LUMO and IP of a system lie with respect to one another. Although it clear from figure 7.2 that the three conditions cannot be exactly satisfied, the three crossing points lie pleasingly close together, and the density error $\Delta\rho$ (see Figure caption) is small in their vicinity. Generally, we find that densities obtained from α values lying between crossing points (A) and (C) are in excellent agreement with the exact case.

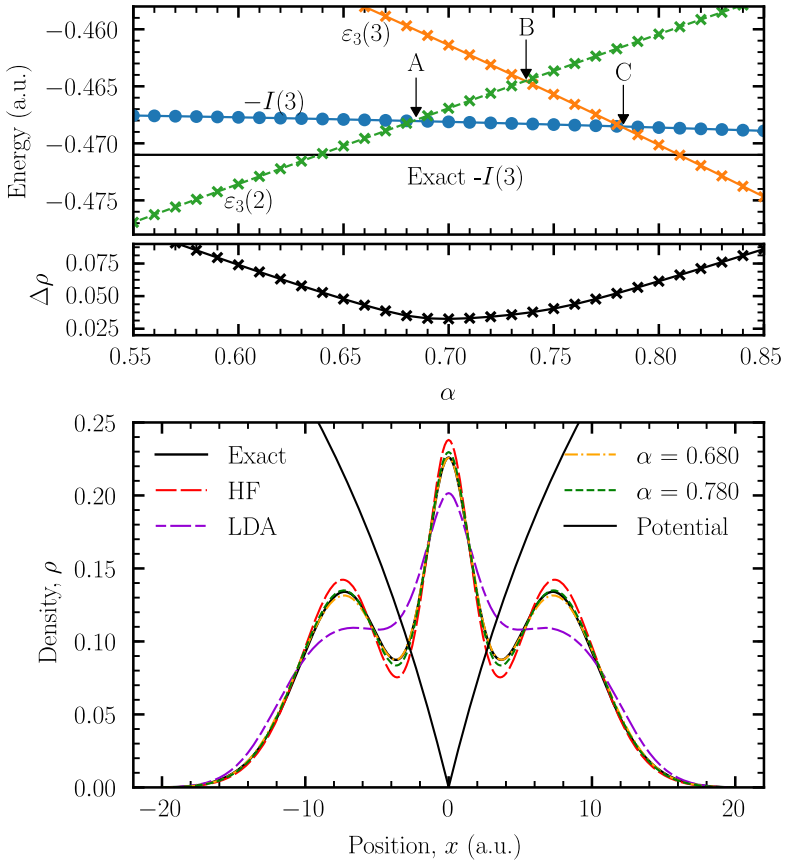

Figure 7.3: As figure 7.2, for three electrons in an atom-like external potential ($V_{\text{ext}}(x) = -1/(0.05|x| + 1)$). The system is correlated as HF fails to predict the exact density and energy.

7.3.2 Correlated systems

Given that both of the underlying functionals usually fail to produce a near-exact density in these systems, we ask: is a hybrid functional capable of reproducing a near-exact density for any value of α? We show the results in figure 7.3 for three electrons in an atom-like potential. Once again, all three conditions (A)–(C) produce values of α that yield strikingly accurate densities.

Although in the exchange-dominated case crossing points (A) and (C) correspond to an α differing by only one percent, in the correlated system we find that they differ more ($\sim 10\%$). Crucially, however, the density error $\Delta\rho$ corresponding to condition (A) and (C) is better than 0.03. Hence, as before, each density corresponding to these conditions is in excellent agreement with the exact. We note that condition (A) corresponds to a *slightly* better density than (C), the GKT, for both this correlated system and the exchange-dominated system. The alternative hybrid strategy of mixing only the exchange potentials yields accurate, but slightly inferior densities, as shown in figure 7.4, this is due to the breaking of the cancellation of errors between the exchange and correlation terms of the LDA.

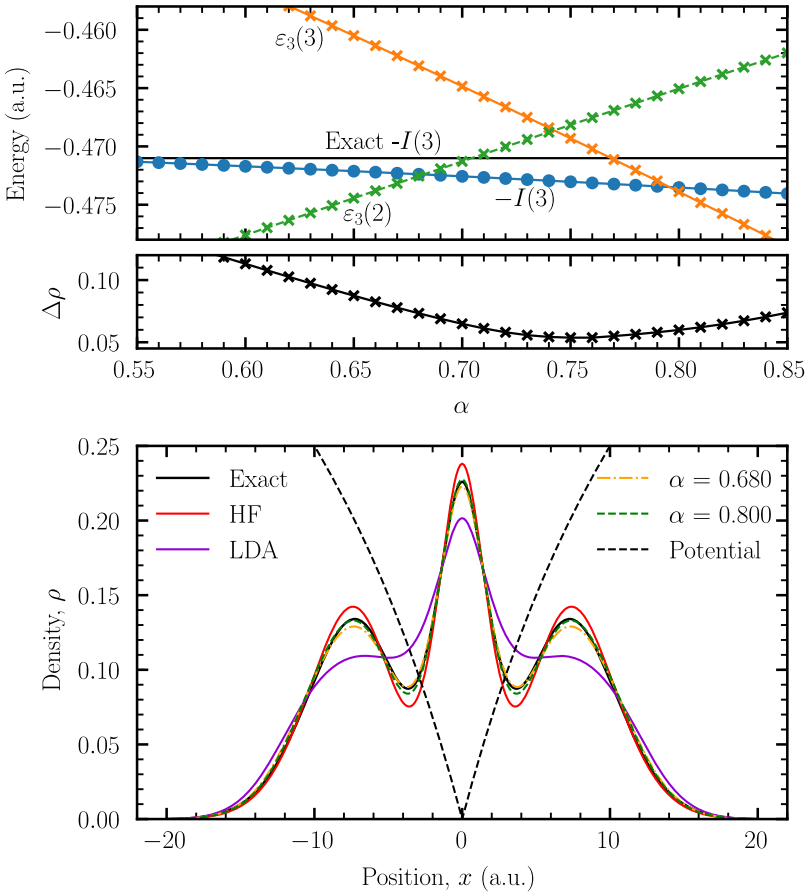

Figure 7.4: To be compared with figure 7.3. Three electrons in the atom-like external potential. In this case the hybrid uses the exchange only form of mixing. This illustrates that both forms of mixing yield similar densities. However, we note that the (global) density error minimum is higher when using exchange-only-mixing (0.05) compared to exchange-and-correlation mixing (0.025), used in the main paper.

In order to verify that the curvature $\partial^2 E/\partial N^2$ in our functionals is indeed better using the constrained hybrid approach, we calculate the derivative of energy with respect to number of electrons $\partial E/\partial N$, shown in figure 7.5 [3]. It can be seen that the HF case is exact for values leading up to one–electron, however curvature is present for anything larger. This is as expected, as the HF energy and density are exact for one electron systems. Unlike HF, the LDA is inexact for all numbers of electrons. The α values corresponding to conditions (A) and (C) in the atom-like potential follow the exact line much more closely than the LDA and HF between 2 and 3 electrons, the region where conditions (A)–(C) have been imposed. This suggests that the curvature has indeed been reduced. Comparing the curvature for conditions (A) and (C), we see that the two are comparable to one another.

[3] As calculated in Reference [93]

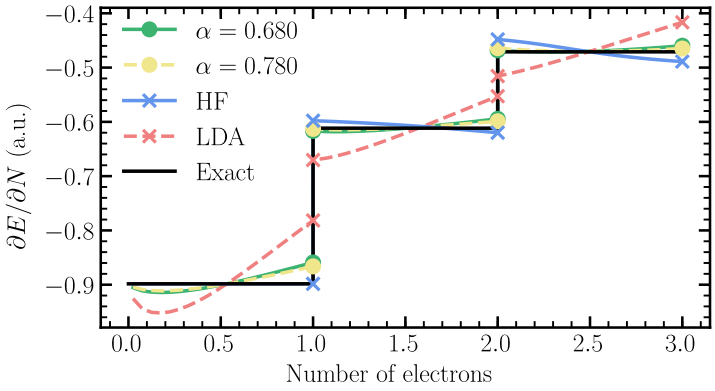

Figure 7.5: The derivative of energy with respect to total number of electrons N, $\partial E/\partial N$, for a number of approximations. The external potential and α values chosen are the same as that of figure 7.3. We verified that the $\partial E/\partial N$ curve lies exactly on that of the HOMO eigenvalue within each approach. Each node at integer numbers of electrons corresponds to the HOMO and LUMO, with the lower energy value being the HOMO.

7.3.3 The fractional dissociation problem

We now demonstrate that hybrids are capable of rectifying the fractional charge problem common to many xc approximations for molecular dissociation. Specifically, we test a system with two separated wells where the usual DFT approximations inaccurately predict the amount of charge present in each well. Figure 7.6 demonstrates that, when compared with the exact case, the constrained hybrid approach and HF yield near-exact densities. In addition, we show that even for a small fraction of exact exchange ($\alpha = 0.200$), the correct charge in each well is obtained, and hence a large range of values of α yield accurate densities. However, the density has an incorrect shape within each well when an α not corresponding to conditions (A)–(C) is used [4]. This large range of α values that yield a highly accurate density shows the advantage of the nearsightedness of the exact-exchange operator present in the hybrid Hamiltonian.

[4] We anticipate than bonded open-shell atoms would constrain α more closely.

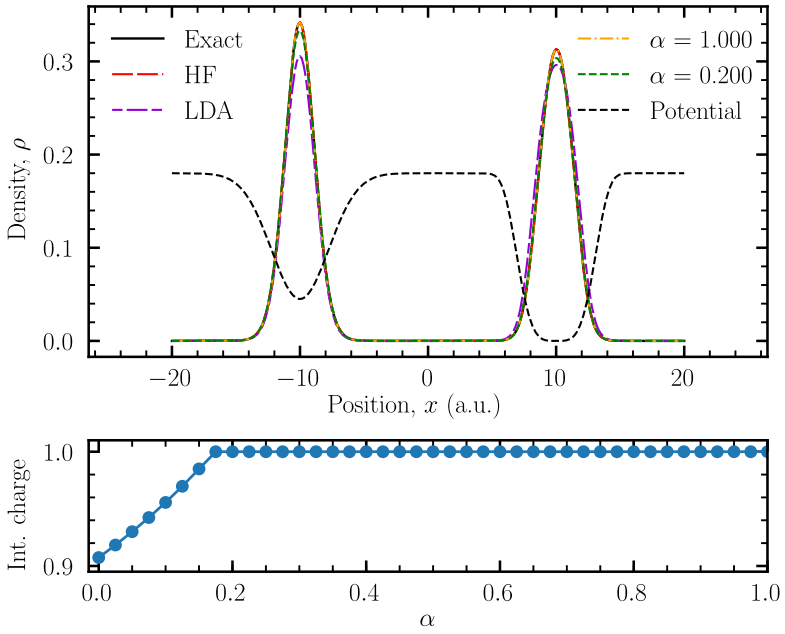

Figure 7.6: (Upper) Densities for various approximations are shown for an exchange-dominated asymmetric double-well potential. The dashed line, illustrating the potential (scaled by 0.15), shows that the two wells are asymmetric. The HF case follows the exact one, placing one electron in each well of a strongly localized system. The LDA predicts that an additional 0.1 electrons are present in the deeper well. The GKT yields $\alpha \approx 1$, effectively HF. We show the density for $\alpha = 0.2$, which places the correct charge in each well, but has an incorrect density shape. (Lower) The integrated charge of the left (shallower) well is shown for a range of α values.

7.3.4 Accuracy of quasiparticle energies

We now show in Table 7.1 that the accuracy of hybrid functionals for densities is not at the expense of energies. Of particular interest is the quasiparticle energy gap $(I - A)$, which the LDA and HF usually under- and over-estimate, respectively, as well as the values of I and A individually. This establishes contact with the performance of Koopmans-compliant hybrids in 3D systems [86, 96, 99] and suggests that useful quasiparticle energies can be extracted from functionals which also produce an accurate density. The tendency of constrained hybrids to reduce these energy gaps from HF to near-exact levels further supports the idea that this approach is similar to a screened-exchange method.

Table 7.1: The quasiparticle gap of two-electron systems as extracted from the LDA, HF and hybrid[5] HOMO-LUMO eigenvalue differences, compared to the exact gap calculated from many-body total energies. Gaps are compared for the exchange-dominated (harmonic) and correlated (atom-like) systems. The two-electron IPs are shown for the same systems.

(a.u.)	LDA	HF	Hybrid	Exact
Quasiparticle gaps				
Harmonic	0.222	0.491	0.472	0.469
% error	53%	5%	1%	–
Atom-like	0.037	0.172	0.152	0.141
% error	74%	22%	8%	–
Ionization potentials				
Harmonic	-0.761	-0.620	-0.629	-0.628
% error	21.2%	1.3%	0.2%	–
Atom-like	0.551	0.620	0.608	0.612
% error	9.9%	1.4%	0.5%	–

7.4 Summary

Through direct comparison of solutions to the exact many-body Schrödinger equation, we have shown that hybrid functionals yield accurate densities *and* quasiparticle energy gaps in both exchange-dominated and correlated systems, if the fraction of exact exchange, α, is chosen using physically justified constraints, such as the generalized Koopmans' theorem. Particularly accurate densities are obtained from a hybrid strategy that mixes LDA correlation, as well as LDA exchange. The three studied constraints are all in close agreement with one another and all yield accurate densities and gaps. In double-well systems, we find that hybrid functionals perform well and are free from the fractional dissociation problem for a large α range. Once the accuracy and reliability were confirmed in this study, hybrids of this type were successfully applied to model the formation of polarons in TiO_2 [100]. A key perspective is the interpretation of a hybrid method as a simple screened-exchange approximation within many-body perturbation theory, which brings with it the benefits of nearsightedness as described in Chapter 6.

Chapter 8

Time-dependent densities from many-body perturbation theory

Common approximations to the exchange-correlation (xc) potential within time-dependent density functional theory (TDDFT), such as the adiabatic local density approximation (LDA) yield extremely poor electrical properties when applied to systems driven by electric fields, predicting largely incorrect currents [12]. In order to systematically improve upon such methods, we must investigate the nature of such failings by considering the erroneous features in the predicted time-dependent densities. The approach we take is to compute the exact real-time evolving density for a series of systems that exhibit the characteristic physical phenomena of atoms being driven by electric fields, this includes strong electron interaction effects. We show that the adiabatic LDA, as expected, yields very poor time-dependent densities for such systems. Many-body perturbation theory (MBPT), in particular the Hartree-Fock (HF) and the *GW* approximation, is successfully used to calculate the ground-state properties of materials as well as the spectral function [14, 101], yet is more rarely used for real-time evolution of the electron density owing to the computational cost. The most significant contribution to this computational cost is the requirement to explicitly store the two-point quantities required for non-equilibrium Green's function approaches, such as the propagation of the Kadanoff-Baym equations [36, 38, 37, 39].

In this chapter we investigate a significantly cheaper and simpler form of time-dependent many-body perturbation theory (MBPT), using both the HF and *GW* approximations to the self-energy. This is motivated by the accurate account of strongly localized electrons captured by the exact-exchange operator as illustrated in chapter 6, and the accurate modeling of ground-state correlation of the inertial flavor of the *GW* approximation as presented in chapter 4. We show the quality of real-time evolving densities produced by such methods greatly improves upon the adiabatic LDA for our set of challenging model systems.

8.1 Introduction

Time-dependent density functional theory (TDDFT) is in principle a powerful method for simulating dynamic properties of matter. It is commonly used within chemistry to calculate the optical absorption spectra. However, existing approximations to its exchange-correlation (xc) potential are unreliable in the presence of strong currents. Within the Kohn-Sham (KS) approach, TDDFT employs an auxiliary system of non-interacting electrons subject to the effective time-dependent KS potential, $V_{\mathrm{KS}}[n](x,t)$, which yields the exact many-electron time-dependent electron density. The KS potential is usually split into the external potential of the many-electron system, the Hartree potential, and the exchange-correlation (xc) potential, $V_{\mathrm{xc}}[n](x,t)$. In practice the xc potential must be approximated. The most common approximation is the adiabatic LDA, which has a local and adiabatic dependence on the density which completely neglects important memory effects.

We assess the accuracy of the time-dependent electron density yielded from MBPT, and the adiabatic LDA within TDDFT, by comparing to the exact many-electron density. We construct simple one-dimensional model nanostructures consisting of 2 electrons whose time-dependent many-body wavefunction, and hence time-dependent density, can be computed exactly using the iDEA code. We construct several model systems that each capture the physical phenomena present in molecular junctions, such as correlated electrons within an atom being driven by an external electric field. These systems are designed to exhibit dynamic exchange and correlation effects in order to fully test the ability of each approximation. For this set of systems we compare the exact time-dependent density to those computed by the adiabatic LDA of TDDFT and time-dependent Hartree-Fock (TDHF). In addition, we assess the accuracy of a novel method of TDGW, by using our static model of screening – inertial screening – to screen the exchange potential within TDGW.

We also test the performance of these approximations for a particularly challenging system in which correlation increases over time: two electrons colliding in an atom. Dynamic correlation effects of this type are extremely difficult for adiabatic approximations with TDDFT. We show that the MBPT approaches yield more accurate densities owing to the spatially non-local potential.

8.2 Time-dependent many-body perturbation theory

The time-dependent density within TDHF can be calculated from the occupied orbitals obtained by solving

$$\left(-\frac{1}{2}\frac{\partial^2}{\partial x^2} + V_{\mathrm{ext}}(x,t) + V_{\mathrm{H}}(x,t)\right)\phi_i(x,t) + \int \Sigma_{\mathrm{x}}(x,x',t)\phi_i(x',t)dx' = i\frac{\partial}{\partial t}\phi_i(x,t), \quad (8.1)$$

where $V_{\mathrm{H}}(x,t)$ is the Hartree potential, $\Sigma_{\mathrm{x}}(x,x',t)$ is the Fock operator and $V_{\mathrm{ext}}(x,t)$ is the external potential which includes the perturbation. The flow chart in Figure 8.1 (black arrows only) details how the TDHF orbitals are propagated through time.

We now propose screening the exchange potential in order to take account of correlation while maintaining the propagation of single-particle orbitals. We first con-

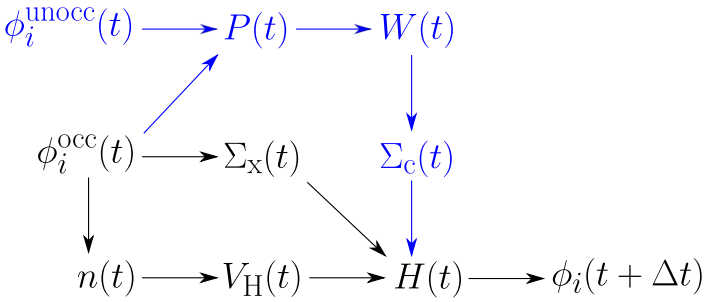

Figure 8.1: Flow chart depicting the TDHF method (black arrows only). The Hamiltonian H is used to evolve the TDHF orbitals over a time-step Δt using the Crank-Nicholson method. In addition to the single-particle kinetic energy and the external and perturbing potentials, H is constructed from the Hartree, V_{H}, and exchange, Σ_{x}, potentials. We then modify this approach to approximately take account of correlation using our proposed TDGW method (additional blue arrows). The correlation potential Σ_{c} is computed from a statically screened Coulomb interaction W which also depends on the unoccupied orbitals via our static approximation to the polarizability P.

sider the usual approximation to P; the RPA. As discussed in Chapter 4 this approximation neglects the electron-hole interactions. If we used this dynamic P to screen the exchange potential we could not evolve the wavefunctions in the same way as in the TDHF case, as the self-energy would become non-Hermitian. One viable alternative is to use an energy-independent self energy. An example of which is the Coulomb-hole-screened-exchange (COHSEX) approximation

$$P_{\text{COHSEX}}(x,x') = P_{\text{RPA}}(x,x',i\omega=0). \tag{8.2}$$

An alternative method which in Chapter 4 was shown to yield more accurate ground-state densities is inertial screening, which is described by

$$P_{\text{inertial}}(x,x') = P_{\text{RPA}}(x,x',it=0). \tag{8.3}$$

As well as its increased accuracy, inertial screening is advantageous as P only depends on the single-particle orbitals and not energies. Written in terms of the orbitals the inertial polarizability is given by

$$P_{\text{inertial}}(x,x') = -\left(\sum_k^{\text{occ}} \phi_k(x)\phi_k^*(x')\right)\left(\sum_k^{\text{unocc}} \phi_k(x')\phi_k^*(x)\right), \tag{8.4}$$

without needing to compute the full many-body Green's function. This then allows us to compute the screened Coulomb interaction by solving a single Dyson-like equation

$$W(x,x') = v(x,x') + \int v(x,x')P(x,x'')W(x'',x')dx''. \tag{8.5}$$

and from this at each timestep we can compute an approximate correlation potential

$$\Sigma_{\text{c}}^{\text{inertial}} = -\sum_k^{\text{occ}} \phi_k(x,t)\phi_k^*(x',t)\left(W(x,x') - v(x,x')\right); \tag{8.6}$$

This is then included in the Hamiltonian H, which can be used to propagate the single-particle orbitals as shown in Figure 8.1 (additional blue arrows).

8.3 Perturbing an atom with an electric field

In this next section we will look at applying our various approximate methods to a series of systems designed to exhibit the physical characteristics of several key parts of a molecular junction, and comparing the time-dependent density in each case to the exact. In each case we begin by computing the ground-state density, and then we turn on a uniform electric field at $t = 0$ of the form

$$V_{\text{perturb}}(x) = -0.01x \tag{8.7}$$

that causes a current to begin to build up as the electrons are driven out of their ground state.

We begin with a single atom, containing two electrons. In figure 8.2 we show the performance of each of our approximations at reproducing the exact time-dependent density. In panel (a) we show the ground-state density of our system and in panel (b) we show the time-dependent density at 100 atomic units of time after the electric field was turned on[1]. We find the expected result that the adiabatic LDA is very poor for this system due to significant correlation. Both it's ground state and time dependent density exhibit a largely incorrect shape. TDHF on the other hand is substantially more accurate over all times. It still does not have the correct density profile in the central highly delocalized region of the system. TDGW performs much better than TDHF for this correlated system until very large times, in order to extend the method to even larger times, vertex corrections could be included in the static P and also Σ.

[1]The propagation algorithm was tested for numerical stability for these long simulation times by verifying the harmonic potential theorem is obeyed by a comparable harmonic oscillator.

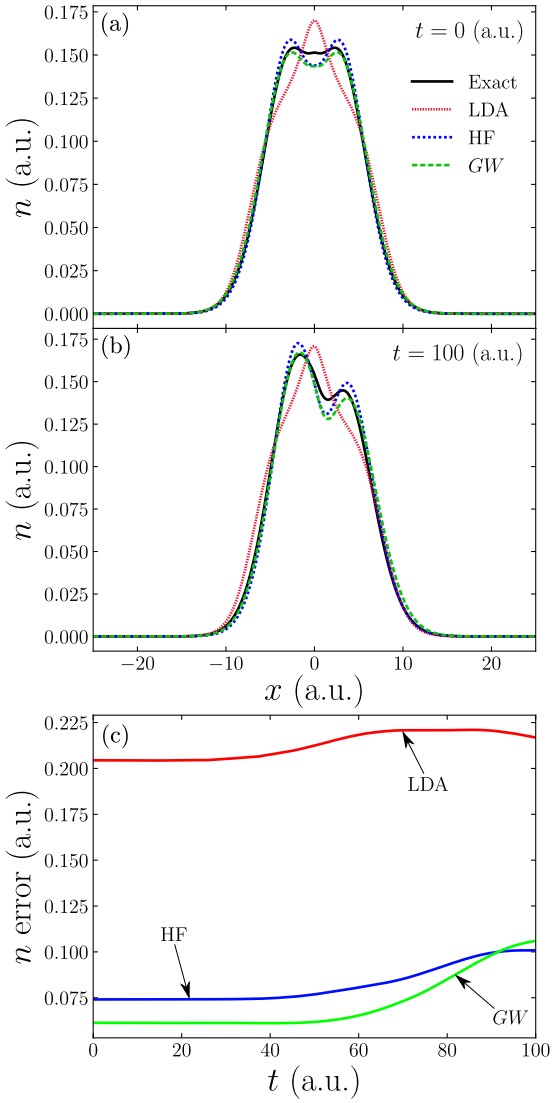

Figure 8.2: Exact and approximate ground-state and time-dependent densities for two like-spin electrons in a 1D correlated atom responding to an electric field. (a) The exact ground-state density for this system compared to approximate methods. The LDA yields a very poor density for this system giving a large spurious bump in the centre of the system, and a incorrect decay rate far towards the edges. Hartree-Fock (HF) performs much better than the LDA, yielding a much more accurate decay rate, but exhibiting a largely incorrect shape in the highly delocalized central region. It is this noteworthy difference between the exact and HF densities that shows the significant effect of correlation in this system. Finally, the static *GW* density is the most accurate method, yielding a marked improvement over the HF density. (b) Here we show the exact and approximate time-dependent density of this system at 100 atomic units of time after the electric field is applied, the electrons have been driven toward the right side of the well. The relative performance of each of the method remains much the same as in the ground-state case. (c) Here we show the error in the density for each of our approximate methods as a function of time. The time-dependent MBPT methods perform much better than the adiabatic LDA. The TD*GW* method outperforms TDHF for most of the evolution, as correlation is approximately accounted for. We see that this approximation begins to break down towards the larger times, although is still a large improvement upon the adiabatic LDA.

In figure 8.3 we show the exchange and correlation parts of the TD*GW* self energy for this system at $t = 100$. The upper left panel shows the real part of the exchange potential Σ_x and the lower right panel shows the real part of the correlation potential Σ_c. The correlation potential acts to screen the exchange potential by a factor of approximately 5.3%. The right panels show the corresponding imaginary parts, which is due to the time-dependent orbitals used to construct the potentials being complex valued[2].

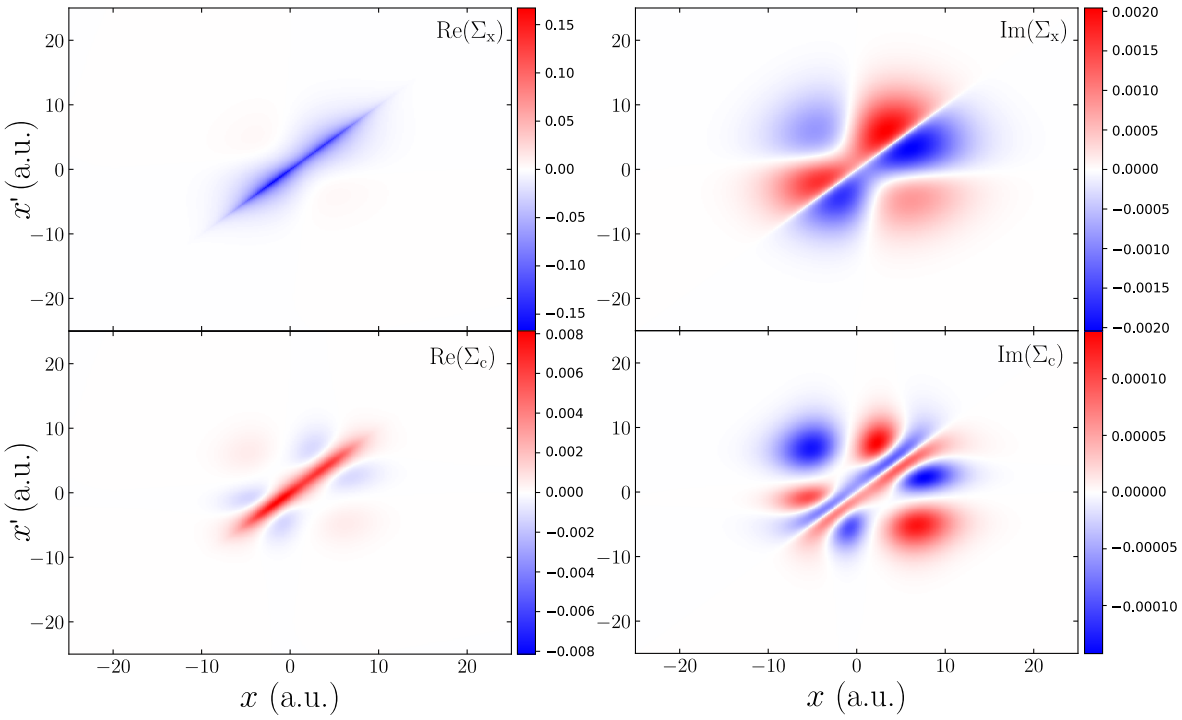

Figure 8.3: The time-dependent self-energy of the TD*GW* method for the two like-spin electrons in a 1D correlated atom responding to an electric field at $t = 100$ (densities shown in figure 8.2 (b)). The left panels show the real parts of both the exchange potential Σ_x (upper left) and correlation potential Σ_c (lower left). The correlation potential acts to non-locally screen the exchange potential. On the right panels we see the imaginary part of both potentials. These arise from the fact the orbitals used to construct the potentials are complex in the time-dependent case.

8.4 Electron collisions

Next we test our approximations for a particularly challenging system that is designed to have significant time-varying correlation. In particular a system that is initially well described by HF, whose driving perturbation causes a rapid increase in correlation. The system we choose is the collision of two electrons in an atom. We have established that the atom potential yields a correlated ground-state density in figure 8.2(a), and so we want to consider two electron being dropped into this atomic well from each side, causing the electrons to collide in the center. To achieve this effect we begin with the initial potential $V_{\text{atom}} + V_{\text{bump}}$ (see figure 8.4), where the bump is designed to hold the electrons away from the center of the system, one on the left and one on the right. For this potential the HF ground-state

[2]It is worth noting that these potentials are still Hermitian and conserve the orthonormality of the orbitals

density is extremely accurate (see figure 8.5(a)). At $t = 0$ we perturb the system by removing the bump (adding $-V_{\text{bump}}$ to the initial potential), and so the electrons begin to accelerate towards the center of the system and collide. We then follow the time-evolution long enough to see the initial collision, although in principle the time-evolution could be continued to see the emergence of an equilibrium state at long times.

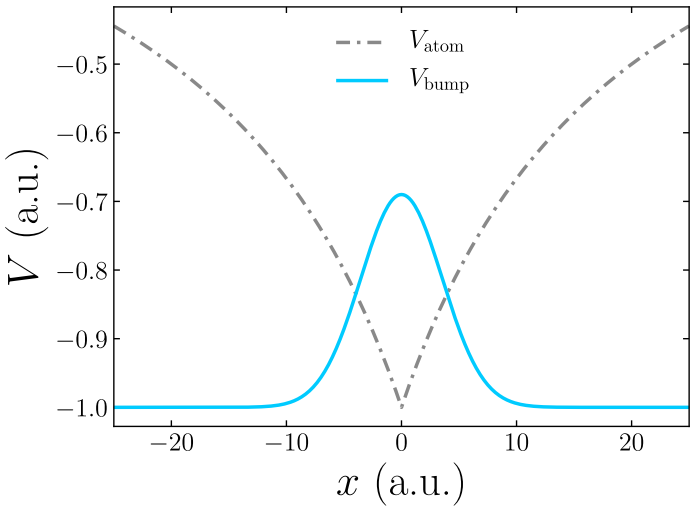

Figure 8.4: The potentials used to simulate two electrons colliding in a atom. Initially the potential is given by $V_{\text{atom}} + V_{\text{bump}}$, where the central bump is designed to hold both of the electrons out of the centre of the atom. At $t = 0$ we apply a perturbation that acts to remove the bump, giving the final potential just to be V_{atom}. This then causes the electrons to respond by falling into the centre of the well and colliding, creating very dynamic correlation effects.

In figure 8.5 we show the performance of each of our approximations at reproducing the exact time-dependent density for this system. In panel (a) we show the ground-state density of our system and in panel (b) we show the time-dependent density at 100 atomic units of time after the bump is removed. We see that the HF ground-state density is, by design, essentially exact. The inertial *GW* density is slightly worse, which is most likely due to the self-screening error, which could be corrected by the inclusion of vertex corrections in the self-energy[3]. The LDA yields a poorer density with the wrong sizes of the peaks. In panel (b) we show the density 100 atomic units of time after the central bump is removed, allowing the electrons to collide with each other in the centre of the atomic well. The TD*GW* method is the most accurate, yielding a relatively accurate shape of the density, in comparison to TDHF and adiabatic LDA, which both predict far too much charge in the centre of the system. In panel (c) we show the error in the density for each of our approximate methods as a function of time. The time-dependent MBPT methods perform much better than the adiabatic LDA. TDFT begins by outperforming TD*GW* but at the correlation begins to increase over time TD*GW* begins to become a larger improvement over TDHF.

[3]Such as our local self-screening correction developed in Chapter 5.

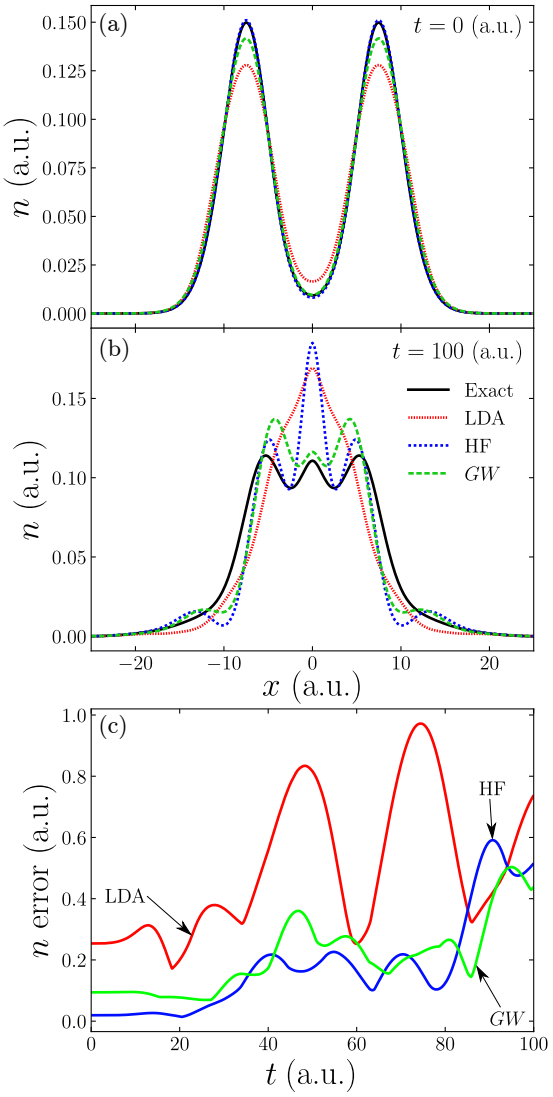

Figure 8.5: Exact and approximate ground-state and time-dependent densities for two like-spin electrons colliding 1D correlated atom. (a) The exact ground-state density for this system compared to approximate methods. By design, Hartree-Fock (HF) performs very well for the ground-state of this system, as there is little overlap between the orbitals as they are held away from the centre of the system by the bump (as shown in figure 8.4). The inertial *GW* method performs slightly worse, this is likely due to the self-screening error, which could be corrected by our local vertex correlation. The LDA yields a much poorer density, although it has the correct characteristic shape, just with the wrong sizes of the peaks. (b) Here we show the exact and approximate time-dependent density of this system at 100 atomic units of time after the bump is removed. As the electrons collide together the exact density becomes extremely dynamic (see supplemental material for full animation of time-dependence). At this large time after the perturbation the TD-MBPT methods slightly outperform the adiabatic LDA, with the TD*GW* yielding a qualitatively better density than TDHF. (c) Here we show the error in the density for each of our approximate methods as a function of time. The time-dependent MBPT methods perform better than the adiabatic LDA in particular for the qualitative shape of the density.

8.5 Summary

In this chapter we have presented a simplified form of time-dependent many-body perturbation theory that is able to give time-dependent densities that are significantly more accurate than conventional TDDFT approaches and substantially cheaper than non-equilibrium Green's function methods. We combine the simplicity of propagating single-particle orbitals, with the nearsighted non-local exact exchange potential, and a simple yet effective approximation to the static correlation potential. For challenging test systems these approaches yield promisingly accurate densities, and show further potential to be systematically improved via the inclusion of dynamic correlation effects and vertex terms in the self-energy.

Chapter 9

Conclusions

Accurate modeling of electron correlation is crucial to investigating and understanding many quantum systems that are integral to quantum technologies, such as molecular junctions. There are many approaches to this problem, such as ground-state and time-dependent density functional theory (DFT), and many-body perturbation theory (MBPT). In key systems that exhibit significant static and dynamic correlation, the ability of such methods to yield accurate results varies tremendously. A systematic understanding of the strengths and weaknesses of these methods is key to overcoming their limitations, and formulating improvements.

The approach we took in this thesis was to construct a set of model systems inspired by challenging large-scale systems, that are sufficiently simple such that the key quantities can be determined exactly by efficient numerical solution to the many-body Schrödinger equation. We compare these quantities to those predicted by commonly used methods in order to gain an understanding of the underlying causes of their merits and shortcomings. Once we attained a sufficient understanding of the reason why the common methods break down, we develop corrections and improvements. We then show, in our model systems, what advancements have been made over the usual methods, and what further limitations are yet to be remedied. We adopt the pragmatic view that these improvements should be computationally simple enough to be applied to large-scale problems.

We demonstrated that the accuracy of densities predicted by the *GW* approximation vary considerably depending on the flavour used. We showed that a pervasive systematic error that leads to substantial inaccuracy in the prediction of both the density and ionisation potential is the self-screening error, particularly in the most sophisticated fully self-consistent case. Following in-depth analysis of this error, we constructed a vertex correction in the form of a simple, computationally inexpensive, local density functional. When applied to our test systems this correction eliminated the unwanted effects of the self-screening error. It is hoped that in the future this correction can be implemented in large-scale codes and applied to systems consisting of many atoms and molecules. We show that further improvements beyond this correction are needed in order to accurately predict the density of particularly delocalized electrons, where electron-hole interactions must be accounted for.

We illustrated that many-body perturbation theory methods, such as Hartree-Fock and the *GW* approximation exhibit Kohn's concept of nearsightedness, unlike Kohn-Sham density functional theory. This means that the potential describing one sub-

system need not contain features to account for the presence of neighboring subsystems. This is due to the spatial non-locality of the potentials of MBPT, which we show need not contain the pathological features required in the spatially local exact Kohn-Sham potential, which are beyond most commonly used DFT approximations. Hence, advanced approximations which employ a non-local potential more easily encapsulate advanced aspects of exchange and correlation. One such method that builds upon the non-local exact exchange potential is hybrid functionals. We demonstrate that these hybrid functionals, when the fraction of exact exchange is chosen using physically justified constraints, yield extremely accurate densities. A further investigation will determine to what extent this concept can be applied to extended systems.

Finally, we apply our approach to the improvement of methods to compute time dependent densities. We use a form of time-dependent many-body perturbation theory that employs the propagation of single-particle orbitals, as in the TDDFT case, but with non-local potentials describing the exchange and correlation effects. We show that these methods significantly outperform the adiabatic LDA, yielding much more accurate time-dependent densities, but without the more onerous computational cost of non-equilibrium Green's function methods. Our presented method can in principle be systematically improved via the application of more advanced approximations to the non-local potential, such as the inclusion of vertex corrections.

Bibliography

[1] James L. McDonagh, Arnaldo F. Silva, Mark A. Vincent, and Paul L. A. Popelier. Quantifying electron correlation of the chemical bond. *The Journal of Physical Chemistry Letters*, 8(9):792–794, 2017.

[2] Maria Hellgren, Fabio Caruso, Daniel R. Rohr, Xinguo Ren, Angel Rubio, Matthias Scheffler, and Patrick Rinke. Static correlation and electron localization in molecular dimers from the self-consistent RPA and GW approximation. *Phys. Rev. B*, 91, Apr 2015.

[3] Fabio Caruso, Daniel R. Rohr, Maria Hellgren, Xinguo Ren, Patrick Rinke, Angel Rubio, and Matthias Scheffler. Bond breaking and bond formation: How electron correlation is captured in many-body perturbation theory and density-functional theory. *Phys. Rev. Lett.*, 110:146403, Apr 2013.

[4] O. Anatole von Lilienfeld, Ivano Tavernelli, Ursula Rothlisberger, and Daniel Sebastiani. Optimization of effective atom centered potentials for london dispersion forces in density functional theory. *Phys. Rev. Lett.*, 93:153004, Oct 2004.

[5] Gordon E. Moore. Cramming more components onto integrated circuits. *Institute of Electrical and Electronics Engineers*, pages 0–4, Apr 1965.

[6] Max Schulz. The end of the road for silicon? *Nature*, Jun 1999.

[7] James R. Heath and Mark A. Ratner. Molecular electronics. *Physics Today*, 56, 5 2003.

[8] C. Gimzewski Joachim and A. J. K. Aviram. Electronics using hybrid-molecular and mono-molecular devices. *Nature*, Nov 2000.

[9] N. J. Tao. Electron transport in molecular junctions. *Nature Nanotechnology*, 2006.

[10] Paula Mori-Sanchez, Aron J. Cohen, and Weitao Yang. Localization and delocalization errors in density functional theory and implications for band-gap prediction. *Phys. Rev. Lett.*, 100:146401, Apr 2008.

[11] C. A. Ullrich. Time-dependent density-functional theory beyond the adiabatic approximation: Insights from a two-electron model system. *The Journal of Chemical Physics*, 125(23):234108, 2006.

[12] Aron J. Cohen, Paula Mori-Sanchez, and Weitao Yang. Insights into current limitations of density functional theory. *Science*, 321(5890):792–794, 2008.

[13] Lars Hedin. New method for calculating the one-particle Green's function

with application to the electron-gas problem. *Phys. Rev.*, 139:A796–A823, Aug 1965.

[14] F. Aryasetiawan and O. Gunnarsson. The GW method. *Reports on Progress in Physics*, 61:237–312, Mar 1998.

[15] Lucia Reining. The GW approximation: content, successes and limitations. *Wiley Interdisciplinary Reviews: Computational Molecular Science*, 8(3):e1344.

[16] J. C. Slater. A generalized self-consistent field method. *Phys. Rev.*, 91:528–530, Aug 1953.

[17] J. C. Slater. Magnetic effects and the Hartree-Fock equation. *Phys. Rev.*, 82:538–541, May 1951.

[18] J. C. Slater. A simplification of the Hartree-Fock method. *Phys. Rev.*, 81:385–390, Feb 1951.

[19] K. Kaasbjerg and K. S. Thygesen. Benchmarking GW against exact diagonalization for semiempirical models. *Phys. Rev. B*, 81:085102, Feb 2010.

[20] Fabio Caruso, Matthias Dauth, Michiel J. van Setten, and Patrick Rinke. Benchmark of GW approaches for the GW100 test set. *Journal of Chemical Theory and Computation*, 12(10):5076–5087, 2016.

[21] C. Rostgaard, K. W. Jacobsen, and K. S. Thygesen. Fully self-consistent GW calculations for molecules. *Phys. Rev. B*, 81:085103, Feb 2010.

[22] P. Romaniello, S. Guyot, and L. Reining. The self-energy beyond GW: Local and nonlocal vertex corrections. *The Journal of Chemical Physics*, 131(15):154111, 2009.

[23] Andrew J. Morris, Martin Stankovski, Kris T. Delaney, Patrick Rinke, P. Garcia-Gonzalez, and R. W. Godby. Vertex corrections in localized and extended systems. *Phys. Rev. B*, 76:155106, Oct 2007.

[24] M. Shishkin, M. Marsman, and G. Kresse. Accurate quasiparticle spectra from self-consistent GW calculations with vertex corrections. *Phys. Rev. Lett.*, 99:246403, Dec 2007.

[25] W. Nelson, P. Bokes, Patrick Rinke, and R. W. Godby. Self-interaction in Green's-function theory of the hydrogen atom. *Phys. Rev. A*, 75:032505, Mar 2007.

[26] Alan M. Lewis and Timothy C. Berkelbach. Vertex corrections to the polarizability do not improve the GW approximation for molecules. *https://arxiv.org/abs/1810.00456*.

[27] Yao-Wen Chang and Bih-Yaw Jin. Self-interaction correction to GW approximation. *Physica Scripta*, 86(6):065301, 2012.

[28] J. Wetherell, M. J. P. Hodgson, and R. W. Godby. GW self-screening error and its correction using a local density functional. *Phys. Rev. B*, 97:121102, Mar 2018.

[29] P. Hohenberg and W. Kohn. Inhomogeneous electron gas. *Phys. Rev.*, 136:B864–B871, Nov 1964.

[30] W. Kohn and L. J. Sham. Self-consistent equations including exchange and correlation effects. *Phys. Rev.*, 140:A1133–A1138, Nov 1965.

[31] Kieron Burke. Perspective on density functional theory. *J. Chem. Phys.*, 136:150901, 2012.

[32] E. Prodan and W. Kohn. Nearsightedness of electronic matter. *Proceedings of the National Academy of Sciences*, 102(33), 2005.

[33] Carl-Olof Almbladh and Ulf von Barth. *Density-Functional Theory and Excitation Energies*. 1985.

[34] A. R. Elmaslmane, J. Wetherell, M. J. P. Hodgson, K. P. McKenna, and R. W. Godby. Accuracy of electron densities obtained via koopmans-compliant hybrid functionals. *Phys. Rev. Materials*, 2:040801, Apr 2018.

[35] Erich Runge and E. K. U. Gross. Density-functional theory for time-dependent systems. *Phys. Rev. Lett.*, 52:115164, Mar 1984.

[36] Robert van Leeuwen Nils Erik Dahlen and Adrian Stan. Propagating the kadanoff-baym equations for atoms and molecules. *Journal of Physics: Conference Series*, 35(1), 2006.

[37] Adrian Stan, Nils Erik Dahlen, and Robert van Leeuwen. Time propagation of the kadanoffbaym equations for inhomogeneous systems. *The Journal of Chemical Physics*, 130(22), 2009.

[38] R. Bersohn. Quantum statistical mechanics. l. p. kadanoff and g. baym. benjamin, new york, 1962. 203 pp. illus. paper, 4.95; *cloth*,6.95. *Science*, 139(3553), 1963.

[39] Karsten Balzer. Solving the two-time kadanoff-baym equations. application to model atoms and molecules. *Dissertation*, 2011.

[40] David Bohm and David Pines. A collective description of electron interactions. i. magnetic interactions. *Phys. Rev.*, 82:625–634, Jun 1951.

[41] David Pines and David Bohm. A Collective Description of Electron Interactions: II. Collective vs Individual Particle Aspects of the Interactions. *Phys. Rev.*, 85:338–353, Jan 1952.

[42] David Bohm and David Pines. A collective description of electron interactions: Iii. coulomb interactions in a degenerate electron gas. *Phys. Rev.*, 92:609–625, Nov 1953.

[43] E. E. Salpeter and H. A. Bethe. A relativistic equation for bound-state problems. *Phys. Rev.*, 84:1232–1242, Dec 1951.

[44] F. Aryasetiawan, R. Sakuma, and K. Karlsson. GW approximation with self-screening correction. *Phys. Rev. B*, 85:035106, Jan 2012.

[45] W. Kohn and L. J. Sham. Self-consistent equations including exchange and correlation effects. *Phys. Rev.*, 140:A1133–A1138, 1965.

[46] M. J. P. Hodgson, J. D. Ramsden, J. B. J. Chapman, P. Lillystone, and R. W. Godby. Exact time-dependent density-functional potentials for strongly correlated tunneling electrons. *Phys. Rev. B*, 88:241102, Dec 2013.

[47] M. T. Entwistle, M. J. P. Hodgson, J. Wetherell, B. Longstaff, J. D. Ramsden, and R. W. Godby. Local density approximations from finite systems. *Phys. Rev. B*, 94:205134, Nov 2016.

[48] J. Crank and P. Nicolson. A practical method for numerical evaluation of solutions of partial differential equations of the heat-conduction type. *Mathematical Proceedings of the Cambridge Philosophical Society*, 43(1), 1947.

[49] H. N. Rojas, R. W. Godby, and R. J. Needs. Space-time method for ab initio calculations of self-energies and dielectric response functions of solids. *Phys. Rev. Lett.*, 74:1827–1830, Mar 1995.

[50] Tathagata Biswas and Manish Jain. Quasiparticle band structure and optical properties of hexagonal-ymno3. *Journal of Applied Physics*, 120(15):155102, 2016.

[51] Jack Deslippe, Georgy Samsonidze, David A. Strubbe, Manish Jain, Marvin L. Cohen, and Steven G. Louie. Berkeley GW: A massively parallel computer package for the calculation of the quasiparticle and optical properties of materials and nanostructures. *Computer Physics Communications*, 183(6):1269 – 1289, 2012.

[52] Andrea Damascelli, Zahid Hussain, and Zhi-Xun Shen. Angle-resolved photoemission studies of the cuprate superconductors. *Rev. Mod. Phys.*, 75:473–541, Apr 2003.

[53] Brian Cunningham, Myrta Gruning, Pooya Azarhoosh, Dimitar Pashov, and Mark van Schilfgaarde. Effect of ladder diagrams on optical absorption spectra in a quasiparticle self-consistent GW framework. *Phys. Rev. Materials*, 2:034603, Mar 2018.

[54] J. J. Fernandez. GW calculations in an exactly solvable model system at different dilution regimes: The problem of the self-interaction in the correlation part. *Phys. Rev. A*, 79(5), may 2009.

[55] Giovanna Lani, Pina Romaniello, and Lucia Reining. Approximations for many-body Green's functions: insights from the fundamental equations. *New Journal of Physics*, 14(1):013056, 2012.

[56] Xinguo Ren, Patrick Rinke, Christian Joas, and Matthias Scheffler. Random-phase approximation and its applications in computational chemistry and materials science. *Journal of Materials Science*, 47(21):7447–7471, Nov 2012.

[57] Johannes Rekkedal, Sonia Coriani, Maria Francesca Iozzi, Andrew M. Teale, Trygve Helgaker, and Thomas Bondo Pedersen. Communication: Analytic gradients in the random-phase approximation. *The Journal of Chemical Physics*, 139(8):081101, 2013.

[58] Thomas M. Henderson and Gustavo E. Scuseria. The connection between self-interaction and static correlation: a random phase approximation perspective. *Molecular Physics*, 108(19-20):2511–2517, 2010.

[59] A. Hebelmann and A. Gorling. Random-phase approximation correlation methods for molecules and solids. *Molecular Physics*, 109(21):2473–2500, 2011.

[60] M. J. P. Hodgson, J. D. Ramsden, T. R. Durrant, and R. W. Godby. Role of

electron localization in density functionals. *Phys. Rev. B*, 90:241107, Dec 2014.

[61] Paul Hessler, Jang Park, and Kieron Burke. Several theorems in time-dependent density functional theory. *Phys. Rev. Lett.*, 82:378–381, Jan 1999.

[62] M. J. P. Hodgson, J. D. Ramsden, and R. W. Godby. Origin of static and dynamic steps in exact Kohn-Sham potentials. *Phys. Rev. B*, 93:155146, Apr 2016.

[63] E. Prodan. Nearsightedness of electronic matter in one dimension. *https://arxiv.org/abs/cond-mat/0506687*.

[64] M. Shishkin and G. Kresse. Self-consistent GW calculations for semiconductors and insulators. *Phys. Rev. B*, 75:235102, Jun 2007.

[65] Sahar Sharifzadeh. Many-body perturbation theory for understanding optical excitations in organic molecules and solids. *Journal of Physics: Condensed Matter*, 30(15):153002, 2018.

[66] R.M. Dreizler and E.K.U. Gross. *Density Functional Theory*. Springer Verlag, Berlin, 1990.

[67] R. O. Jones. Density functional theory: Its origins, rise to prominence, and future. *Rev. Mod. Phys.*, 87:897–923, Aug 2015.

[68] Aron J Cohen, Paula Mori-Sanchez, and Weitao Yang. Challenges for density functional theory. *Chemical reviews*, 112(1):289–320, 2011.

[69] Michael G. Medvedev, Ivan S. Bushmarinov, Jianwei Sun, John P. Perdew, and Konstantin A. Lyssenko. Density functional theory is straying from the path toward the exact functional. *Science*, 355(6320):49–52, 2017.

[70] John P. Perdew, Robert G. Parr, Mel Levy, and Jose L. Balduz. Density-functional theory for fractional particle number: Derivative discontinuities of the energy. *Phys. Rev. Lett.*, 49:1691–1694, Dec 1982.

[71] Robert van Leeuwen, Oleg Gritsenko, and Evert Jan" Baerends. Step structure in the atomic Kohn-Sham potential. *Zeitschrift fur Physik D Atoms, Molecules and Cluster*, 33(4), Dec 1995.

[72] A. Seidl, A. Gorling, P. Vogl, J. A. Majewski, and M. Levy. Generalized Kohn-Sham schemes and the band-gap problem. *Phys. Rev. B*, 53:3764–3774, Feb 1996.

[73] Andrea Ferretti, Ismaila Dabo, Matteo Cococcioni, and Nicola Marzari. Bridging density-functional and many-body perturbation theory: Orbital-density dependence in electronic-structure functionals. *Phys. Rev. B*, 89:195134, May 2014.

[74] John P. Perdew, Weitao Yang, Kieron Burke, Zenghui Yang, Eberhard K. U. Gross, Matthias Scheffler, Gustavo E. Scuseria, Thomas M. Henderson, Igor Ying Zhang, Adrienn Ruzsinszky, Haowei Peng, Jianwei Sun, Egor Trushin, and Andreas Gorling. Understanding band gaps of solids in generalized Kohn-Sham theory. *Proceedings of the National Academy of Sciences*, 114(11):2801–2806, 2017.

[75] John P. Perdew, Kieron Burke, and Matthias Ernzerhof. Generalized gradient

approximation made simple. *Phys. Rev. Lett.*, 77:3865–3868, Oct 1996.

[76] W. Kohn. Density functional and density matrix method scaling linearly with the number of atoms. *Phys. Rev. Lett.*, 76:3168–3171, Apr 1996.

[77] John P Perdew and John R Smith. Can desorption be described by the local density formalism? *Surface science*, 141(1):L295–L303, 1984.

[78] M. J. P. Hodgson, Eli Kraisler, Axel Schild, and E. K. U. Gross. How interatomic steps in the exact Kohn-Sham potential relate to derivative discontinuities of the energy. *The Journal of Physical Chemistry Letters*, 8(24):5974–5980, 2017. PMID: 29179553.

[79] John P. Perdew, Matthias Ernzerhof, and Kieron Burke. Rationale for mixing exact exchange with density functional approximations. *The Journal of Chemical Physics*, 105(22):9982–9985, 1996.

[80] J. Paier, M. Marsman, K. Hummer, G. Kresse, I. C. Gerber, and J. G. Ángyán. Screened hybrid density functionals applied to solids. *The Journal of Chemical Physics*, 124(15):154709, 2006.

[81] Ismaila Dabo, Andrea Ferretti, Nicolas Poilvert, Yanli Li, Nicola Marzari, and Matteo Cococcioni. Koopmans' condition for density-functional theory. *Phys. Rev. B*, 82:115121, Sep 2010.

[82] A. D. Becke. Density-functional exchange-energy approximation with correct asymptotic behavior. *Phys. Rev. A*, 38:3098–3100, Sep 1988.

[83] J. P. Perdew and Alex Zunger. Self-interaction correction to density-functional approximations for many-electron systems. *Phys. Rev. B*, 23:5048–5079, May 1981.

[84] E. J. Baerends. Exact exchange-correlation treatment of dissociated h2 in density functional theory. *Phys. Rev. Lett.*, 87:133004, Sep 2001.

[85] Axel D. Becke. A new mixing of HartreeFock and local densityfunctional theories. *The Journal of Chemical Physics*, 98(2):1372–1377, 1993.

[86] Leeor Kronik, Tamar Stein, Sivan Refaely-Abramson, and Roi Baer. Excitation gaps of finite-sized systems from optimally tuned range-separated hybrid functionals. *Journal of Chemical Theory and Computation*, 8(5):1515–1531, 2012.

[87] Viktor Atalla, Igor Ying Zhang, Oliver T. Hofmann, Xinguo Ren, Patrick Rinke, and Matthias Scheffler. Enforcing the linear behavior of the total energy with hybrid functionals: Implications for charge transfer, interaction energies, and the random-phase approximation. *Phys. Rev. B*, 94:035140, Jul 2016.

[88] Sivan Refaely-Abramson, Sahar Sharifzadeh, Manish Jain, Roi Baer, Jeffrey B. Neaton, and Leeor Kronik. Gap renormalization of molecular crystals from density-functional theory. *Phys. Rev. B*, 88:081204, Aug 2013.

[89] Stephan Lany and Alex Zunger. Polaronic hole localization and multiple hole binding of acceptors in oxide wide-gap semiconductors. *Phys. Rev. B*, 80:085202, Aug 2009.

[90] Monika Srebro and Jochen Autschbach. Tuned range-separated time-

dependent density functional theory applied to optical rotation. *Journal of Chemical Theory and Computation*, 8(1):245–256, 2012.

[91] Arteum D. Bochevarov and Richard A. Friesner. The densities produced by the density functional theory: Comparison to full configuration interaction. *The Journal of Chemical Physics*, 128(3):034102, 2008.

[92] Mel Levy, John P. Perdew, and Viraht Sahni. Exact differential equation for the density and ionization energy of a many-particle system. *Phys. Rev. A*, 30:2745–2748, Nov 1984.

[93] J. F. Janak. Proof that edni=e in density-functional theory. *Phys. Rev. B*, 18:7165–7168, Dec 1978.

[94] Weitao Yang, Aron J. Cohen, and Paula Mori-Sanchez. Derivative discontinuity, bandgap and lowest unoccupied molecular orbital in density functional theory. *The Journal of Chemical Physics*, 136(20):204111, 2012.

[95] John P. Perdew, Weitao Yang, Kieron Burke, Zenghui Yang, Eberhard K. U. Gross, Matthias Scheffler, Gustavo E. Scuseria, Thomas M. Henderson, Igor Ying Zhang, Adrienn Ruzsinszky, Haowei Peng, Jianwei Sun, Egor Trushin, and Andreas Gorling. Understanding band gaps of solids in generalized KohnSham theory. *Proceedings of the National Academy of Sciences*, 114(11):2801–2806, 2017.

[96] Tamar Stein, Helen Eisenberg, Leeor Kronik, and Roi Baer. Fundamental gaps in finite systems from eigenvalues of a generalized Kohn-Sham method. *Phys. Rev. Lett.*, 105:266802, Dec 2010.

[97] Miguel A. L. Marques, Julien Vidal, Micael J. T. Oliveira, Lucia Reining, and Silvana Botti. Density-based mixing parameter for hybrid functionals. *Phys. Rev. B*, 83:035119, Jan 2011.

[98] Nicholas P. Brawand, Marton Voros, Marco Govoni, and Giulia Galli. Generalization of dielectric-dependent hybrid functionals to finite systems. *Phys. Rev. X*, 6:041002, Oct 2016.

[99] Sivan Refaely-Abramson, Roi Baer, and Leeor Kronik. Fundamental and excitation gaps in molecules of relevance for organic photovoltaics from an optimally tuned range-separated hybrid functional. *Phys. Rev. B*, 84:075144, Aug 2011.

[100] A. R. Elmaslmane, M. B. Watkins, and K. P. McKenna. First-principles modeling of polaron formation in tio2 polymorphs. *Journal of Chemical Theory and Computation*, 14(7):3740–3751, 2018. PMID: 29874462.

[101] M. Schuler and Y. Pavlyukh. Spectral properties from matsubara Green's function approach: Application to molecules. *Phys. Rev. B*, 97:115164, Mar 2018.